

POLITECNICO DI TORINO

---

Corso di Laurea Magistrale in Ingegneria Elettrica

Tesi di Laurea

**Computational framework for evaluating the  
impact of power-to-gas technology on European  
transmission system with large penetration of  
renewable sources**



**Relatore**

Dr. Mazza Andrea

**Correlatori**

Prof. Bompard Ettore Francesco

Dr. Estebansari Abouzar

**Candidato**

Andrea Rogin

---

Anno Accademico 2017 - 2018



# Table of Contents

Table of Contents.....	3
Acronyms.....	5
1 Introduction.....	7
2 The “electrical” PtG node: plant model assumptions .....	10
2.1 Understanding power to gas .....	10
2.2 Algorithm of the AEC-based PtG plant model .....	13
3 Network resolution methods.....	15
3.1 Power Flow and Optimal Power Flow .....	15
3.1.1 Power flow resolution methods: AC power flow vs DC power flow .....	15
3.1.2 Optimal power flow: description of the problem and resolution methods .....	16
3.2 Day-ahead market and Intra-day market.....	17
3.3 Matpower.....	17
4 Proof of Concept.....	19
4.1 Description of the Network #T1 .....	19
4.2 Description of the algorithm for the case study #T1 .....	21
4.2.1 Time function .....	25
4.2.2 Power redistribution function.....	25
4.2.3 Feasibility check function .....	27
4.2.4 Protection function .....	27
4.3 Results for the case #T1 .....	28
5 Description of the European transmission networks.....	34
5.1 Existing models of the European transmission system.....	34
5.2 Description of the Network #T2.....	35
5.3 Description of the Network #T3.....	37
5.4 PV production for the European case .....	39
5.5 Wind production for the European case .....	39
5.6 Load profiles for the European case .....	41
5.7 Generation scenario for the European case.....	41
5.8 Future scenarios for the European case .....	42
6 Description of the algorithm for the case studies #T2 and #T3.....	44
6.1 Main characteristics .....	44
6.2 Description of the input data .....	44
6.3 Limitations .....	45
6.4 Execution of the DAM algorithm.....	46
6.5 Execution of the ID (or real time) algorithm .....	47

6.6	Introduction of the PtG node into the calculation loop .....	50
7	Results for the cases #T2 and #T3 .....	53
7.1	Network #T2 .....	53
7.2	Network #T3, present scenario .....	59
7.3	Network #T3, future scenarios .....	66
8	Conclusions .....	77
Appendix A	PtG plant model .....	78
A.1	AEC electrolyser model .....	78
A.2	AEC electrolyser efficiency .....	80
A.3	Methanation unit .....	81
A.4	Compression and pumping power consumptions.....	81
Appendix B	Calculation of the AC power for PV fields .....	83
Appendix C	Wind Profile Elaboration .....	84
C.1	Network #T1 .....	84
C.2	First approach for Europeans networks .....	84
C.3	Second approach for Europeans networks .....	86
C.4	Final approach for Europeans networks.....	87
Appendix D	NUTS 2 and Regions association.....	90
Appendix E	OPF convergence problems and their possible solutions .....	93
References	.....	95
Ringraziamenti	.....	98

## Acronyms

AC	Alternate current
DA	Day-Ahead
DCOPF	DC Optimal Power Flow
DG	Distributed Generation
DUOPF	DC Unit de-commitment Optimal Power Flow
GDP	Gross Domestic Product
HV	High Voltage
ID	Intra-Day
mpc	Matpower Case-file
MV	Medium Voltage
OC	Overcurrent
OV	Overvoltage
PtG	Power-to-Gas
pu	per unit
PV	Photovoltaic
RES	Renewable Energy Sources
RPF	Reverse Power Flow
ROR	Run-On-River plant (hydro power plant)
SA	Simulated Annealing
SNG	Synthetic Natural Gas
TYNDP	Ten Year Network Development Plan



# 1 Introduction

The outline of transmission and distribution electrical networks relies on old infrastructures, conceived as pluri-decennial investments, and Transmission and Distribution System Operators (TSOs and DSOs) need to serve consumers and producers with this same infrastructure along the years.

The electrical system underwent a major transition, evolving from a vertical integrated model, in which a single monopoly manages generation, transmission and distribution, to a free market, in which TSOs and DSOs, except for security reasons, have no control over the power flows. Power exchanges are decided through a market logic, in order to create competition and lower the costs. The separation between the generation and the transportation of energy brought a new wave of investments and incentives in the field of generation, and who in the past was only a consumer, had the possibility to become also a producer, creating the figure of the “prosumer”. Besides the conventional power plants, technological advancements improved photovoltaic (PV) and wind production feasibility and accessibility, overturning the principle, true for vertically integrated networks, in which the direction of the power flows in the lines is known beforehand.

The integration of such large amounts of renewable energy sources into the electrical grid poses technological difficulties, as those sources, like wind and solar irradiance, are volatile and generate electricity intermittently. At times there will be a surplus of energy when there is no demand for it, and vice versa there will be at times high demand when there is not enough renewable energy available. In case of surplus of RES production, reverse power flow from the distribution networks to the transmission one is a possibility, and the continuously increasing RES penetration means additional work for system operators in order to maintain the network’s security and avoid interfering with the market due to networks’ limitations.

The necessity of focused investments is undiscussed, but after seeing the importance of the evolution that has happened to the electrical system, it’s important to accurately re-evaluate the technics of problem-solving that have been deployed until now, in the light of the fact that they could not be the optimal ones anymore.

The users have changed, the producers have changed, and moreover the increasing capacity of uncontrollable RES generation brings new problems to the networks. Despite the need of CO<sub>2</sub> emissions’ reduction, which requires the discontinuation of conventional power plants, these networks need those very same conventional power plants now more than ever, in order to compensate wind speed and irradiance variability, and therefore the RES power production variability. It’s true that RES aggregates are more predictable than single units, but the resulting power flows in the lines are not, creating not only problems to producers, but also to system operators. Conventional generators are then still needed for reliability purposes, but they are more and more in difficulty in the highly competitive energy market.

The classical solution to these problems would be the construction of additional lines, in order to limit congestions, and leave the market to self-regulate, but the now constantly evolving topologies of production sites brings added difficulty to identify the optimal configuration for these investments.

The problems are of a dynamic nature, so it is legit to question ourselves if the passive nature of lines can be the solution we are looking for. Maybe a new, active participant of the network is needed, and this is where the power to gas (PtG) technology could step-in. PtG plants are able to use electricity and a CO<sub>2</sub> supply to produce synthetic natural gas (SNG) and its development is the goal of the project STORE&GO, funded by European Union’s Horizon 2020 research and innovation programme. The project STORE&GO aims to investigate all the aspects regarding the integration of large-scale Power-to-Gas (PtG) at European level, by exploiting it as means for long term storage.

The question is why PtG is chosen over other long term storage solutions. Nowadays the largest energy storage capacity is offered by pumped hydro power, but still it would not be able to last more than few hours if used to help the European transmission grid ([www.storeandgo.info](http://www.storeandgo.info)). The other possibility is the use of batteries, much more versatile than pumped hydro power, but still they are difficult to implement for this kind of usage due to low energy density, high costs and the problem of self-discharging.

Producing SNG does not seem to add any benefit over usual storage solutions at first glance, but PtG plants have some peculiarities:

- The interface with the electrical network is an electrolyser, a device that can modify its power consumption way faster than any normal load, introducing a new kind of load shedding, with faster response, less consequences, and the ability to increase the power consumption if necessary.
- The PtG plants also interface themselves with the gas market by completing a bi-directional link to the gas network, opening to unfathomed possibilities. The SNG can be stored in tanks or in the existing 2.2 million km long gas grid, which in Europe reaches approximately 70 million consumers.
- SNG offers the highest energy density of available storage technologies and it is by far the most promising way to store large amounts of energy and reach the targets of the Paris climate agreement, which has been signed as legally binding global climate deal in December 2015 by 195 countries. EU committed itself to reduce emission by 40% by 2030 and by 80 to 95% by 2050, compared to 1990.

One of the aspects that should be properly addressed is the impact that the integration of PtG plants may have on the electricity system stability. Being a multiple year project, this thesis will present the models which will be used during the next investigations about PtG effects on transmission networks.

But before diving into this realm of possibilities, it is important to understand on which solid bases the considerations will be made. A single PtG plant can be easily modelled without any regard to the network in which it is inserted. But a big scale application needs the context of the transmission system since it represents the backbone of the entire electricity system and traditionally represented the link between the generation units (usually located far from cities) and the load centres. For matter of clearness, the simplified schematic of the entire electricity system is shown in Figure 1-1.

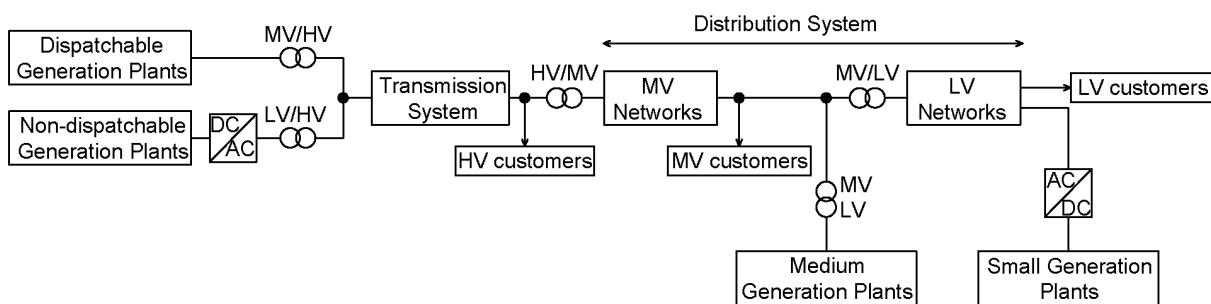


**Figure 1-1: Representation of the electricity system [1]**

First of all, a model of PtG plant takes into account the entire chain of the plant, by eventually introducing the electrical "PtG node". It is able to emulate the limits in accepting electricity due to the different elements composing the plant.

Then the second step is the creation of a computational framework, built from the ground up, capable to insert PtG nodes in the network. It also needs to accurately represent the variability of RES and their effects on intra-day market of transmission networks, and to compare the latter to the assumptions made in the day-ahead market. Through the execution of optimal power flows it enables the possibility to make economic considerations on the networks.

In order to take advantage of this framework, it is important to use representative networks. In fact, the detailed study of the integration of PtG into the transmission network needs the following features:

1. Proof of concept, for testing purposes
2. Proper description of the transmission network: this means the implementation of realistic transmission systems, in terms of physical parameters (e.g., resistance, reactance, length, line thermal limits and so on)
3. Geographical coverage: in the usual load flow analysis, the geographical coverage is not so much important. However, by handling a new technology which aims to support the integration of RES in Europe, the geographical information is necessary
4. Proper values of generation and loads: the mix of generation and loads regarding the next decades (e.g., 2030 and 2040)
5. Application of the algorithm on the European network model

This thesis will present how to evaluate the effect of PtG, and if there is any benefit by using PtG in transmission systems from a technical standpoint. In these considerations PtG plants number, sizing and siting will not be a variable, so a single PtG system will be considered, in order to show its effect in different present and future scenarios. The economical aspect, and therefore the optimization of the PtG plants siting and sizing, will be addressed in future researches.

More in detail, this work is organised as it follows: after this introduction, the second chapter will explain the concept of PtG and its integration in a Matlab model. The third chapter is dedicated to the chosen network resolution methods and the reasoning behind the choices made. More detailed information about electricity markets is also present in this chapter. The description of the case #T1, which has been used as a proof of concept, is presented in chapter four, along the description of the algorithm used and the relative results. The case study #T2 and #T3 are more complex, and they are detailed in chapters five to seven. The fifth chapter is dedicated to the modelling of the two European networks, while in the sixth one the used algorithms, along the PtG model implementation, are presented. Results of the European cases are presented in the seventh chapter. The eighth chapter include the conclusions taken from this work.

The process of modelling a PtG unit from the data of a real plant is shown in Appendix A, since it has been developed for another work but it's been crucial for this work since it represents the basis of the PtG application. Appendix B shows how to calculate the ac power produced by PV plants starting from irradiance values.

Appendix C presents the process needed to model the wind production, which is only one part of the European network modelling but required much time and efforts. Appendix D instead shows a particular case of problem solving which has been necessary while modelling the European networks: after offering some information about the NUTS classification, it shows the process I've gone through in order to be able to correlate the geographical location of buses to their belonging territorial region, information needed in order to assign to each bus its RES installed capacity. Appendix E is a collection of problem-solving steps to be deployed in case of non-convergence of PF in Matpower.

## 2 The “electrical” PtG node: plant model assumptions

### 2.1 Understanding power to gas

Before observing the effect of the PtG on the grid, it's important to understand what is meant by “power to gas” (PtG). PtG represents a chain of processes that by absorbing electrical energy from the network allows the production of synthetic natural gas (SNG). A PtG plant is composed by three main components, an electrolyser, a hydrogen buffer, and a methanation unit.

- The electrolyser's aim is to produce hydrogen through water electrolysis.
- The hydrogen buffer is a tank that can accumulate hydrogen. It is responsible to guarantee methanation unit's autonomy when hydrogen production fluctuates, in order to provide more flexibility to the PtG plant.
- The methanation unit produces methane through carbon oxide's hydrogenation (Sabatier reaction). It has a slower dynamic than the electrolyser and therefore the hydrogen buffer is necessary to interface the two devices.

This modularity gives the possibility to scale up the plants, or even change the technology for a given stage along plant's lifespan. A simplified scheme of the PtG process can be seen in Figure 2-1. The electrolyser is the interface of the PtG plant with the electrical system and the fast response to working point changes is the peculiarity which will be analysed.

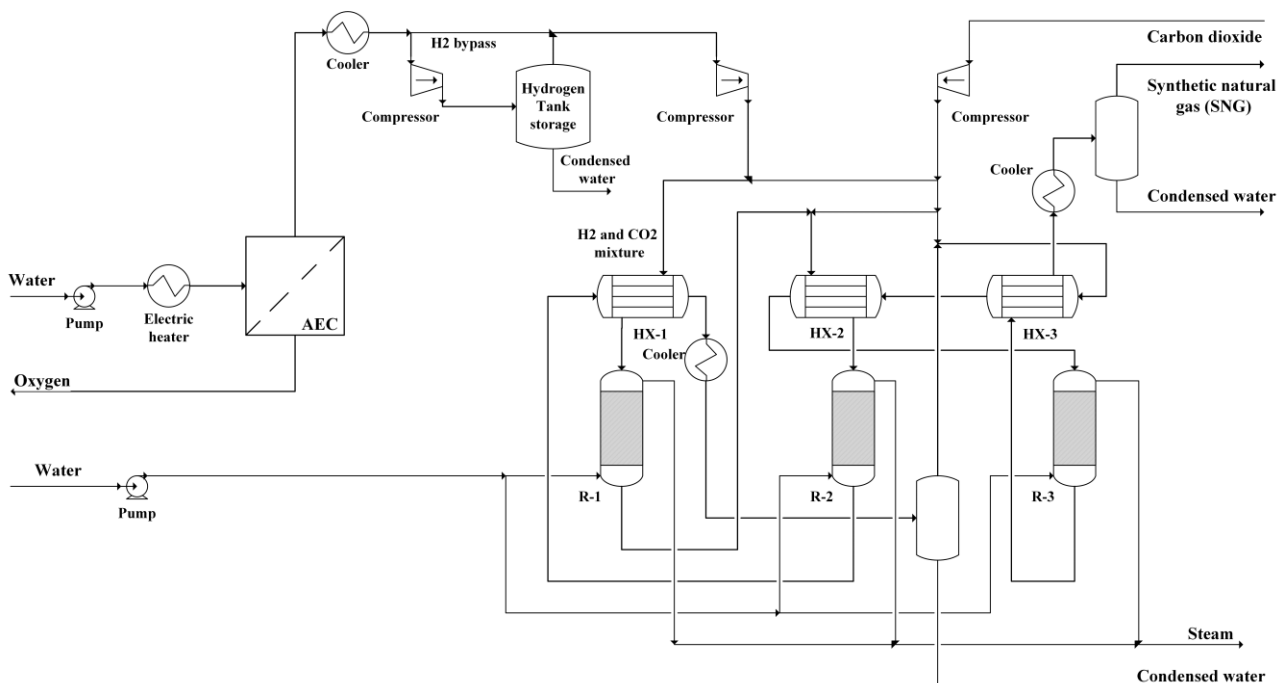


Figure 2-1: Power-to-Gas process scheme (the methanation unit refers to a work of Giglio et al. [2]).

More in detail, the electrolyser uses an electrical current to decompose water into hydrogen and oxygen. In an electrolytic cell two electrodes are present, in which a half reaction is caused by the passage of the electrons. At the cathode a reduction reaction happens:



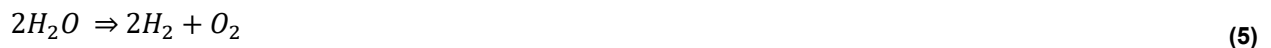
At the anode, instead, hydroxide ions are subjected to an oxidation reaction:



It is then necessary to balance the two half reactions with either acid or base, for example as base:



By summing them the overall electrolysis reaction is obtained, in which from water are obtained both hydrogen and oxygen:



This is the principle of electrolysis, but different technologies are deployed. In particular there are three main categories of commercial electrolyzers:

- **Alkaline electrolyzers (AEC):** they are based on the alkaline electrolysis, well known technology used in most commercial applications. Despite the use of corrosive electrolytes, which prevents any cost reduction at increased plant size, their advantages are multiple. For example, their cells work at atmospheric pressure with an efficiency from 40% to 80% (calculated as hydrogen energy over electricity spent) and relatively low working temperatures (below 100°C). For our application another negative aspect emerges: it is required for PEM electrolyzers a minimum stable power absorption of 20% of their nominal power, in order to retain the best response to power variation requests.
- **Proton exchange membrane electrolyzers (PEM):** they are characterized by a semipermeable membrane, which allow the passage of protons but prevent it for hydrogen and oxygen. The resulting device is simple and compact, with great response. The downsides are noteworthy investment costs and limited lifespan of the system.
- **Solid oxide electrolyzers (SOEC):** they rely on a newly adopted technology. The principle is similar to AEC, the difference being the use of solid electrolytes. The construction costs are lower than PEM and they offer great efficiency, but the technology is not ready yet for large scale deployment, being high working temperatures the limiting factor of the plant's lifespan.

The methanation unit instead takes advantage of Sabatier's process: it is an exothermic reaction between carbon dioxide and hydrogen which happens in presence of a catalyser, the result being the production of synthetic natural gas (SNG) and water:



It is important to highlight the fact that none of these processes involve the production of CO<sub>2</sub>. If these plants are in order to help the electrical system absorbing the variation of RES power production, the result is the production of SNG without any CO<sub>2</sub> emission.

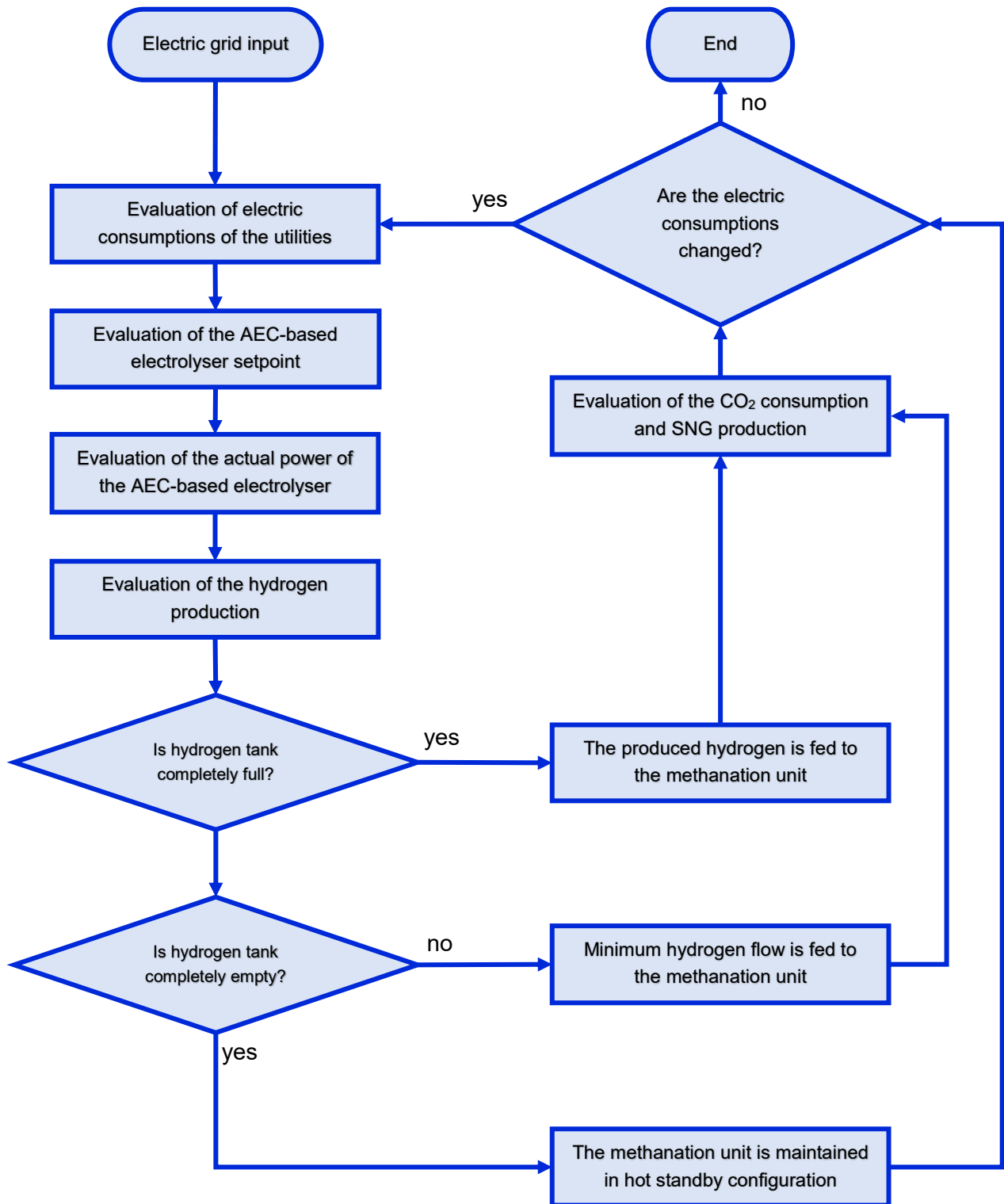


Figure 2-2: AEC-based P2G plant flowchart of the algorithm.

## 2.2 Algorithm of the AEC-based PtG plant model

The AEC-based PtG plant model, which was developed for this work, simulates the dynamic behaviour of a real AEC-based electrolyser coupled with a methanation unit. Implemented and tested by established private enterprises the demonstration site in Falkenhagen (Germany) is dedicated to the application of PtG technology to the transmission grid. The location is a rural area in the North East of Germany, characterized by high wind power production and low overall electricity load consumption. The plant is composed of a 2MW alkaline electrolyser, a hydrogen injection plant and a methanation unit. The latter one has the purpose of showcase two technologies an isothermal catalytic honeycomb and structured wall reactors. A biogas and a bioethanol plant are the sources of the necessary CO<sub>2</sub>. Up to 57 Nm<sup>3</sup>/h SNG (volumetric flow of synthetic natural gas) can be produced equivalent to approximately 600 kWh per hour. In addition, the heat generated during conversion will be supplied to a nearby veneer plant.

The modelling of the PtG unit is a crucial point in this work, but since it has been developed internally by PoliTo it has been detailed in Appendix A. The algorithm, which is illustrated in

Figure 2-2, was developed in MATLAB environment and consists of these main instructions:

- **Setpoint power of the AEC-based electrolyser:** given a random setpoint, the model calculates an internal setpoint, by capping the value between AEC electrolyser's maximum and minimum power levels, which are the 20% and 100% of its nominal power. Moreover, it's calculated as the difference between the electric available input and all the auxiliary consumptions of the PtG plant.
- **Actual power consumption of the AEC-based electrolyser:** the actual electric power consumption could be calculated using the dynamic model of the AEC-based electrolyser (first order system with delay, see Appendix A.1).
- **Hydrogen production:** the hydrogen flow could be evaluated taking into account the efficiency of the AEC-based electrolyser (see Appendix A.2).
- **Hydrogen tank:** the methanation unit is always fed with a minimum hydrogen flow (20% of the nominal power), if the electrolyser is operative. In addition, a certain amount of hydrogen could be sent to a hydrogen tank storage until the tank is completely full (filling of the tank is a priority). If the hydrogen tank is completely full the hydrogen produced by the AEC-based electrolyser is completely fed to the methanation unit. On the contrary, if the electrolyser does not produce hydrogen, the stored hydrogen is fed to the methanation unit, which works at the minimum power load until the hydrogen tank is completely empty.
- **Auxiliary consumptions:** all the consumptions of the auxiliary items of equipment scale to the amount hydrogen production. Firstly, the hydrogen could be compressed; secondly, the carbon dioxide has to be compressed; thirdly, the water has to be pumped and lastly it must be heated up to the AEC-based electrolyser.
- **Control of the setpoint:** the setpoint power of the electrolyser must be recalculated considering the new auxiliary consumptions, because the available electricity is comparable with the power absorbed by the electrolyser.
- **Methanation unit:** eventually, the amount of methane could be calculated using the CO<sub>2</sub> conversion; thus, the SNG productivity could be estimated.

The summary of the assumption used for implementing the model is shown in Table 2-1.

**Table 2-1: Parameters used for the PtG model**

<b>Parameter</b>	<b>Value</b>
$K$	1
$\tau$	11.73 [s]
$\alpha$	14.62 [s]
$\eta_{power-to-H_2}$	57.6 %
Conversion CO <sub>2</sub> in methanation unit	99 %
$\eta_c$	85 %
$\eta_p$	85 %
$WC$	75 %
$P_{min}$	$0.2P_n$
$P_{max}$	$P_n$

## 3 Network resolution methods

### 3.1 Power Flow and Optimal Power Flow

The resolution of problems related to the electricity networks involved the calculation of the status of the network starting from an operational point. Given a particular network condition, the aim is to calculate the currents flowing in the branches and the voltage at every node. This process is called “power flow” (PF) study. The resolution is complicated by the structure of the transmission network, which is meshed for allowing enough connection redundancy for guaranteeing the security of the system and by the technological limits of branches and generators.

In the network resolution, the nodes of the network can be divided in three categories:

- **PQ:** they traditionally represented the passive load of the network. The two letters “P” and “Q” indicate that the node is defined through an active power value (“P”) and reactive power value (“Q”). Today, this kind of representation is also used for generation nodes which are not acting for voltage regulation (such as non-dispatchable generators producing only active power P, without any injection of reactive power Q)
- **PV:** these nodes are representative of the traditional generators. They are defined through a power injected P and the nodal voltage V. They are characterised by a “capability curve”, which delimitates the possible combined production of active and reactive power
- **Slack bus:** this is also called swing bus. It represents the reference node in the network calculation. Furthermore, it allows to cover all those quantities (such as the network losses) which are unknown at the beginning of the process, and are only known at the end of the calculation

In order to define a network condition to be solved, all the generators but the slack one need a given setpoint. The generator in the slack bus is the only one which can not have a setpoint given beforehand, since it is the generator which will supply the network losses, which can not be known in advance.

Different is the case in which economic information about the generators is also available. By considering the economic costs (or biddings) of power generation, through an optimization process it is possible to dispatch the generators in such a way the total network costs reach a minimum. This process is called “optimal power flow” (OPF) and will be detailed in Section 3.1.2.

#### 3.1.1 Power flow resolution methods: AC power flow vs DC power flow

The resolution of the network is based on the use of iterative methods, which can solve both the active and reactive dispatching (i.e., AC-power flow methods) or only the active power dispatching (i.e., Decoupled power, also called DC-power flow). The choice to use either the AC methods or the DC power flow depends on the type of network under analysis, the constraint in terms of time for executing the calculation, and on the available information of network’s parameters.

The most used AC power flow methods are the so-called Newton-Raphson and Gauss-Siedel methods [3].

However, the solution of large-scale network can be efficiently made by applying the decoupled power flow method, which provides an approximate result of the load flow calculation. The principles

which drive towards the use of this simplified method are the presence, in the transmission network, of two well defined “control channels”, which are the “active control channel” and the “reactive control channel”. The active control channel refers to the control of the active power, which in the transmission system is mainly based on the voltage angle values, whereas the reactive control channel refers to the reactive power control, mainly depending on the amplitude of the nodal voltages. These two channels are so “well defined” in the transmission network thanks to the low resistance value of the electrical conductor. This kind of consideration led to simplify the mathematical formulation of the Newton-Raphson methods, by making possible to have good enough results in less time [3].

The Decoupled Power Flow has been used for the European networks considered in this work in order to decrease computational time, given their size.

### 3.1.2 Optimal power flow: description of the problem and resolution methods

The presence of several generators connected to the same infrastructure leads to consider which of them should be dispatched as first. This kind of choice can be done by making a ranking based on an economic merit order, by minimizing the total cost  $f(\mathbf{x})$  through on an optimization problem, i.e.:

$$\min_{\mathbf{x}} f(\mathbf{x}) \tag{1}$$

subject to equality  $\mathbf{g}(\mathbf{x})$  and inequality  $\mathbf{h}(\mathbf{x})$  constraint, as well as to the limits of the state variables  $\mathbf{x}$ :

$$\mathbf{g}(\mathbf{x}) = \mathbf{0} \tag{2}$$

$$\mathbf{h}(\mathbf{x}) \leq \mathbf{0} \tag{3}$$

$$\mathbf{x}_{min} \leq \mathbf{x} \leq \mathbf{x}_{max} \tag{4}$$

In our cases, the problem variables are the angle of the voltages and the generated power of the generators, which cannot exceed their technical limits. The existence of time variant loads implies a variation in the production of the different units: this variation is physically limited by ramp rate constraints, which do not allow the sudden change of the generation<sup>1</sup>. Branches thermal limits also play as constrains which need to be enforced by redispatching generators differently, causing additional costs for the system and different zonal prices.

The main role of PtG is to produce SNG by exploiting the excess of electricity produced by RES, and the installation of a number of PtG plants can help to stabilise the network. In this framework, the PtG plants operate as a balancing element, by making possible the long-term storage of the excess of electricity produced by RES. In this work, the integration of PtG into the electricity system passes through an intra-day OPF based on the results of day-ahead OPF. These two OPF aim to find the set of generators allowing the operation of the system at minimum generation cost. In particular, the first OPF dispatches the expected value of RES and the traditional generation through an economic merit order, whereas the second one aims to redispatch the traditional generators and the PtG for facing the unbalances caused by the variable nature of the RES. These two OPF aim to represent the day-ahead market and a (quasi) real-time market, on which PtG can operate for providing its services to the network. A short overview of the concept of day-ahead market and the real-time market is presented in the following Section 3.2.

---

<sup>1</sup> This condition affects only the structure of the inequality constraints, which should consider also the transition from one state to the other during the time

### 3.2 Day-ahead market and Intra-day market

Before going further into the model's description, it is important to explain the role of these two electricity markets. After the deregulation of the electrical systems the vertically integrated power system was split up and the state-owned utilities privatized. The deregulation and privatization mainly happened on production: at supply side, many countries established wholesale markets, where the generators can sell generated electricity under competition. Due to the non-storability of electricity in large scales and the constant need for balancing of generation and demand, a real spot market with immediate delivery cannot exist for power. Hence, most electricity markets perform a day-ahead trading, where the generation/demand schedules and prices for the 24 hours of the following day are determined. The price determination is often done by an auctioning process. In addition to the day-ahead trading, markets with trading shortly before delivery (usually 5-15 minutes), called as real-time or intra-day market, also exist. In some markets, both trading mechanisms exist, while the real-time trading is usually used as a kind of balancing market to adjust the predetermined quantities of the day-ahead market [4].

The day-ahead market is the main area for trading power. The day-ahead energy market is a forward market where generation suppliers sell energy and Load Serving Entities (LSEs) buy energy in advance of the time when energy is produced and consumed. An energy buyer needs to assess how much energy it will need to meet demand in the following day, and how much it is willing to pay for this volume of demanded power, hour by hour. The energy seller also needs to decide how much it can deliver and at what price, hour by hour. The market clearing engine performs an optimization program, generally with the objective function of minimizing total costs or maximizing the social surplus, taking into account some technical and financial constraints.

The real-time market starts physical operations at midnight of the operating day, based on schedules obtained from the day-ahead market and updated in the hours before midnight. The role of the real-time market is mainly to re-dispatch the already committed resources and commit new fast-start resources to meet real-time load and other changes to the system conditions. These changes include weather changes leading to deviations in variable renewable energy sources' production, forced outages of the resources and outages of network facilities.

The real-time market clearing prices reflect the actual operation of the resources participating in the market and are used to re-settle all the generation resources and loads that deviate from their day-ahead schedules. The real-time market calculates real-time marginal prices, usually on a 5-minute basis [5]. It is worth to note that the largest part of the actual energy gets settled in the day-ahead market, and only a small percentage gets settled in the real-time market. Usually in European power system, the market-based ancillary services are provided through an independent market, separated from the energy market; whereas in the American markets, energy and ancillary services are co-optimized in the same market. Inside the United States, all ISOs operate electricity markets in a sequence of day-ahead and real-time markets (sometimes called a two-settlement system). Following day-ahead market closure, real-time (or balancing) energy and ancillary service markets are cleared on an hourly basis during the operation day to ensure resources can meet any changing conditions in an efficient manner, e.g. change of load or renewable production with respect to the day-ahead forecasted values [5].

### 3.3 Matpower

Implementing a network resolution and/or optimization routine written from the ground up would not be nor useful nor noteworthy for this work, therefore Matpower [6], an open source collection of Matlab scripts, has been chosen. It provides all the instruments needed in order to solve steady-

state problems and the flexibility of easily changing the network's parameters, as it will be discussed more deeply in the description of the algorithms.

In fact, all of the network's data is gathered in a single structure called Matpower case-file (*mpc*) and also the results of Matpower's power flow functions follow the same structure of the input network file. This is very convenient when trying to create a time-evolving analysis starting from steady state network solutions.

Moreover Matpower, when creating the output structure, copies the structure of the input *mpc* and it only modifies the necessary output values. This allows additional columns to be stored in the *mpc* without interfering with its functionality. For example, within the bus field a column that stores all the information regarding the bus country has been added, and in generator field a new column allows to store the information of the type of generator. This simplifies a lot the application of properties to some elements only, as well as the filtering of the data along the algorithm execution. Useful indexes have been created, so, for example, solar, wind and conventional generators can be rapidly selected.

Both PF and OPF (AC and DC) can be easily performed by using simple functions which requires only a *mpc* as input. It is important to note that while calculating OPF solution, Matpower considers all the generators which are marked as "online" in the economic evaluation. The consequence is that pricier generators are kept online at their minimum stable generation, and therefore supplying power to the load at high price, adding shadow costs to the network. Matpower offers for DC OPF a Unit-Decommitment algorithm which recursively turns off some of the pricier generators in order to decrease the total costs of the system by reducing shadow costs. An example of these functions is shown in Table 3-1.

**Table 3-1: Example of Matpower PF functions**

<b>Function</b>	<b>Description</b>
<i>Output</i> = <code>runpf(mpc)</code>	Execute AC PF
<i>Output</i> = <code>rundcpf(mpc)</code>	Execute DC PF
<i>Output</i> = <code>rundcopf(mpc)</code>	Execute DC OPF
<i>Output</i> = <code>runduopf(mpc)</code>	Execute Unit-Decommitment OPF

## 4 Proof of Concept

Before integrating PtG technology in a real transmission network it has been necessary to make some considerations on a test network with certain characteristics. The example provided includes a small network, characterized by three conventional generators, 15-minute load profiles for each bus, and a wind farm generating uncontrollable power. It's important to keep in mind that in this analysis loads are constant for 15 minutes and the minute-based fluctuations, the consequence being that all the fluctuations are caused by the wind farm. Generation profiles of traditional generators are based on forecasts of the wind power production and on a given load, but what happens when the actual fluctuating power is injected into the network? What can PtG be used for?

In this case study the focus is about the power output of generators, in particular the slack one, that could be required in a certain instant, but can not be reached due to technical ramp rates. That amount of power, which prevents the equality between loads and generation, can be only provided by conventional generators' kinetic energy, causing a variation in voltage frequency in the system.

In this chapter PtG can find an application in absorbing the amount of power that the slack generator cannot provide, limiting effectively frequency changes. The algorithm shown will present a way to use steady-state network resolution methods in discrete time-varying analysis.

After the initial calculations and tests, this network has not been longer used anymore, due to the lack of the geographical information of the nodes and the limited applications, by leaving the room to more meaningful networks, as the network #T2 and #T3 (presented in Section 5.2 and Section 5.3, respectively). Moreover, the shift of view from an operational but not optimized standpoint (network #T1) to an operational optimized one (network #T2 and #T3) brought the need to change the approach used in the algorithm.

### 4.1 Description of the Network #T1

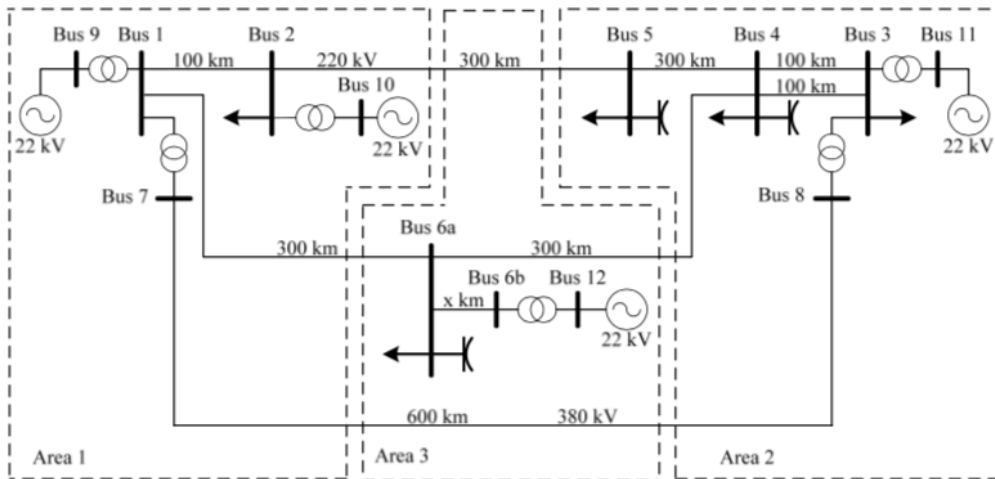
The first network used was the CIGRE European Configuration network [7]: the network is composed of 13 buses and all its elements are referred to the European network standards (e.g., voltage level, types of lines and so on).

The representation of the network is shown in Figure 4-1a. In the initial configuration, no RES power plants were installed. However, the taskforce have found as possible node for installation of a wind farm the bus 12, obtaining the configuration shown in Figure 4-1b: as it is possible to see, an additional line has been added, as well as new reactors (for reactive power control).

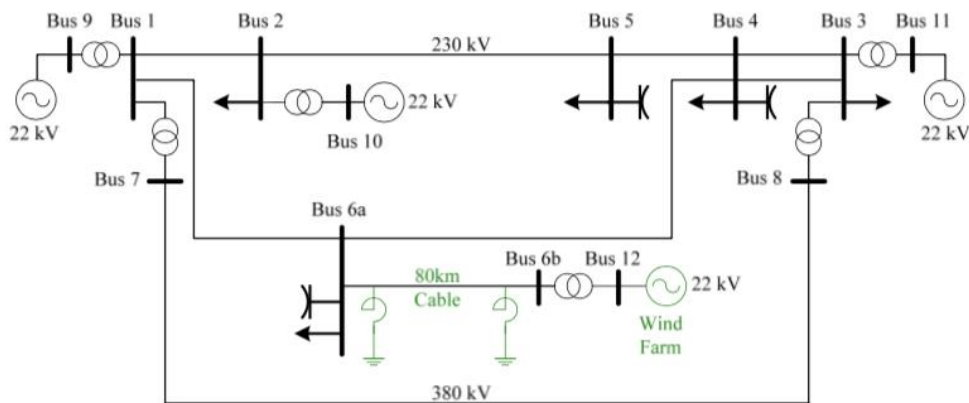
This network has been chosen in order to develop and validate the algorithm. By having few buses, the focus could be shifted from the network itself to the program. Furthermore, managing a smaller network helped to create a proper input file, which can be easily scaled up with larger network.

The case study considered a wind power plant connected to the node 12 and a PtG plant (in which only the dynamic characteristics of the electrolyser were considered) in node 6b. As suggested in [7], node 6b is in fact referred as a suitable location for studying the incorporation of large-scale renewable energy sources such as wind energy conversion systems (WECS) in node 12.

A real wind farm per unit profile has been assigned to the wind generator, and its nominal power has been scaled up in order to match a certain percentage of the daily energy consumed by the loads. In our tests two percentages have been used, 10% and 20% of the total load energy.



(a) Version without RES plants



(b) Version with wind power plant

**Figure 4-1: CIGRE HV Transmission Network: European configuration**

The loads and the generators of the model are shown in Table 4-1 and Table 4-2, respectively<sup>2</sup>. By applying a combination of load profiles, the maximum peak power of the network was 8.65 pu.

**Table 4-1: Load of the case study #T1**

Node	P [pu]	Q [pu]
2	2.85	2.00
3	3.25	2.44
4	3.26	2.44
5	1.03	0.62
6a (PtG)	4.35	2.96
6b	0.5	0

<sup>2</sup> The values expressed in pu are referred to  $S_b=100$  MVA

**Table 4-2: Generators of the case study #T1**

<b>Node</b>	<b>S<sub>rated</sub> [pu]</b>	<b>P<sub>out</sub> [pu]</b>
9 (slack)	7.00	5.00
10	7.00	5.00
11	5.00	2.00
12 (wind)	3.92	3.92

The minimum power at which the plants can work is 20% of its nominal power, and only the generators in bus 9 and bus 10 offer ramp service, with a ramp rate value equal to 0.17 pu/min. PtG ramp rate is equal to 50% of its nominal power, at 0.25 pu/min.

## 4.2 Description of the algorithm for the case study #T1

The algorithm developed and tested with the network #T1 is different from the one used in the following Chapter 6 for network #T2 and #T3. Briefly the differences are:

- No OPF existing: generators try to follow their generation profiles, compatible with their ramp rates and minimum/maximum power output
- The network calculations are made by means of Newton-Raphson power flow algorithm and so it is possible to find one slack node, which has to face the load variations and supply the network's losses
- Only one RES power plant is considered

The idea behind this algorithm was to apply a steady state network resolution method to a time-varying study, since a dynamical approach would not be feasible both for computational times, and for the quantity of additional information needed (for example, generators' statistics for frequency analysis). The limitation derived by the use of a steady state network resolution is the simplifications around the frequency, which it is supposed constant. The goal of the algorithm was to keep track, from a minute to another one, not of the changing rate of frequency but of the quantity of power that caused it.

This was done by using the slack's characteristic in Newton-Raphson's network's resolution:

- For all the generators but the slack one the setpoint equals to the actual power output, so these generators' limits are not a concern
- Slack generator will be the one to supply the network's losses, regardless its limits, set in the mpc
- These limits, since are not enforced by Matpower's resolution, are enforced externally, and the missing power quota is classified as  $dP$ , power that should be provided by the slack, but could not, and then it is safe to assume that it is the power is provided by system's kinetic energy
- This  $dP$  should be provided by conventional generators in the following time steps

The other problem was the necessity to link the discrete time steps one to another. In fact, for the single steady state network resolution the only limits for the generators are maximum and minimum power output, but when a time variation is considered another limit must be taken into account, the ramp rate. It is the amount of power output variation that a generator can sustain in a given amount of time, it allows to differentiate generators' types, and it's the key parameter that permits PtG to be competitive against conventional fossil fuels power plants. To give the scale of the difference, where coal power plants have ramp rates equal to 3% of their nominal power, PtG plants, as it can be seen in Section A.1, can modify their power from their minimum power to their maximum (and vice versa) in a matter of few minutes.

In order to enforce ramp rate limits, it is necessary to keep track of the power output of each generator at the previous discrete time step and compare it with the one at the current time, and if the difference exceed the ramp rate, the power output has to be capped. Note that this situation also produces a quantity of power that, if it will not be produced by other generators which have not reached any technical limitation, it will be part of the  $dP$  that will be seen at slack bus.

Both of these two problems have been solved by creating a re-dispatching algorithm based on the generator technical features. If a  $dP$  is present from the previous iteration, or has been created in the current iteration, part of that quantity of power will be assigned to each generator that offers ramp service and have not reached any constraint. If all generators reach their technical limits, and there is still power that needs to be redistributed, it will be assigned to the slack by the power flow resolution. The information about this amount of  $dP$  is passed to the next iteration.

Network's problems are created by the wind power plant: in fact, for the creation of the generation's profiles only the hourly average values of the wind power plant output are considered, like if their calculation would be based on a forecast. This way, during the power flow the conventional generators will try to follow their profiles, the wind power plant will follow its "real time" 1-minute based power output, and the redistribution logic will have to adapt to the evolving condition.

After running the network with conventional power plants only, a raw model of PtG plant has been implemented, in this case considering only the electrical interface, i.e., the electrolyser characteristics. Furthermore, a complete and scalable input data format has been introduced for the following applications. The main loop of the code is shown in Figure 4-2.

The algorithm has been developed with modularity in mind, dividing it through dedicated functions for each task, in particular:

- Time function: manages time-related operations, for example it updates the current time, the loads and generation based on the load and generation profiles in the current time step
- Power redistribution function: evaluates the existence of residual load  $dP$ , caused by new scheduled values of the generation (due to the variation of the load). By considering the generator characteristics (i.e. current generation value and ramp rates values), it redistributes  $dP$  among generators that can do it, based each generators ramp value and size
- Feasibility check function: checks the feasibility of the system and adds warnings to the mpc if violations are found, resets the warnings if they're not. Also calculates apparent power flowing in the network branches
- Protection function: it triggers protections based on warnings and timers. This functionality has been used only in this proof of concept

- Execute PF: it calculated the solution of the network based on the Newton-Raphson algorithm. The native code of Matpower [6] has been modified for accepting further fields not existing in the original version

PF is executed two times: the first time it acts as a “virtual” power flow, which is needed in order to check if any infeasibility triggers any protection. If it does, the network configuration changes abruptly and then another power flow calculation is needed.

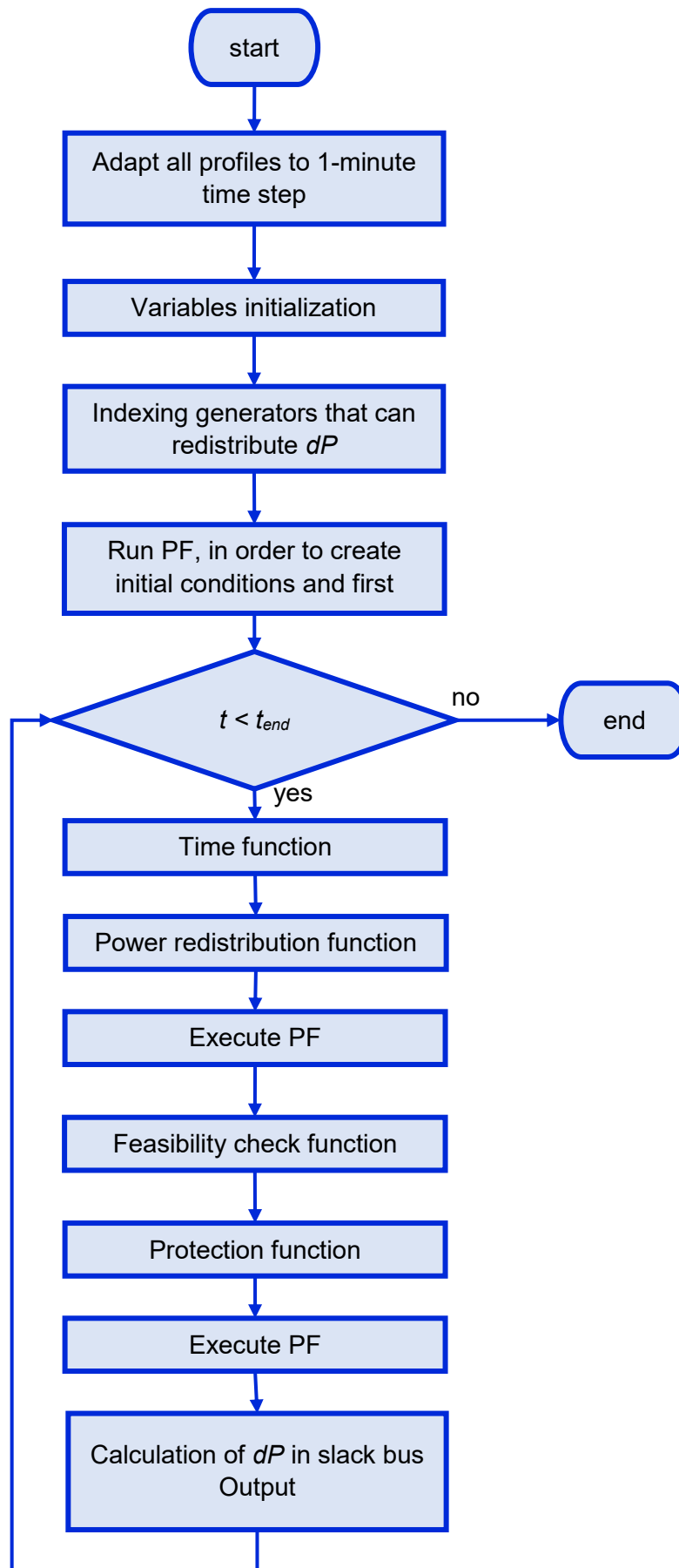


Figure 4-2: Main loop of the algorithm applied to network #T1

### 4.2.1 Time function

It is responsible for increasing the discrete time variable and all the other time-related variables by the user-defined discrete time-step  $dt$ . A representation of the code can be seen in Figure 4-3. All the timers necessary for protections are updated if the warning flags are active. Loads for each bus are updated using the profiles at the current time, like generation setpoints for both conventional and wind generators. For branches that has been opened previously due to thermal limit violations, a restoration timer is updated.

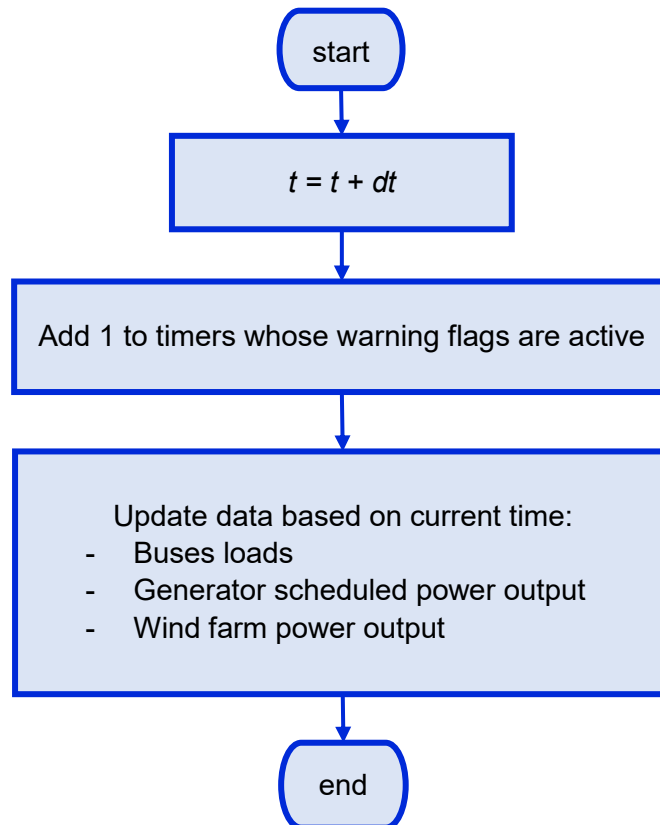


Figure 4-3: Flow chart of time function

### 4.2.2 Power redistribution function

It's the most complex function of the algorithm. By comparing the results of the first "virtual" power flow and the power output of generators at the previous time iteration, it calculates an amount of  $dP$  caused by technical constrains, like maximum and minimum power output and ramp rate. This quantity is added to the residual slack's  $dP$  from the previous time iteration, if present.

The second part of the routine consists in a loop which redistributes the amount of  $dP$  between the generators that offer ramp service and eventual PtG plants. At each iteration it keeps track of the availability of power of these units in relations to their technical limits and redistributes the  $dP$  among them by size. If a generator reaches a constrain in this while loop, part of the  $dP$  remains unallocated and it is redistributed in the next loop iteration among all the remaining generators which have not reached any of their constrains yet. The loop ends when all the  $dP$  is redistributed, or all the generators have reached their technical limits (and thus allocating the remaining  $dP$  to the slack generator at the end of the time iteration), or a maximum number of iterations has been reached.

A flowchart representing this function is presented in Figure 4-4.

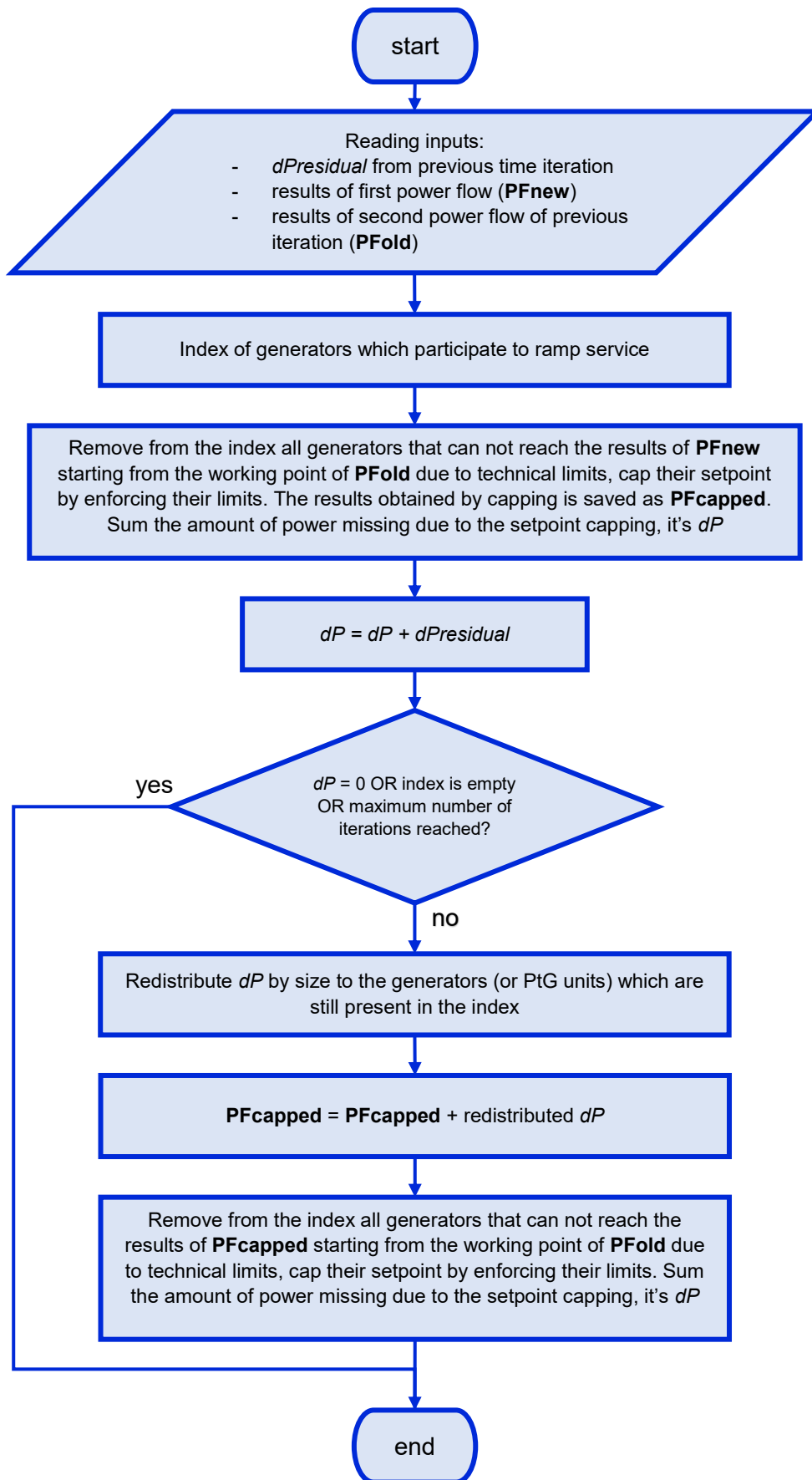


Figure 4-4: Flow chart of power redistribution function

### 4.2.3 Feasibility check function

The feasibility check function is a simple routine which checks for bus voltage limit and branch thermal limit violations, and if they are present it enables some warnings flags in the mpc. For buses, if there is no further violation, the flag is resetted without the use of any timer

This functionality is represented in Figure 4-5.

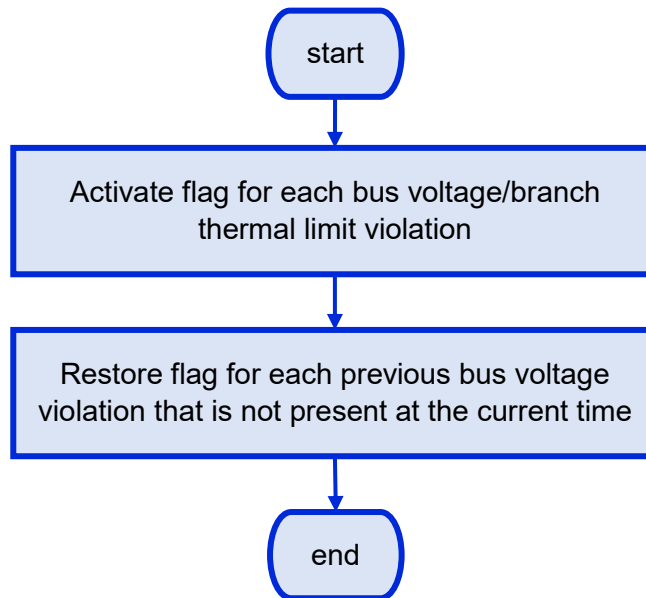


Figure 4-5: Flow chart of feasibility function

### 4.2.4 Protection function

This function takes advantage of the results of the warnings-and-timers system, and if a timer reaches a certain threshold contained in the mpc, the corresponding branch/bus gets opened. Protection functionality can be turned on or off by a control input variable. This function has been implemented for universal use of the algorithm, and it is not intended to be triggered in this case study, since it is not aimed to analyse emergency situations.

This function can be observed in Figure 4-6.

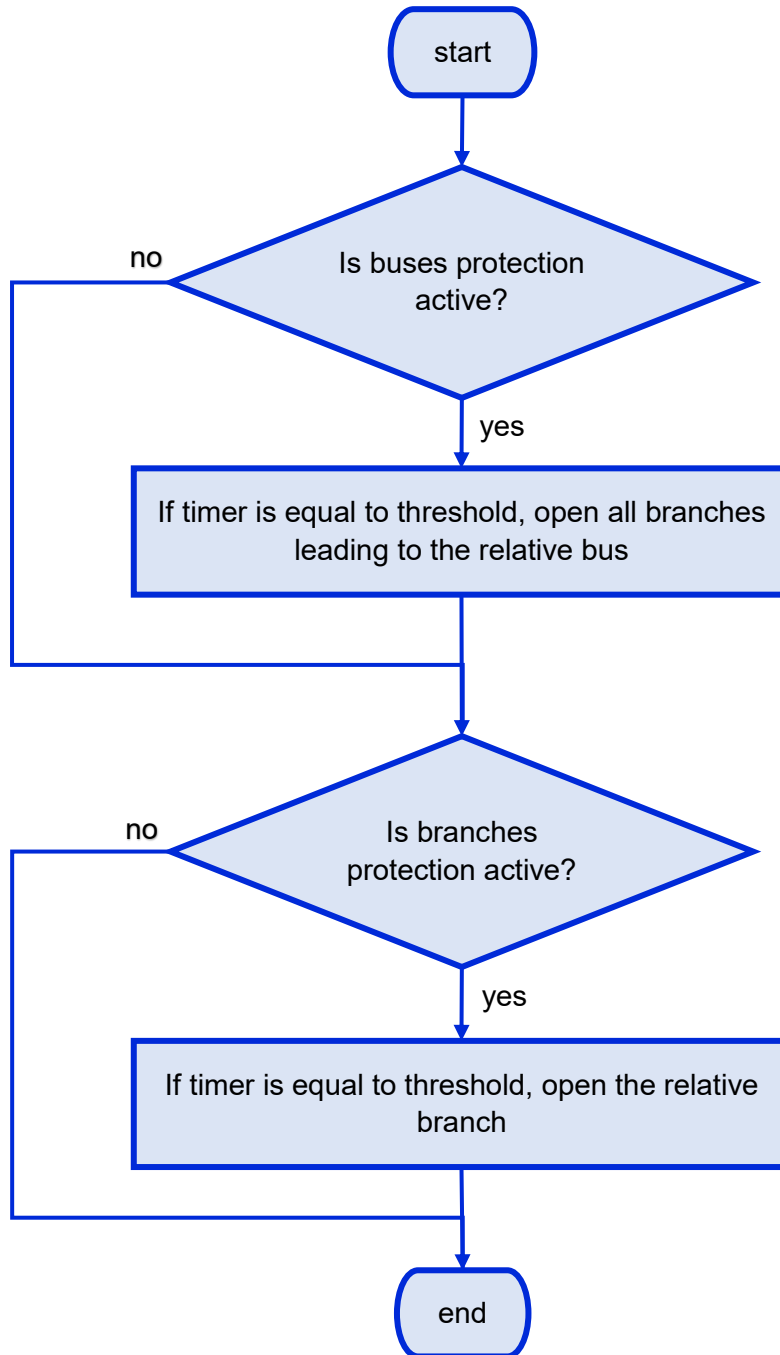


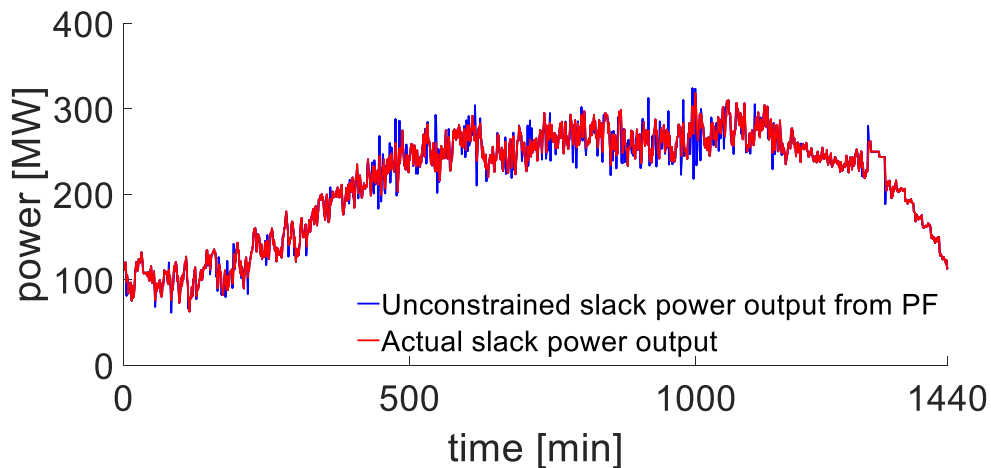
Figure 4-6: Flow chart of protection function

### 4.3 Results for the case #T1

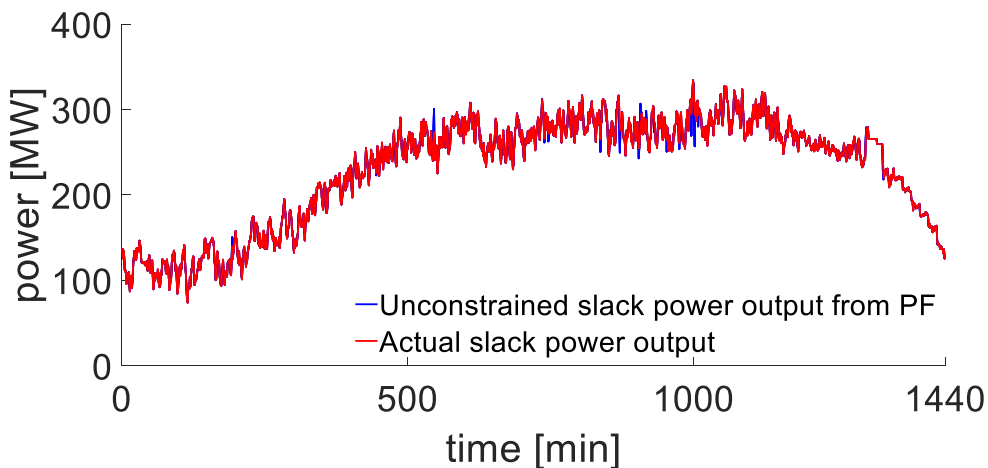
The network #T1 has been analysed by means of the algorithm presented in Section 4.2, that is essentially based on power flow algorithm. This implies that the largest generator is considered as the slack bus, and thus any excessive load variation (which cannot be face properly by any of the generators connected to the network) will be assigned to the slack bus itself. In that case, if the slack generator is not able to provide that amount of power, the total power generated is not equal to the total network load plus losses, therefore in a real system a frequency variation would be needed. It therefore is important to quantify the amount of  $dP$  and the effect that PtG can have over this amount of imbalance at slack bus.

As explained in Section 4.1, two wind scenarios have been considered, in order to show two different levels of RES penetration in the network.

The results of this simplified case study are reported in Figure 4-7 and Figure 4-8. These two figures show, for the two wind profiles considered, the actual power output of slack generator (obtained considering all of the technological constrains of the slack generator) as a red line, while the blue line represents the power output of slack generator that would be required in order not to have any frequency variation. Ideally the two lines would be indistinguishable, symptom of a well-balanced network.



a) Without PtG installed

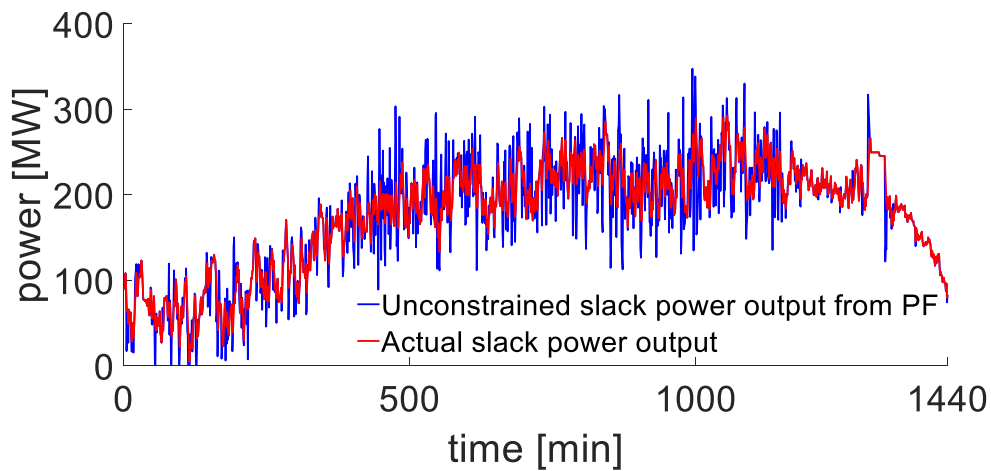


b) With PtG installed

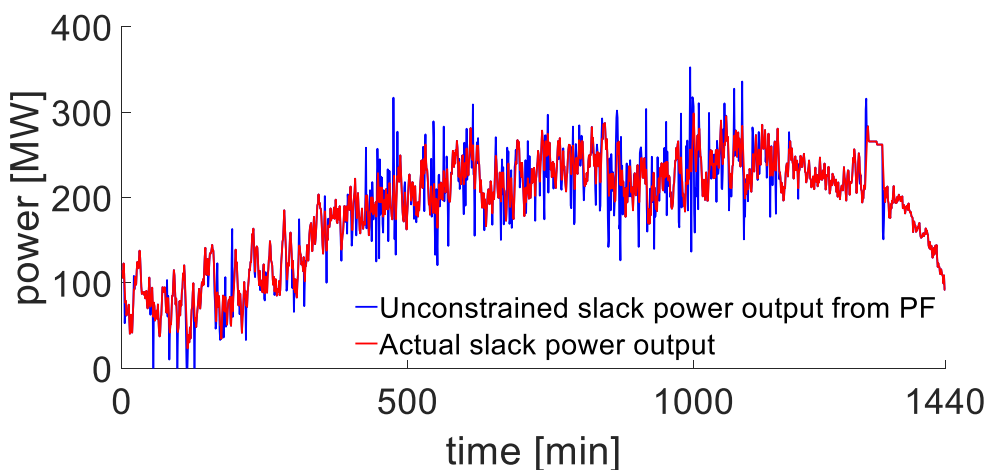
**Figure 4-7: Slack generator's power output, network #T1, 10% energy case**

The more the blue line deviates from the red line, the more often and more intensively power is drawn/injected from/to the kinetic energy reserve of conventional power plants. As it can be observed, in both cases the application of the PtG unit reduces both the peaks and the recurrence of these energy draws/injections. It is important to note that slack bus provides more power when

PtG is deployed, since PtG units aim to draw about 50% of their nominal power in order to provide ramp service as their best.



b) Without PtG installed



c) With PtG installed

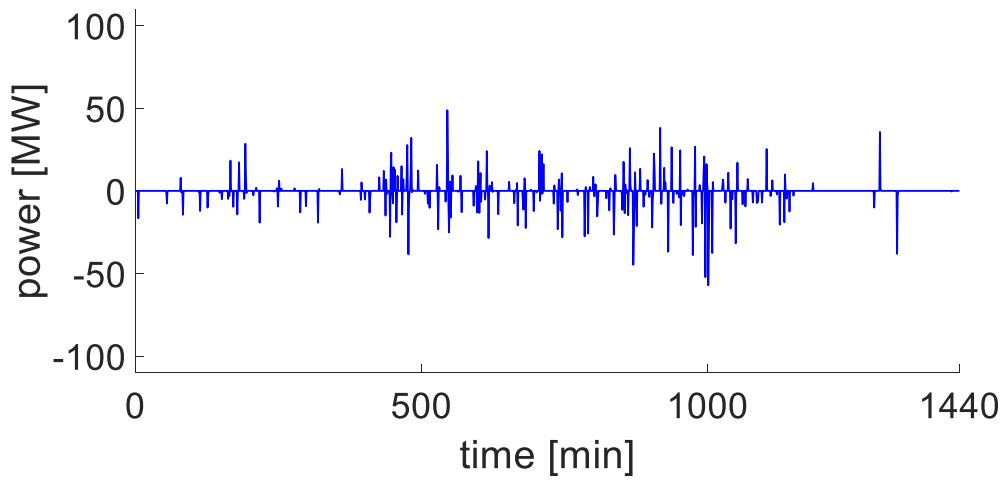
**Figure 4-8: Slack generator's power output, network #T1, 20% energy case**

Therefore,  $dP$  can be easily represented as difference of the two types of slack power output. Figure 4-9 and Figure 4-10 show this difference which represent the amount of power that the slack cannot provide, ad each minute: it is evident that the installation of a relatively small the PtG is able to help the stabilisation of the network, by reducing the variation of power that the slack has to face. Improvements can be seen as both reductions of the peaks of imbalance, and removal of the minor fluctuations.

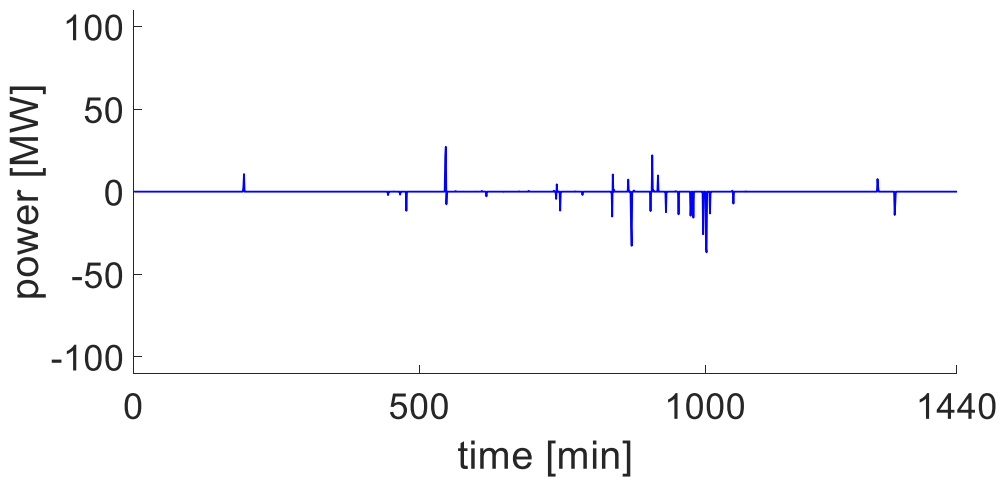
These results, summarized in Table 4-3, showed the goodness of the approach, which has been further developed for the network #T2 and #T3.

Table 4-3: Results for network #T1

Wind energy penetration	PtG status	RES imbalance					
		Energy [MWh]	Energy difference [%]	Duration [min]	Duration difference [%]	Peak [MW]	Peak difference [%]
10%	Off	46	-83%	246	-76%	57.1	-36%
	On	8		58		36.8	
20%	Off	288	-45%	687	-38%	119	-9%
	On	157		427		109	

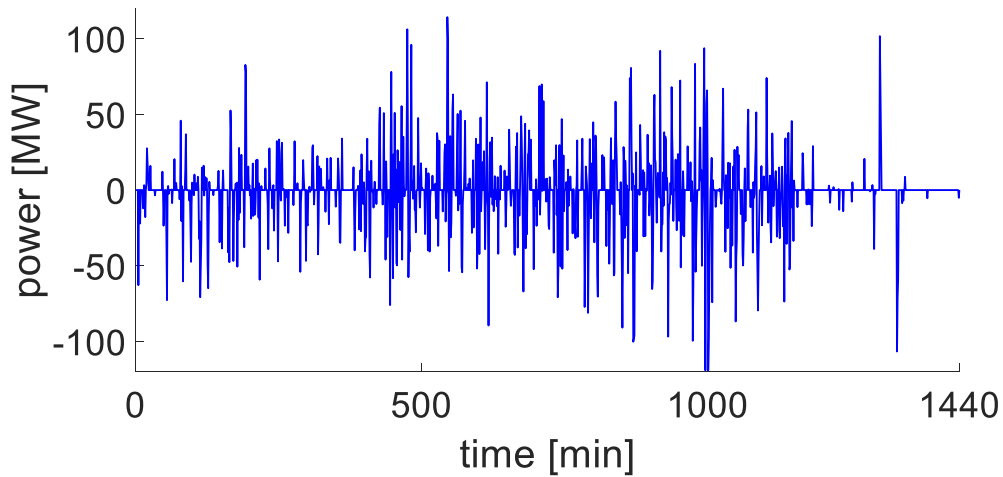


c) Without PtG installed

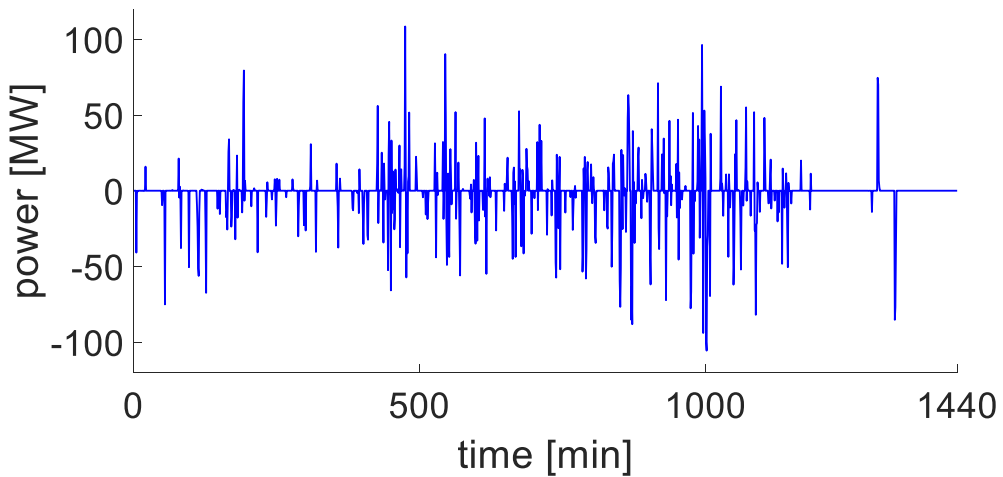


d) With PtG installed

Figure 4-9: Power imbalance at slack bus, network #T1, 10% energy case



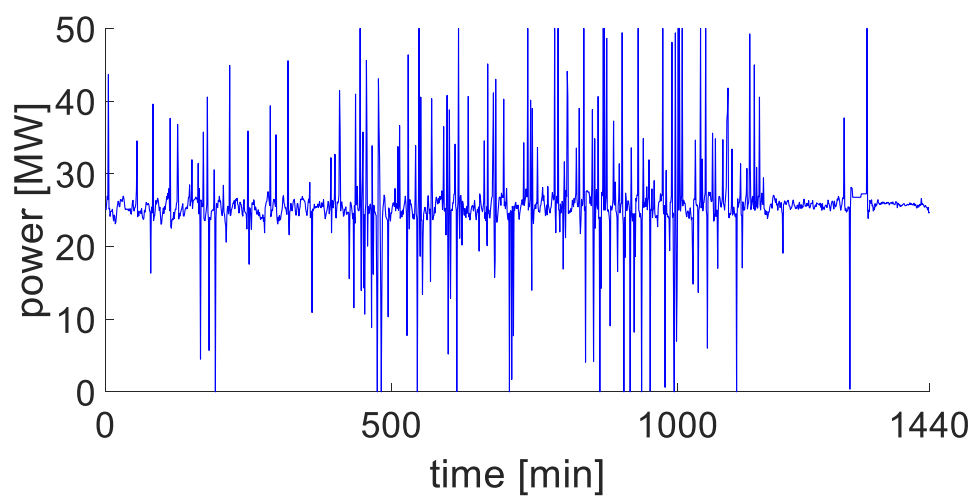
a) Without PtG installed



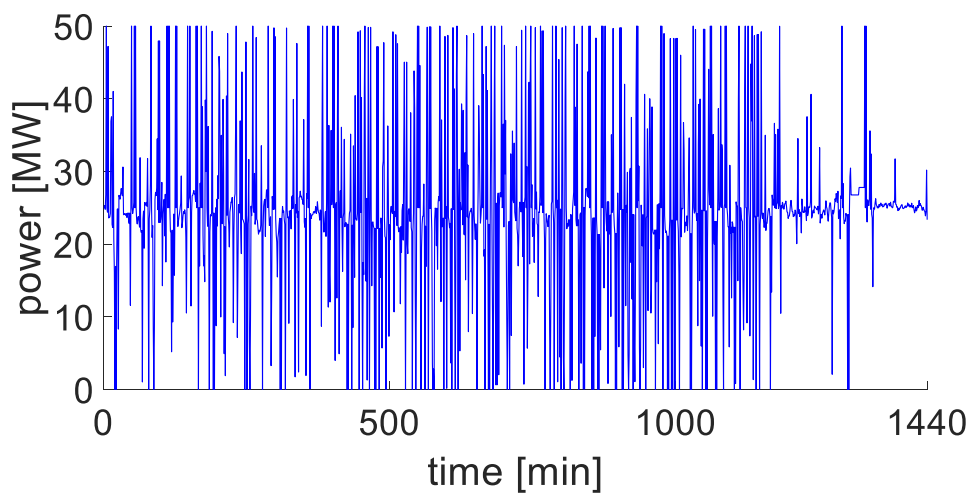
b) With PtG installed

**Figure 4-10: Power imbalance at slack bus, network #T1, 20% energy case**

In Figure 4-11 the power consumption of the PtG unit during the day in the two cases considered is shown. It is clear that a higher penetration scenario, as the 20% energy one, causes the PtG unit to deviate more often from its working point. In fact, PtG unit is set to consume at 50% of its nominal power (0.25 pu) when it is not offering any ramp service, and more deviation from the 0.25 pu level mean more engaging of the system stabilisation routine.



a) 10% wind energy case



b) 20% wind energy case

Figure 4-11: PtG power consumption in network #T1

## 5 Description of the European transmission networks

The transmission system represents the backbone of the entire electricity system and traditionally has been the link between the generation units (usually located far from cities) and the load centres. For matter of clearness, the simplified schematic of the entire electricity system is shown in Figure 5-1.

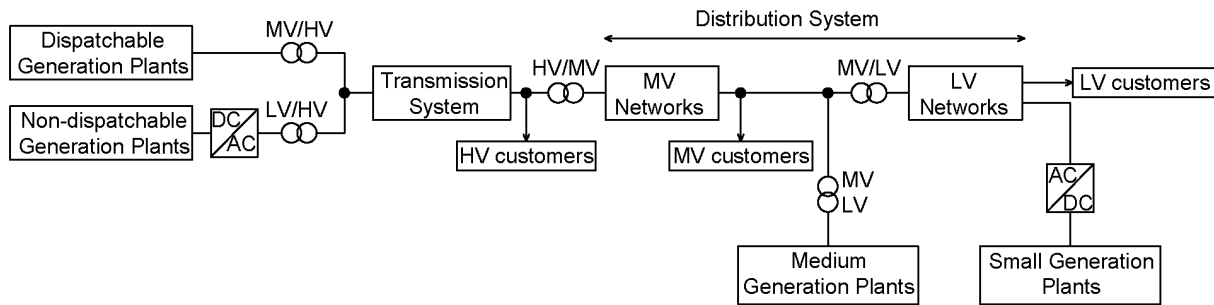


Figure 5-1: Representation of the electricity system [1]

In Europe, the number of nodes of the transmission network is about 6000, and it is operated with different level of voltages, as reported in Table 5-1.

Table 5-1: Number of nodes composing the EU transmission system [8]

Voltage $V_n$ [kV]	Number of Nodes
<220	327
$220 \leq V_n < 400$	3683
400	2592
>400	19
Total number of nodes	6621

The detailed study of the integration of PtG into a real transmission network needs the following features:

1. **Proper description of the transmission network:** this means the implementation of realistic transmission system, in terms of physical parameters (e.g., resistance, reactance, length, line thermal limits and so on)
2. **Geographical coverage:** in the usual load flow analysis, the geographical coverage is not so much important. However, by handling with a new technology which aims to support the integration of RES in Europe, the geographical information is necessary
3. **Proper values of generation and loads:** the mix of generation and loads regarding the next decades (e.g., 2030 and 2040)
4. **Proper economic data:** the operational study with optimization needs more information in order to recreate the electricity markets

### 5.1 Existing models of the European transmission system

The most updated model of the European transmission system is the one related to the Ten Years Network Development Plan (TYNDP) 2016 [8], that is the so called "Stum Model". Unfortunately, the model does not report any information regarding the geographical location of the different node, so cannot be used due to the lack of the point 2 of the above-mentioned feature list.

A further source is [9], presented in the paper [10]: the model assumed value of the transmission capacity linked to the voltage level of the line. However, the website does not report any information about the model itself.

Due to the aim of this work, the approach followed in the project Store&Go was to merge different sources, for creating a simplified model of the European transmission system taking into account the characteristics listed above. For this reason, three different databases were merged:

- 1) UCTE model of the European transmission network (internal source of PoliTo), reporting the thermal limits of the lines (no information about neither the geographical coordination nor the types of generation)
- 2) Bialek model from PowerWorld® [11], reporting information about the types of generators installed (no information about neither the geographical coordination nor the thermal limits)
- 3) Geographical coordinates from the Bialek model stored in the repository [12] [13] (no complete information about thermal limits)

The matching of the nodes among the three model was possible thanks to the partial information of the contained in all the model, for example the thermal limits of the transnational connection and the same node. This approach led to obtain the Network #T2, explained in Section 5.2.

Another source can be found in the Zenodo repository [12], and it was mentioned as source by [14]. This database has two drawbacks: it does not report the load for the nodes, and it has not any information about the transfer capacity. The first problem was solved in [14] by dividing the hourly load of all the EU countries based on the density of population at NUTS3 level. The same paper uses clustering technics for reducing the number of nodes by maintaining the main capacity corridor. However, the transmission limits (fully described in [8]) is not present in the repository [12], that thus cannot be used alone. Furthermore, the paper in any case is not taking into account the grid topology and the electrical distance among nodes, fundamental for properly studying the operation of the system.

On May 2018, a new and updated release of the model stored in the repository [12] was uploaded: this model can be found at the weblink [15] and in the repository [16]. The model has been validated in [17]: this model considers as thermal capacity the one obtained by considering, for every level of voltage, a defined type of conductor. The model allows as well to simplify the network, making an equivalent composed of 256 nodes.

Thanks to the presence of the code architecture, the input file has been also adapted for the network reported in [15], by creating the model #T3, further described in Section 5.3.

## 5.2 Description of the Network #T2

The Network #T2 aims to be representative of the entire European transmission system. The network is based on data of Union for the Coordination of the Transmission of Electricity (UCTE) [18], which was the former name of the current European Network of Transmission System Operators for Electricity (ENTSO-E) [19]. This model is the simplified version of the European transmission network<sup>3</sup>.

---

<sup>3</sup> The evolution of this model led to the Bialek model ([11]), whose current version does not provide any information regarding the thermal limits of the network.

The information regarding the network are summarised in Table 5-2.: Information about the Network #T2

**Table 5-2: Information about the Network #T2**

<b>Buses</b>	<b>Branches</b>	<b>Generators</b>	<b>Load [GW]</b>
1254	1944	378	~250

This model covers mostly of the continental Europe, and is representative of the following 17 European countries:

Austria (AT), Belgium (BE), Croatia (HR), Czech Republic (CZ), Denmark (DK), France (FR), Germany (GE), Hungary (HU), Italy (IT), Luxemburg (LU), Netherlands (NL), Poland (PL), Portugal (PT), Slovakia (SK), Slovenia (SI), Spain (SP) and Switzerland (CH).

The graphical representation of the geographical distribution of the model is depicted in Figure 5-2. Despite having the information about buses coordinates, there was not any reference to the corresponding NUTS 2 (Nomenclature des Unités Territoriales Statistiques) region. Therefore, an association has been made by the means described in the Appendix D, along additional information about the NUTS system.



**Figure 5-2: Representation of the model implemented [11]**

The types of generators considered are the following:

- Coal
- Distillate fuel oil
- Fuel oil
- Geothermal
- Hydro
- Lignite
- Import
- Natural gas
- Solar
- Waste
- Wind
- Wood

- Nuclear

A solar generator and a wind power plant has been assigned to each bus, so of the 2886 generators present, 2508 are wind and solar generators. Generators' costs were present in the source data, and when it was not a similar price to the nearest same type generator has been assigned.

### 5.3 Description of the Network #T3

The network #T3 is composed of 256 nodes [17]: it has been created by applying a k-means clustering technique at the European Network (over 6000 nodes) which was obtained by analysing the European Network Map [20]: this simplified network is a 380kV equivalent network, connecting the different nodes, which fall in their own cluster. The capacity among the clusters depend on the connection existing among them: due to the fact that the model considers also lower voltage level (220 kV and 300 kV), the equivalent capacities consider also those connection. Due to the absence of information regarding the real lines composing the original network, a simplification has been carried out, i.e., defined lines geometries have been considered, as shown in Table 5-3 [21].

**Table 5-3: Properties transmission lines**

Voltage [kV]	Current limit [A]	Power limit [MVA]
220	1290	492
300	1935	1005
380	2580	1698

The resulting network's summary is presented in

Table 5-4, whereas the representation of the georeferenced model is shown in Figure 5-3.

**Table 5-4: Information about the Network #T3**

Buses	Branches	DC lines	Generators	Load [GW]
257	460	24	1448	~360

The network #T3 adds the 17 countries to the ones already present in network #T2, for a total of 33 countries, covering all the ENTSOE countries:

Albania (AL), Austria (AT), Bosnia and Herzegovina (BA), Belgium (BE), Bulgaria (BG), Estonia (EE), Finland (FI), Croatia (HR), Czech Republic (CZ), Denmark (DK), France (FR), Germany (GE), Great Britain (GB), Greece (GR), Hungary (HU), Ireland (IE), Italy (IT), Latvia (LV), Lithuania (LT), Luxemburg (LU), Montenegro (ME), The former Yugoslav Republic of Macedonia (MK), Netherlands (NL), Norway (NO), Poland (PL), Portugal (PT), Romania (RO), Serbia (RS), Slovakia (SK), Slovenia (SI), Spain (SP), Sweden (SE) and Switzerland (CH).

The load profiles used are referred to the year 2013: the share of load for every cluster has been obtained by considering a combination between the population and Gross Domestic Product (GDP) of each cluster.

The generation in the original dataset is referred to year 2013: at every node of the network more than one type of generator is connected. The types of generators considered in the model have been adapted at the types of generators requested by the Store&Go project. The types of generators considered are the following:

- Biomass
- Coal
- Geothermal
- Lignite
- Nuclear
- CCGT
- OCGT
- Oil
- Wind onshore
- Wind offshore
- Solar
- Run on River (ROR) power plant
- Hydro-pump

Hourly power profiles are also available for Run on River power plants. Generators' costs are assigned based on generation's type, since the generators of the network are aggregates of real ones. Both generation and loads have been updated according to current and future scenarios, as shown in Sections 5.6, 5.7 and 5.8.

The model also takes into account the presence of DC link existing in Europe, as it can be observed in Figure 5-3.

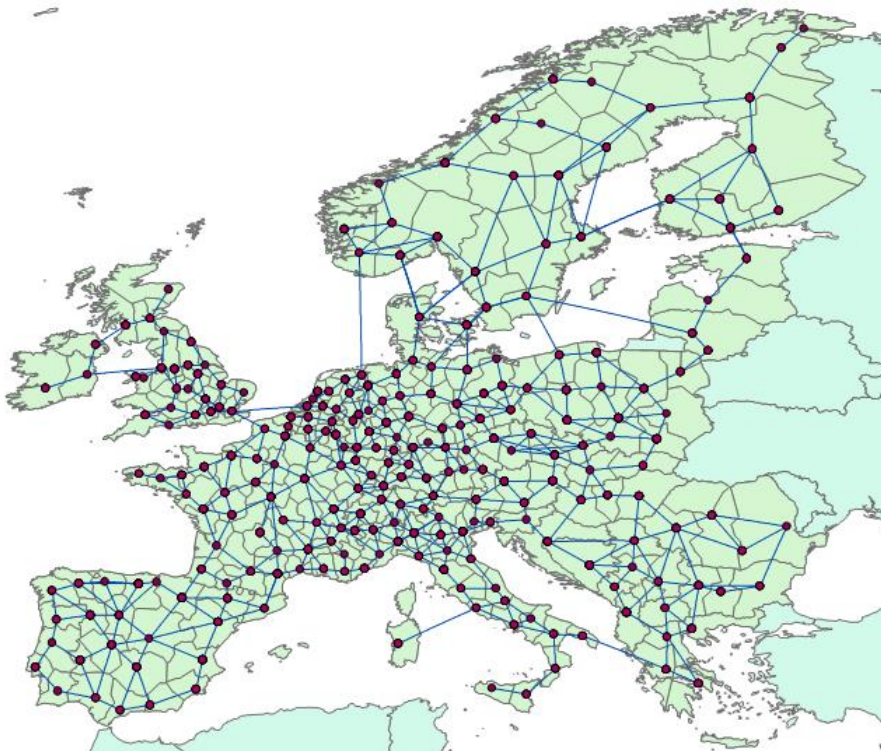


Figure 5-3: Representation of the network #T3

## 5.4 PV production for the European case

The variance of PV production within space and time brings the need to adequately represent PV production in our study case. This is the reason why a proper network model including georeferenced bus data was needed. This information allows to reach a good level of fidelity for both the installed capacity and the generation profile for each bus.

The installed PV capacity data has been gathered from EMHIRES dataset [22], provided by Strategic Energy Technologies Information System (SETIS). EMHIRES dataset provide information about PV installed capacity at country level, by bidding zone, at NUTS 1 level and at NUTS 2 level. By assigning each bus to the corresponding NUTS 2 region it is possible to reach the highest level of spatial resolution available with this dataset.

EMHIRES dataset provide also provide 30 years of hourly production levels, for each one of the previous spatial resolutions. However, this information is enough for hourly analyses only, so another source is needed in order to study the network at a higher temporal resolution. This has been achieved by using Bright's solar model [23] [24]: this model, at given points coordinates, simulates a yearly irradiance profile with a temporal resolution of one minute, that can be averaged according to the user's need.

PV profiles for each bus are then calculated from the irradiance profiles and the given installed PV capacity. Thanks to the formulation reported in Appendix B, the power profiles are calculated [25].

## 5.5 Wind production for the European case

Wind generation has the property to be less distributed than PV generation, and having fewer plants to keep track of brings a high level of fidelity. Since EMHIRES dataset [22] provides for the wind generation the same kind of information as the PV generation, it has also been used in this case.

As for the PV, another source is needed in order to reach a higher temporal resolution. Differently from the irradiance, wind speed cannot be assumed easily, since it highly depends from seasonality, turbine height and ground conformation. Moreover, each turbine model has its unique power characteristic. No reliable data with high spatial and temporal resolution has been found, so a different approach was needed.

Since capacities and hourly profiles were available from EMHIRES dataset, the missing information was wind variability. By analysing a year worth of data from a real wind farm, a per unit profile has been extracted, with a temporal resolution of ten minutes. In fact, as presented in sharper details in Appendix C, wind variance has been characterized statistically through clustering in order to elaborate a plausible profile for each bus. This way, the variability information from the real wind farm is kept among the different created profiles, emulating wind effect on a real network.

This approach has been validated through an autocorrelation check, by comparing the real data, the clustering approach, and an approach which randomize the variance profile. Autocorrelation for profiles visible in Figure 5-4 can be observed in Figure 5-5, which shows the goodness of the approach.

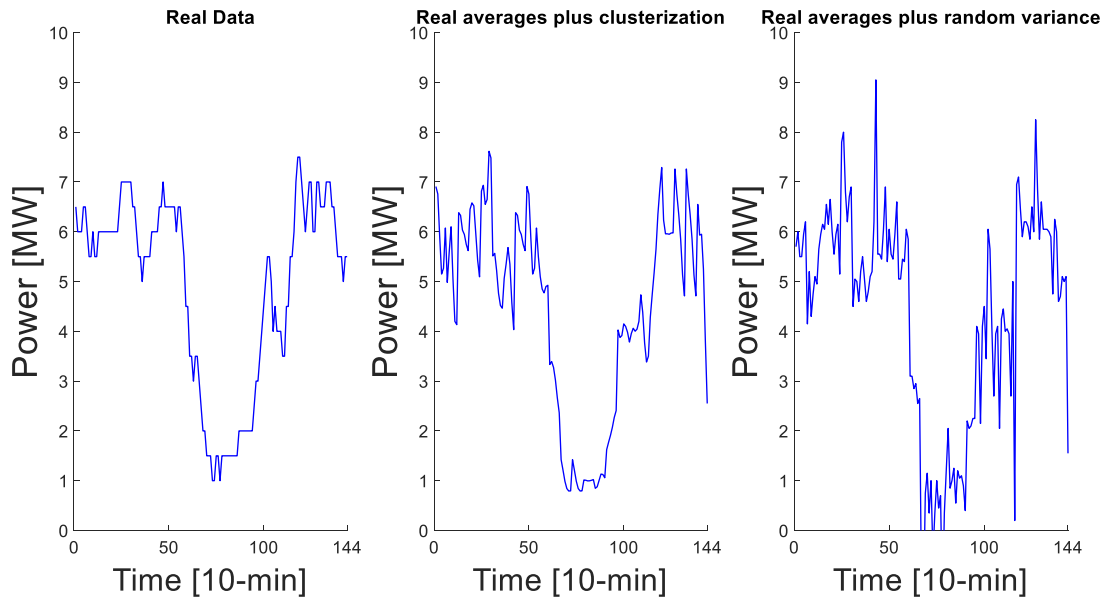


Figure 5-4: Profiles used for autocorrelation test

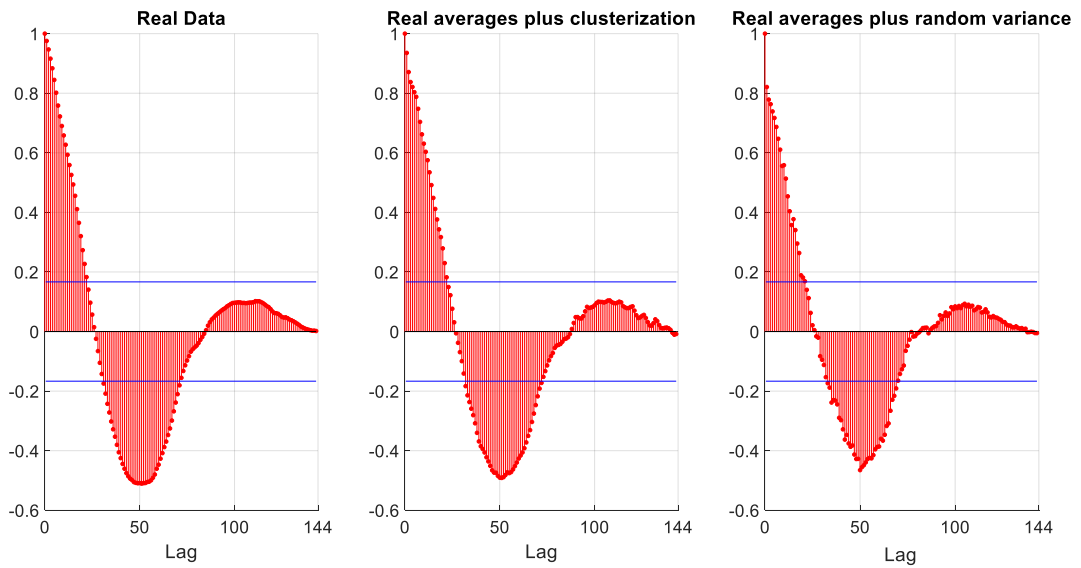


Figure 5-5: Autocorrelation

## 5.6 Load profiles for the European case

The values of loads and their variation with the time have been updated on the basis of the 2017 data provided by [26], for the countries considered. The power statistics offers yearly historical data for power consumption, provided with a temporal resolution of one hour, and country level as spatial resolution. The country-level load has been distributed within the buses of the same country by the nominal load of each bus, provided within the networks' data. Eventual variations of load values from these profiles are not considered in this work. An example of the yearly load profile of the entire #T3 network is shown in Figure 5-6.

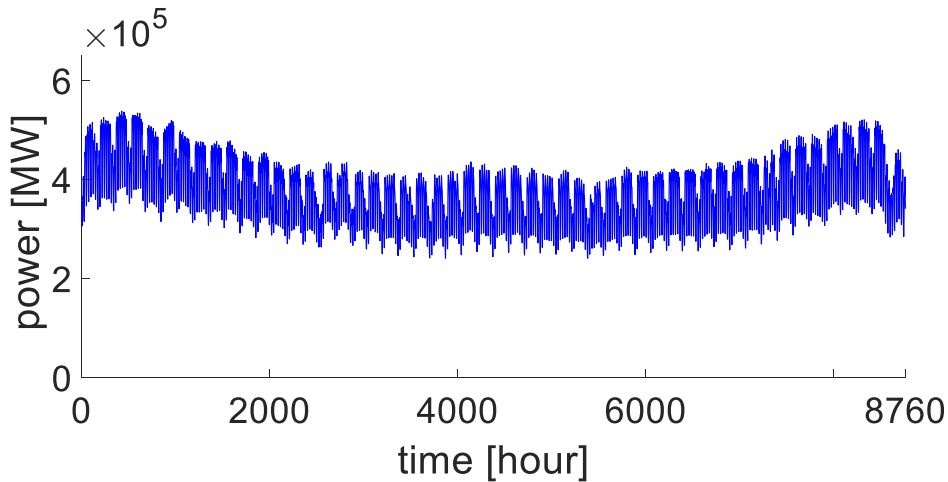


Figure 5-6: Yearly load profile for 2017 scenario, whole #T3 network

## 5.7 Generation scenario for the European case

As for the load profiles, generation capacity of each network has been updated to match 2017 data [27]. The number of generators and their positioning has been kept the same as in networks' data, and then within each country, for each generator's type, the capacity has been scaled. Minimum stable power output, and ramp rate values has been considered for each type of generator as showed in Table 5-5. The data has been collected from [27]. Note that the ramp rate value for hydro generators is not the maximum technical possible, but a value for ordinary operation has been considered, since the model does not aim to recreate emergency situations.

Table 5-5: Generators data

Generator type	Minimum stable generation [% P <sub>n</sub> ]	Ramp rate [% P <sub>n</sub> /min]
Biomass	43%	3%
CCGT	30%	10%
Coal	38%	3%
Geothermal	20%	30%
Hydro turbine	20%	12.5%
Lignite	43%	3%
Nuclear	45%	7%
OCGT	28%	10%
Oil	35%	3%

## 5.8 Future scenarios for the European case

Beyond the most recent historical data, various scenarios can be used in the model. The selection of the scenario implies the choice of the desired load profile and the scaled-up baseline generation, based on the data obtained by [27]. The forecasts are part of the ENTSO-E Ten-Year Network Development Plan (TYNDP), which provides a detailed overview of possible European energy futures up to 2040.

In particular the algorithms are able to handle the following baseline scenarios:

- **2025\_BE Best Estimate:** it represents a medium-term scenario which is on track to meet the decarbonization targets set in place by EU for 2030. It is based on TSO perspective and on following all national and European current regulations.
- **2030\_DG Distributed Generation:** it represents a prosumer-centric development, in which the end user technologies will be the focus. An high PV, batteries, and electric vehicles penetration is considered, and the use of smart home devices and dual fuel appliances, which can allow prosumers to switch energy following market conditions, is a reality.
- **2030\_EUCO European Council:** using the EU reference Scenario 2016 as a base, it models the achievement of the 2030 climate and energy targets agreed by the European Council in 2014. Since its similarities, this scenario replaced the 2030\_GCA within the TYNDP framework
- **2030\_ST Sustainable Transition:** it summarizes a quick, yet sustainable, CO<sub>2</sub> reduction by replacing coal and lignite power plants with gas ones. Oil use in heavy transport is also displaced by gas. This particular focus causes a slower electrification of heat and transports but allows to reach the EU goal of 80-95% CO<sub>2</sub> reduction in 2050.
- **2040\_DG Distributed Generation:** see 2030\_DG.
- **2040\_GCA Global Climate Action:** opposed to ST scenarios, full speed decarbonization is the global objective, achieved by large-scale renewables and nuclear power plants deployment. Electrification of residential and commercial heat leads to an important decrease of gas demand in this sector, and electrification is applied also to transports. The research for better energy efficiency is applied to all the sectors, and PtG production reaches the biggest development in comparison to the other scenarios.
- **2040\_ST Sustainable Transition:** see 2040\_ST.

Each one of these scenarios offers the possibility to choose between three load time-series, built to represent three different climatic condition, i.e.:

- **1982** for dry conditions
- **1984** for normal conditions
- **2007** for wet conditions

A summary of the scenarios is presented in Figure 5-7 [28]. For more information about these scenarios, please refer to [27]. Examples of the yearly load profile of the total #T3 network for 2030DG and 2040GCA scenarios are shown in Figure 5-8 and Figure 5-9.

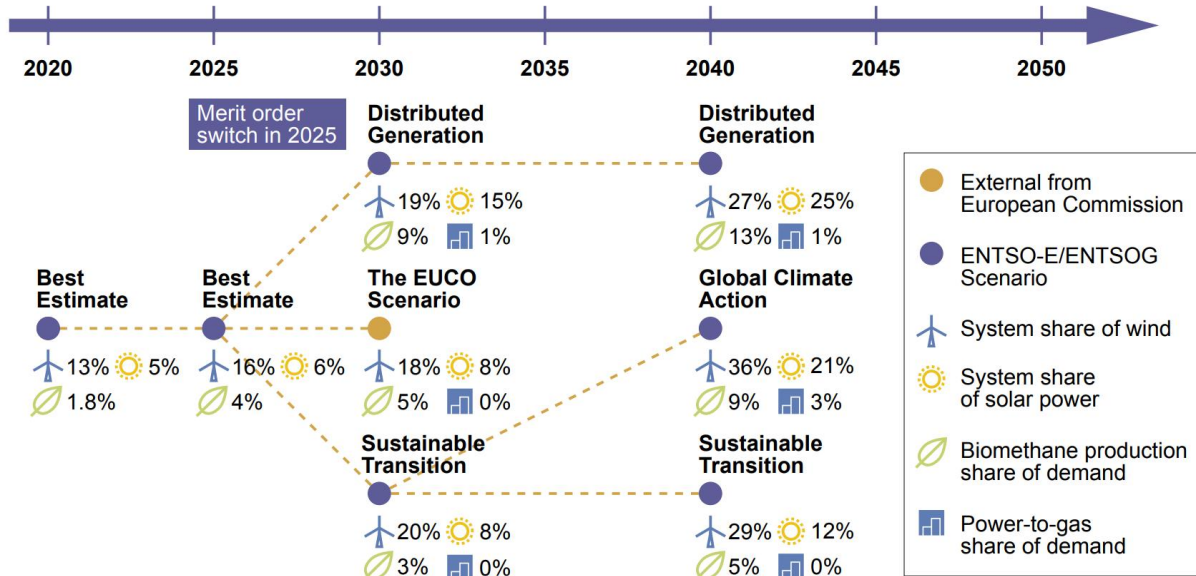


Figure 5-7: The scenario building framework for TYNDP 2018 [28]

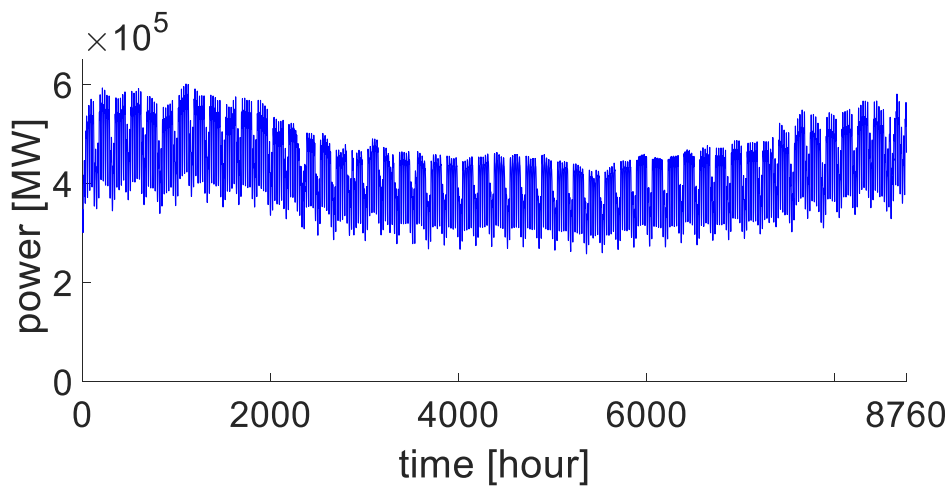


Figure 5-8: Yearly load profile for 2030DG scenario, 1984 climatic conditions, whole #T3 network

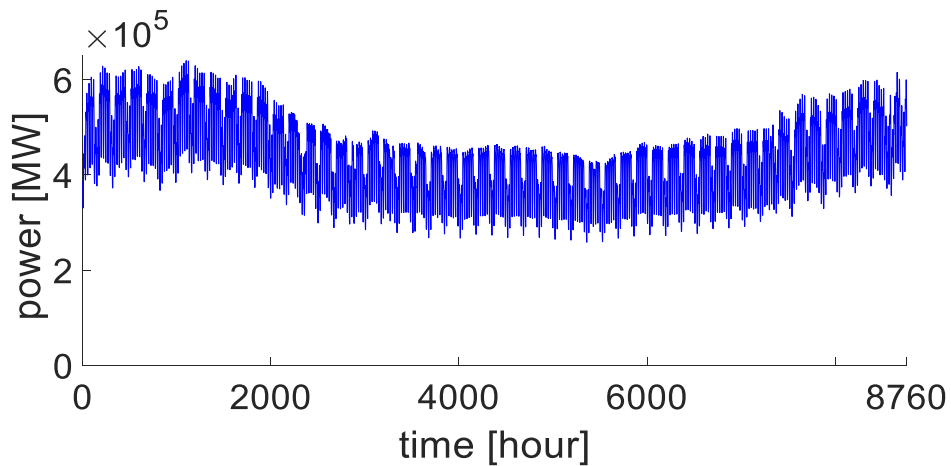


Figure 5-9: Yearly load profile for 2040GCA scenario, 1984 climatic conditions, whole #T3 network

## 6 Description of the algorithm for the case studies #T2 and #T3

### 6.1 Main characteristics

The algorithm is composed of two main parts, which run two optimizations:

- the first one, based on expected values of load and non-dispatchable generation (emulating a day-ahead market, DAM),
- the latter one based on the actual values of PV and wind generation (emulating a real time market).

By comparing the results of the two markets it is possible to evaluate the impact of the variability of PV and wind on the system, and thus, inserting PtG units, also the effect that these units can have on the electrical system.

PtG units are modelled within Matpower as dispatchable loads, which are modelled as negative generators. Within the day-ahead market they are considered as constant loads, working at a fixed percentage of their rated power.

As explained in Section 3.3, the algorithm is based on Matpower [6] since this choice allows to take advantage of Matlab's flexibility. The model does not account for frequency variation and reactive power, since it relies on DC power flow (for reducing the computational time).

Moreover, differently from the algorithm presented in Section 4.2, optimal power flow (OPF) is used, instead of power flow. The consequence of this choice is that generators do not need a generation profile (since the level of production is dictated by their costs, and market logic) and generators limits are already enforced by OPF, leaving only the ramp limit to be managed externally. Finally, the resulting solution is the network configuration providing the lowest possible cost.

Despite OPF being an obvious choice, which should have been used from the beginning with the case #T1, it requires generators costs as additional data. The operational study was the first goal of the research, and only later network's optimization has been requested by STORE&GO. A remnant of this change is a version of network #T2 solved with operational method, not presented in this thesis.

### 6.2 Description of the input data

Both algorithms contain a similar input section, in which the Matpower case-file (called mpc) is loaded. A mpc is a structure that gathers all the necessary network parameters.

The main fields contain all the information regarding:

- Buses (location, load value)
- AC lines (starting and ending nodes, capacity, number of equivalent lines in parallel)
- Generators (type, status, size, ramp up and ramp down, location, marginal cost, minimum power)
- DC lines (starting and ending nodes, capacity)

As explained in Section 3.3, additional columns have been added into the mpc in order to store more information without interfering with Matpower's functionality.

Other variables are needed, in order to store the necessary time-dependent data that at each iteration will be loaded into the mpc. Load profiles for each scenario are loaded from previously created mat files, in order to reduce computational times. They are created by redistributing the available country-level load profiles among buses of the same country, using ratios present in the network data. Profiles for run-on-river (ror) hydro plants were also available and loaded in the same way.

Irradiance profiles are loaded from a mat file, but not using the usual *load* function, which loads the file contents from the memory device to RAM: being the file hundreds of megabytes, it would cause additional computational time. The mat file instead has been accessed using the *matfile* function, which allows to read the variables straight from the memory device. This has been crucial, since only a small part of the irradiance matrix is needed, given a certain date which has been selected as scenario. Generated power profiles are then calculated as explained in Section 5.4.

Wind profiles are instead calculated on the spot by the algorithm. Only average 1-hour profiles and clusters of variances are loaded from mat files, and then by using the provided probability weights, for each value of average profiles and for each wind generator, one variance profile is extracted and applied. Repeatability of the tests is guaranteed by imposing randomizer's seed.

Generation scenario is applied by comparing the 2013 installed capacity for each country and for each generator type with the corresponding capacity from the selected scenario. The result is a matrix, with countries number in one direction and generators' type number in the other, containing multipliers. By applying the corresponding multiplier to each generator, the original 2013 installed capacity is scaled up or down to the desired scenario level.

PtG profiles are easily created, since in this work their goal is to stabilize the network. In fact, they are supposed to work at the power level which grants the possibility to increase or decrease by the same amount the power absorption. This value is the average value between its nominal power and its minimum stable power consumption. For example, if a PtG has a  $P_{MIN}$  equal to 20% of its nominal power, its desired load profile is 60% of its nominal power, granting the possibility to modify its power consumption by  $\pm 40\%$  of its nominal power.

### 6.3 Limitations

From the time calculation point of view, the algorithm performance is strongly depending by the DC Unit De-commitment OPF (DUOPF) implemented in Matpower, which is used for the solution of the DAM. This algorithm calculates the cost of keeping generators online at their minimum working point and considers it when evaluating the OPF solution.

Matpower DUOPF routine is a basic deterministic routine that changes generators' status with a logic similar to the one of the branch exchange method. As stated by [6], the routine is not efficient as the number of generators increases. The original deterministic logic has been modified to include a basic heuristic, which excludes some of the most expansive generators at the minimum power output. By doing this the computational time required decreases significantly, from  $\sim 1500$  seconds circa down to  $\sim 500$  seconds for network #T3.

Another example can show how much DUOPF computational time is directly linked to the number of generators: in network #T3 a single execution of DUOPF takes about 400 to 600 seconds, while in network #T2, which has less generators, computational times are from 40 to 60 seconds for a single execution.

Despite this inconvenient, the split nature of the implemented algorithm allows to solve multiple IDM conditions (for example, with different number of PtG) given only one DAM calculation. Security and emergency problems are not taken in account in the current implementation.

## 6.4 Execution of the DAM algorithm

As shown in Figure 6-1, the DAM is modelled as loop, in which each iteration represents an hour. For each iteration:

- A function updates the time and all the time related variables, for example the nodal loads for the current hour, and the current PV and wind generation forecasts for the hour.
- Then a DUOPF is performed, and it provides the list of generators that are required online in order to supply optimally the load in that iteration, without violating any generator or branch constrain.
- This list of online generators is saved and assigned to the current hour.
- Since it is expected for the RES production to have variations in the intra-day market, it is necessary to add more generators online in order to provide security/reserve /ramp services. These generators are chosen among the cheapest that could not participate to the day-ahead market, and the added capacity depends on two factors, seasonality and time.
- After adding additional generators, a DCOPF is performed, in order to obtain the market clearance for this iteration. The current output is saved, and the iteration ends and another iteration begins

When all the hours of the day have been processed, the day-ahead market algorithm ends.

Additional generators are necessary since there are two time intervals in which the ramp service is highly required: the first is at sunrise when PV production rapidly increases, whereas the second one is at sunset, when PV production rapidly decreases. This is needed since in those hours the averages at five to fifteen minutes do not oscillate around the hourly averaged value, but steadily increase or decrease. Because of this, more generators are needed for ramp service. Seasonality changes the time when these two conditions occur, and this affects also the number of generators required to change along the year.

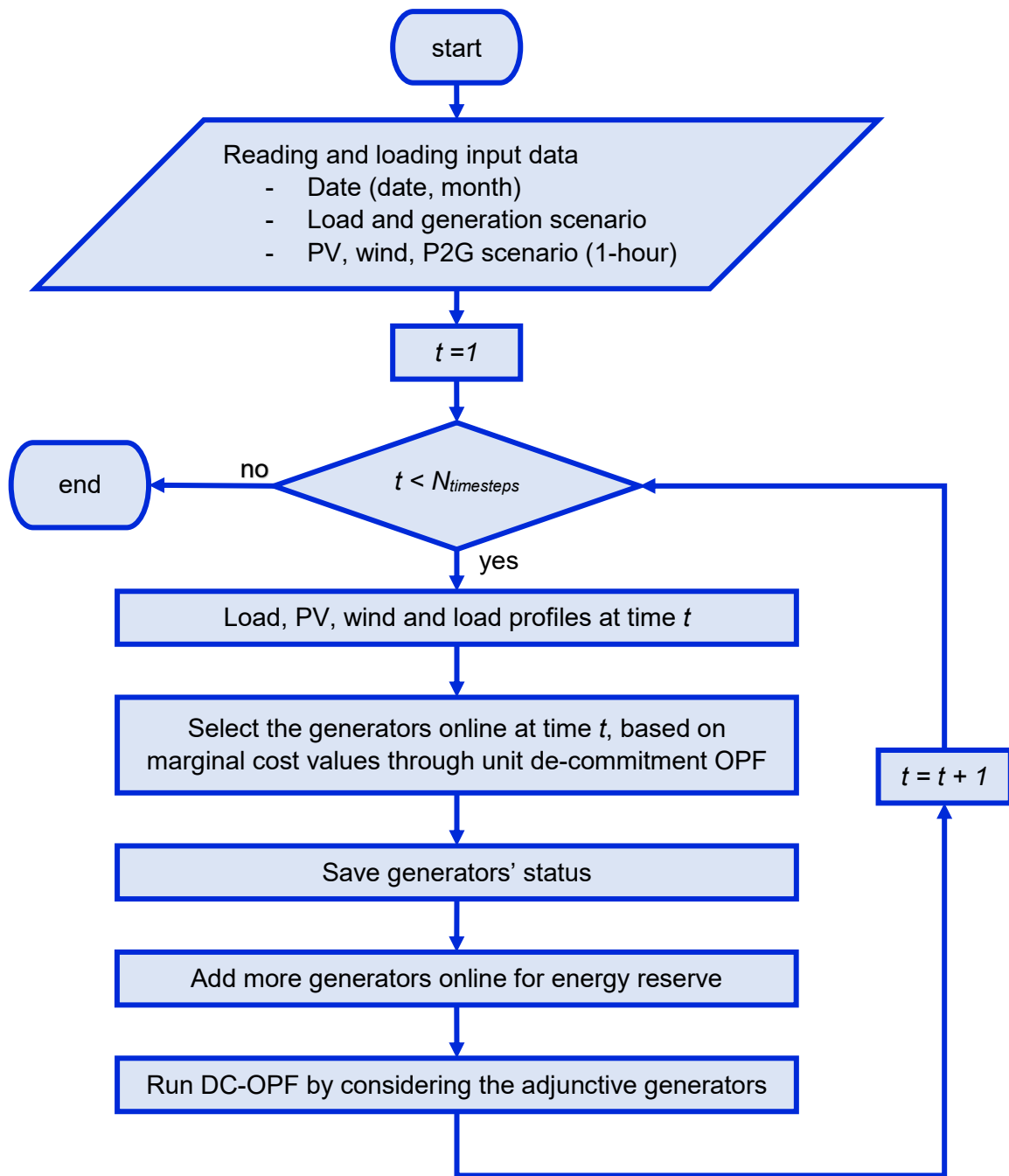


Figure 6-1: Flow chart describing the DAM

## 6.5 Execution of the ID (or real time) algorithm

The real time market flowchart is shown in Figure 6-2. The real time market algorithm, as previously stated, shares most of the input part with the one emulating the day-ahead market. Moreover, it receives as input the status of the generators for every hour from the day-ahead market. There is an hourly time loop that updates every variable that changes hourly (DA time loop), and, within each hour-iteration, another time loop represents the user defined time steps within the hour (ID time loop), e.g., twelve five-minutes time steps, six ten-minutes time steps, four fifteen-minutes time steps.

Within each ID time loop, the PV and wind profiles are averaged according to the user time-step, and the difference of the actual renewable power with respect to the hourly one is calculated for each PV/wind generator. Part of this difference between the actual ID generation and the DA forecast, can be assigned to every PtG unit as setpoint. If this quantity is positive it means that currently there is more PV/wind generation than forecasted, then PtG units can increase their power absorption. Vice versa, if this quantity is negative, there is less PV/wind generation than forecasted, therefore PtG units will have to lower their power absorption in order to help the network. This quantity effectively mirrors the concept of  $dP$  present in case #T1.

When PtG units' setpoints for the current ID time step are known, PtG model is launched for each PtG unit, as explained in more detail in Section 6.6. The outputs of the model executions are the responses of PtG units in the current minute which equals as load values for dispatchable loads in Matpower modelling.

Since Matpower's OPF offers a static resolution of the network, the ramp constrains are enforced through the maximum and minimum power constrains of generators. In each iteration the generation results of the previous time iteration are taken in account, and the maximum/minimum power constrains are updated as the previous results plus/minus the ramp rate applied to the user-defined time step for ID market.

A DCOPF is performed, and the output is saved as the results for the current iteration, ending the iteration.

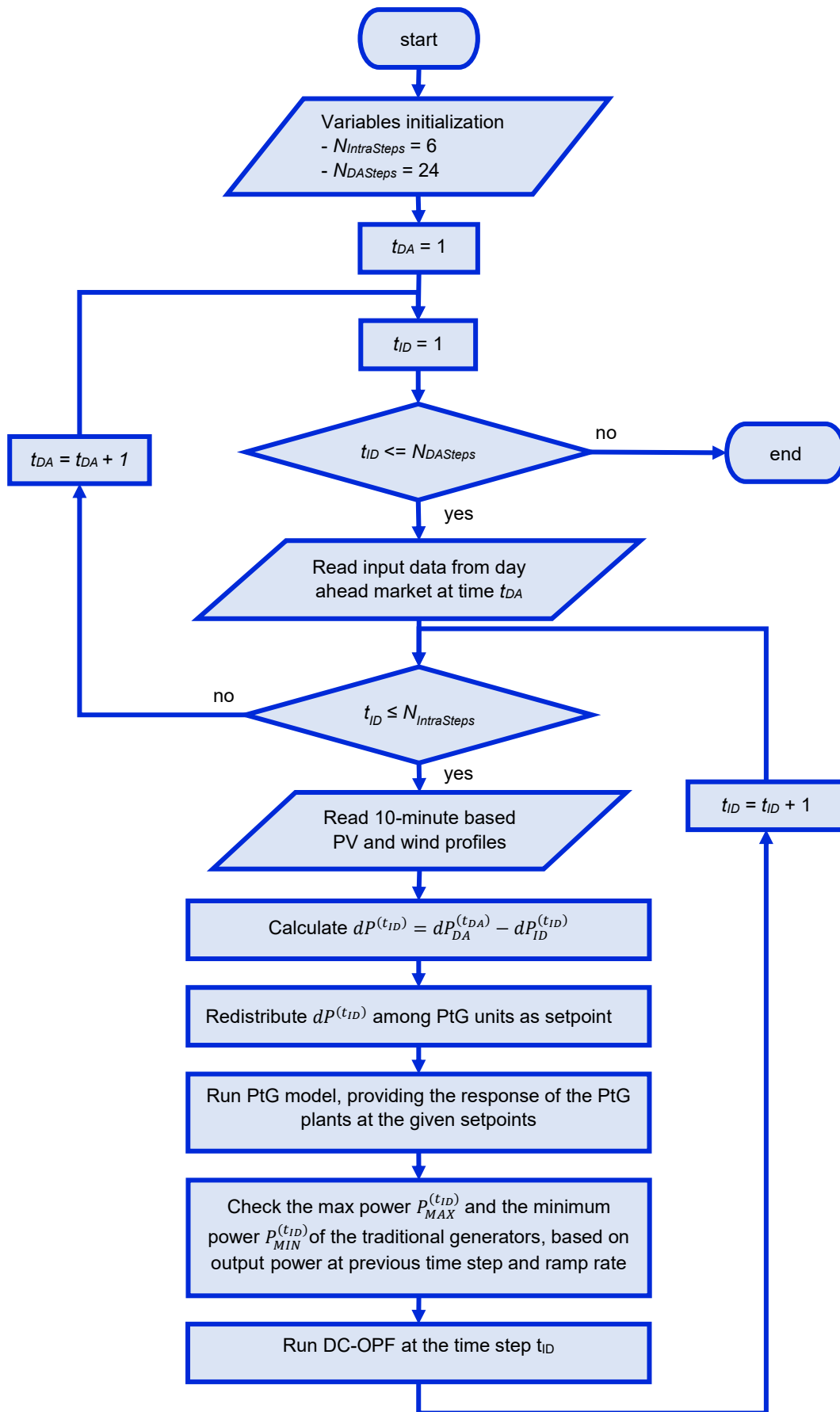


Figure 6-2: Flowchart of the ID (or real time) market

## 6.6 Introduction of the PtG node into the calculation loop

The PtG unit model presented in Section 2.2 has been designed to provide the response to a pre-established consumption target profile. In this network model, however, the desired working point of the PtG unit is calculated at the current time step of the power flow. This means that, when using the previously illustrated PtG model at each power flow iteration, all of the discrete time steps are loaded from the initial to the current one, so the past work points of the electrolysers would be recalculated at every call of the PtG function, leading to an increase of the computation time. However, as explained in Appendix A.1, the response of the PtG unit is modelled as a first order system and it does not need the entire set of the electrolyser’s working points in order to generate the current response, but only few of them. For this reason, to improve the computational times the variable  $N_{keep\_step}$  is introduced: this variable limits the number of working points of the electrolyser, avoiding the recalculation of all the previous work points. The numerical value of  $N_{keep\_step}$  should be enough to rebuild the model response, by maintaining the model’s accuracy with respect to the “correct response” (i.e., the one based on the entire set of past working points). This method, using  $N_{keep\_step}$  equal to 10 time steps, has been tested and the relative error is  $10^{-18}$  respect to the case in which all the working points are calculated.

In particular, the model has been wrapped in a function, which accepts as input all of the characteristics of the PtG unit, such as maximum and minimum stable power consumption, and the information about the current and previous states: the history of  $N_{keep\_step}$  setpoints plus the newly calculated one, the H<sub>2</sub> tank level at the older point and the time step for the model simulation are required in order to run the simulation. A graphical representation of the inputs and outputs of the function can be observed in Figure 6-3. It is suggested to use a value of  $N_{keep\_step}$  equal or bigger than  $dt$  time step, previously defined.

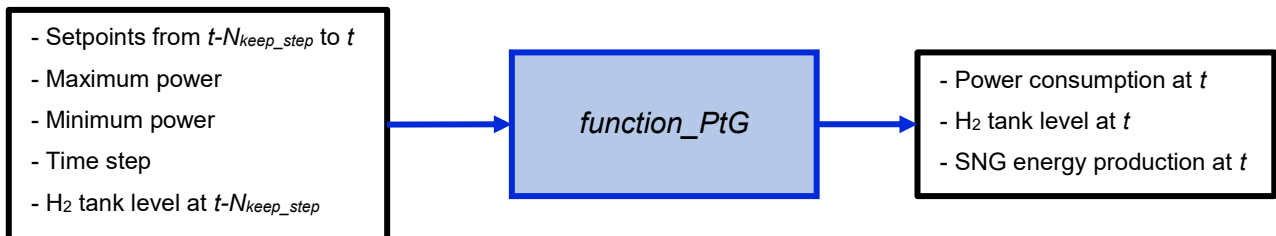


Figure 6-3: PtG model function I/O

The acronyms used for the PtG model are reported in Table 6-1 and are useful to understand the explanation of the algorithm shown in the flowchart of Figure 6-4.

Table 6-1: Set variables used in *function\_PtG*.

Variables	Description
$N_{units}$	Number of PtG units
$N_{keep\_step}$	Number of points for running PtG model
$SP_{PtG}$	Size of PtG plants
$H_{2,tank}(SP_{PtG})$	Initial value of the volume of H <sub>2</sub> in the tank
$dt_{PtG}$	Discrete time step for PtG model
$P_{PtG}$	Power consumption
$ERIP$	Setpoint of PtG units

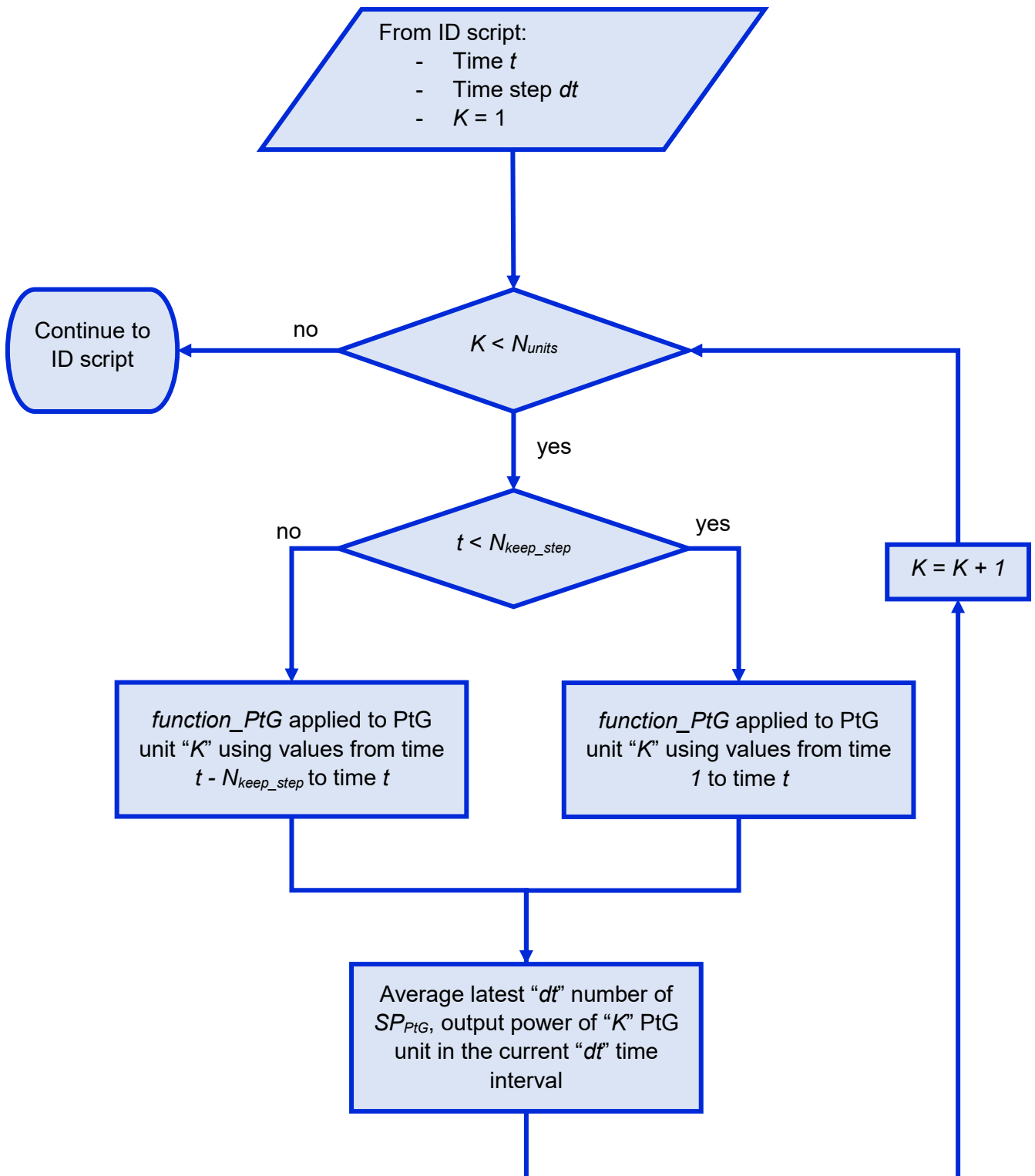


Figure 6-4: Execution of PtG model within ID algorithm. The function called function\_PtG represents the PtG node

Given the fast response of PtG, the model runs with one-minute time steps, for a number of times equal to the user defined time step “ $dt$ ” for ID market. For each loop execution, if the current time  $t < N_{keep\_step}$ , the entire past values of setpoints are passed as input to *function\_PtG*. Otherwise, only the previous  $N_{keep\_step}$  points are passed to PtG node function. In both cases, the value of  $H_{2,tank}$  that needs to be provided is the one corresponding to the oldest setpoint. At each execution, the resulting  $H_{2,tank}$  and  $P_{PtG}$  values are saved, being  $P_{PtG}$  the power absorbed by the PtG system.

For each PtG unit the average power (energy) within the user defined time step for ID market is the response of the unit at the current time iteration.

## 7 Results for the cases #T2 and #T3

Cases #T2 and #T3 use the same algorithm, therefore results of both them share the same structure. Considerations made for one case may be not repeated in the other. As explained previously, the imbalance between the day-ahead forecasts and the real time production of RES is an indicator of RES effect and eventual PtG influence on the network.

The results shown for the network #T2 and #T3 refer to two working days of the year, in January and July. The rationale behind this choice was to show two completely different types of seasonality, both for loads and RES production. In January the load reaches its peak of the year, while in July it is lower. RES production is different both for wind and PV, given the characteristics of winter and summer.

### 7.1 Network #T2

The loads used are based on the European load values of 2017 and the capacity of the generators installed in the network has been updated for approximate the capacity of the same year. Table 7-1 shows RES capacity for the various countries.

Table 7-1: Generation capacity in Network #T2, 2017 scenario

Country	Conventional [MW]	Solar [MW]	Wind [MW]	RES penetration <sup>4</sup> [%]
AT	22135	1031	2730	17.0
BE	15392	3380	2807	40.2
CH	21333	1664	75	8.2
CZ	18497	2040	308	12.7
DE	111449	42020	55072	87.1
DK	9671	907	5497	66.2
ES	75247	6970	23066	39.9
FR	109135	7646	13539	19.4
HR	4191	51	537	14.0
HU	8152	94	323	5.1
IT	103540	19662	9778	28.4
LU	1876	121	120	12.8
NL	21916	38	3641	16.8
PL	32395	186	5697	18.2
PT	14219	489	5090	39.2
SI	3534	270	3.3	7.7
SK	7301	530	3	7.3

Figure 7-1 shows with red line the RES power production imbalance between the forecasted value in day-ahead and the actual value that happens in intra-day, calculated as a sum for all RES plants of the network: this unbalance has to be solved by involving the traditional generators, that should adapt their production for maintaining the system in operation. The same figure shows in dashed

<sup>4</sup> RES penetration is equal to the total installed capacity of wind and solar generators, divided by the total installed capacity of conventional power plants.

blue the effect of 7.2 GW of PtG working in different network nodes<sup>5</sup>. The redistribution of the power among the different PtG has been based on size criterion: this means that, after the calculation of the unbalance of the network, the setpoints of every PtG plant have been fixed according to its size. The model of the PtG plant is the one shown in Section 6.6.

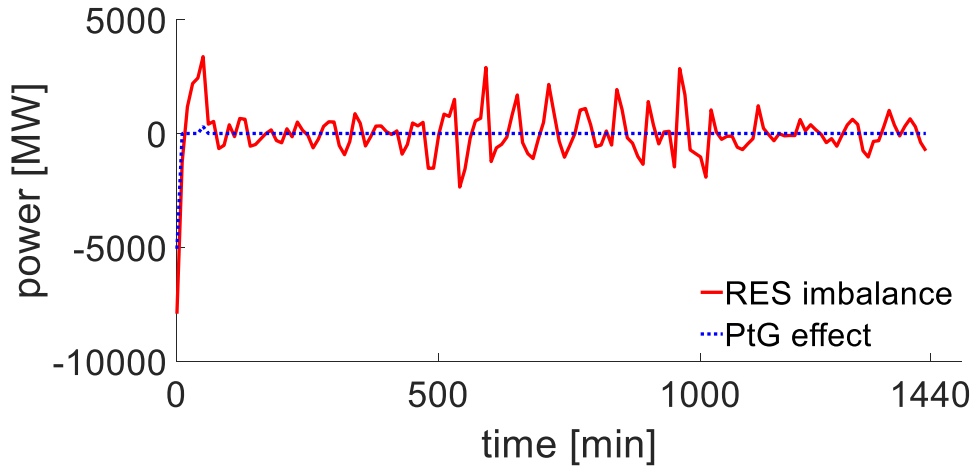


**Figure 7-1: Total network RES imbalance before and after the PtG installation (10<sup>th</sup> January)**

Since PtG plant setpoint is imposed by their size, and in this particular example the sizes of all the PtG plants have been fixed 400 MW, the responses of the PtG plants are also the same. An example of these responses is shown in Figure 7-2: the model follows in very good way the setpoint imposed. A detail of the response can be seen in Figure 7-3, showing the characteristic delay of PtG response, and, around 50 to 60 minutes, a working point not reachable by the PtG unit, since it is above its nominal power.

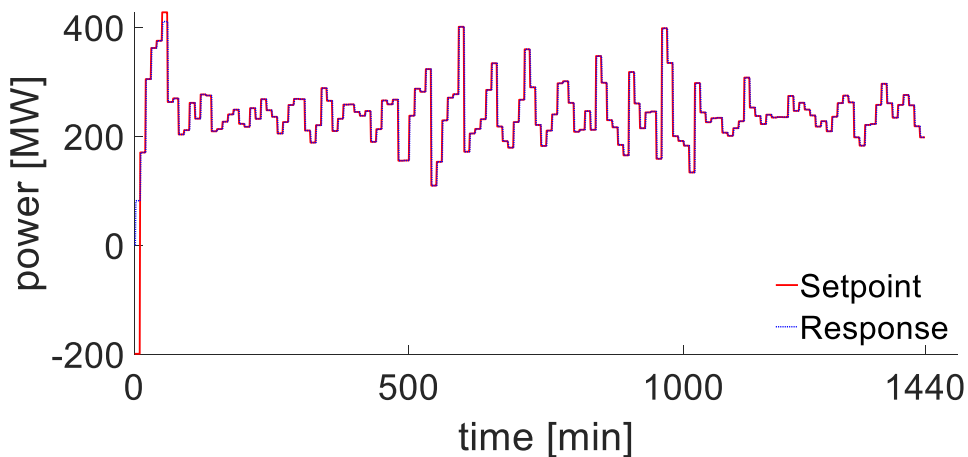


**Figure 7-2: Setpoint and response of 400-MW PtG plant (10<sup>th</sup> January)**

<sup>5</sup> It is worth to note that the siting and sizing of the PtG in the European transmission system, in these case studies, has not been optimized and it will be proper investigate in a future work. In this work, PtG plants has been placed in correspondence of the biggest RES plants.

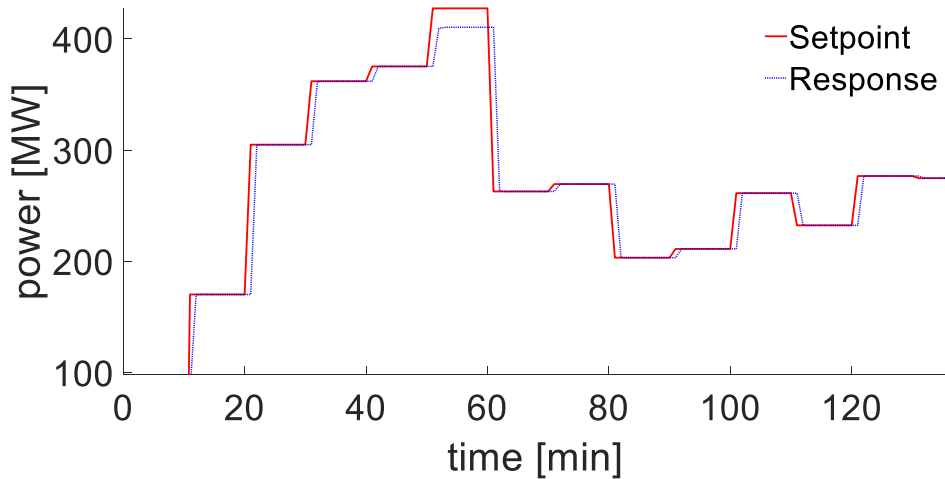


Figure 7-3: Detail of the setpoint and response of 400-MW PtG plant (10<sup>th</sup> January)

The filling of the hydrogen tank is shown in Figure 7-4: the maximum pressure of the tank is 6 MPa and the time for which the tank guarantees the minim H<sub>2</sub> flow at the methanation plant is 24 h. At the initial time step the tank is 50% full. As explained in Section 2, filling the hydrogen tank is the priority, reducing the flow rate to the methanation unit until it is full. After this happens, methanation unit gets the priority over hydrogen flow rate, using hydrogen tank as a buffer. Therefore, Figure 7-4 shows a good example of both the scenarios.

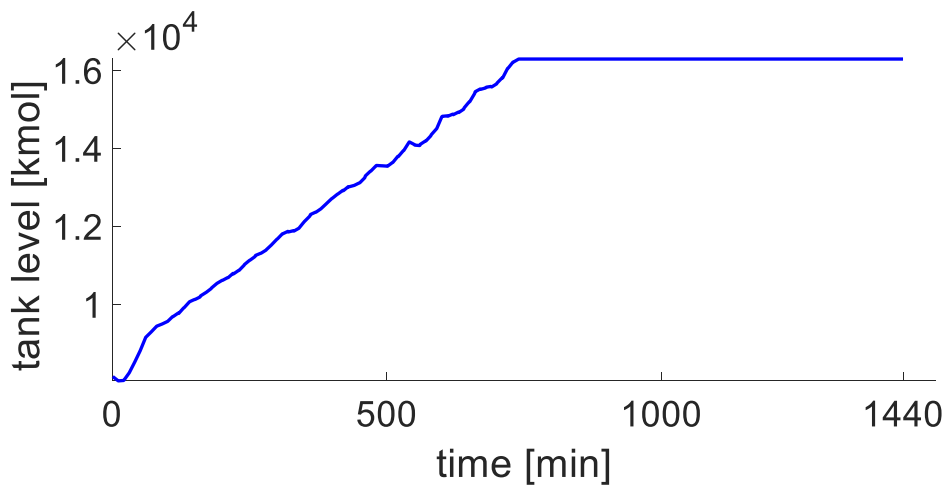


Figure 7-4: Filling of the tank of the 400-MW PtG plant (10<sup>th</sup> January)

It is also possible to track the energy content of the SNG produced by a PtG unit in order to confirm this behaviour. In Figure 7-5 the quantity of SNG produced ad each minute can be observed and clearly shows how the methanation unit works at its minimum stable output until the hydrogen tank is full, around 750<sup>th</sup> minute of the day.

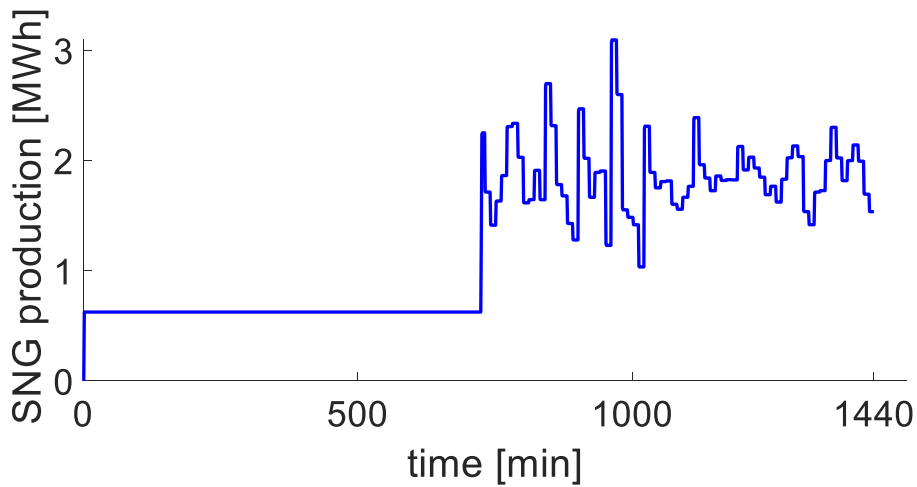


Figure 7-5: Instantaneous SNG production of the 400-MW PtG plant (10<sup>th</sup> January)

A simple manipulation of this information can be seen in Figure 7-6, which shows the amount of SNG produced from the start of the day to each minute.

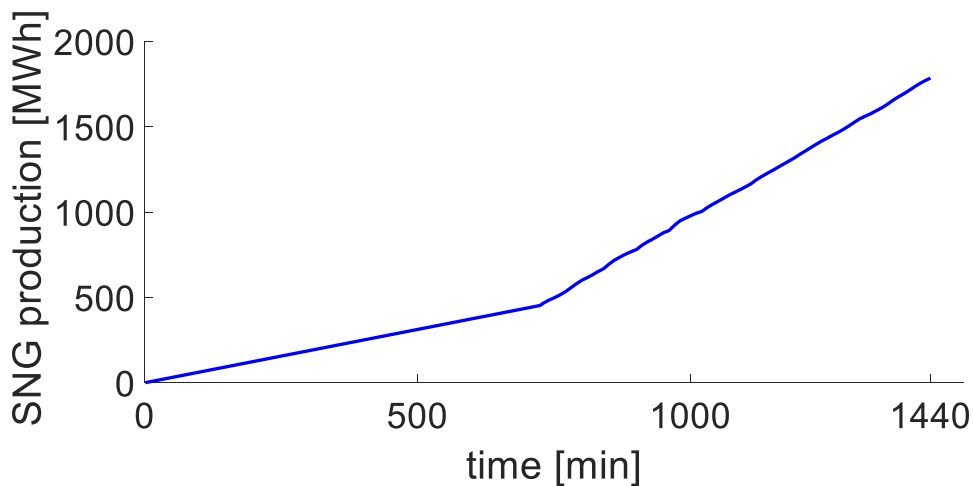


Figure 7-6: Cumulative SNG production of the 400-MW PtG plant (10<sup>th</sup> January)

The same results related to July are shown in Figure 7-7, Figure 7-8, Figure 7-9, Figure 7-10 and Figure 7-11: it is evident that there is more variability to be faced in presence of the sunrise and sunset compared to January, where the power produced by the sun is increasing/decreasing in monotonic way.

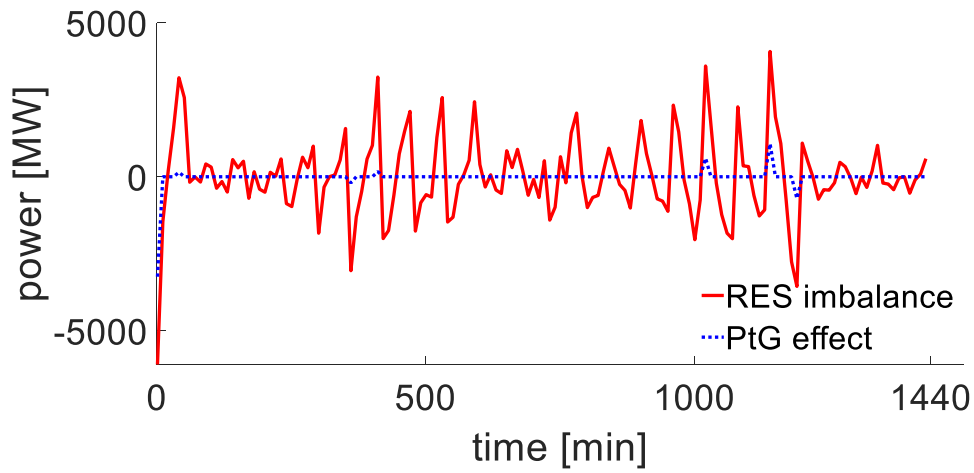


Figure 7-7: Total network RES imbalance before and after the PtG installation (3<sup>rd</sup> July)

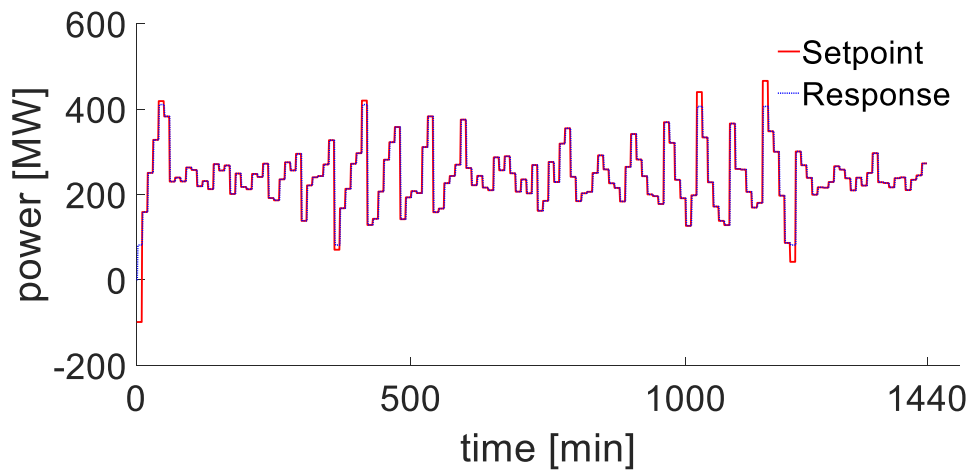


Figure 7-8: Setpoint and response of 400-MW PtG plant (3<sup>rd</sup> July)

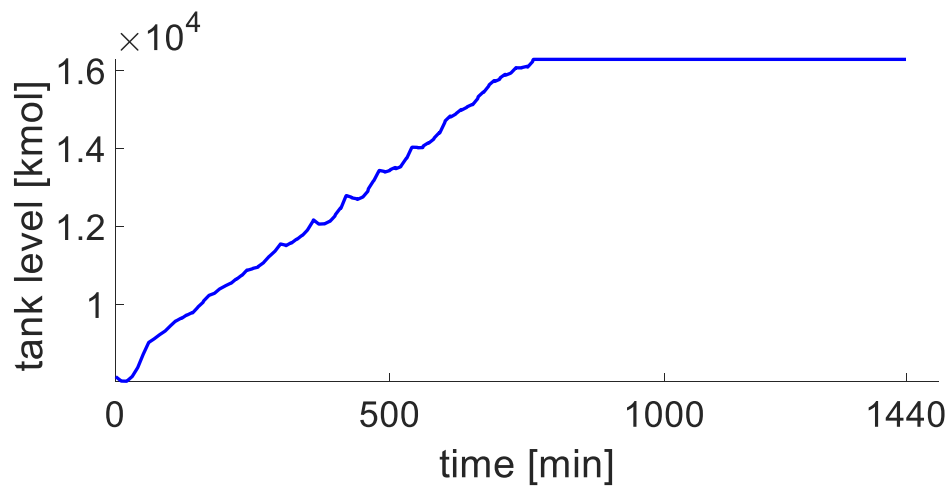


Figure 7-9: Filling of the tank of the 400-MW PtG plant (3<sup>rd</sup> July)

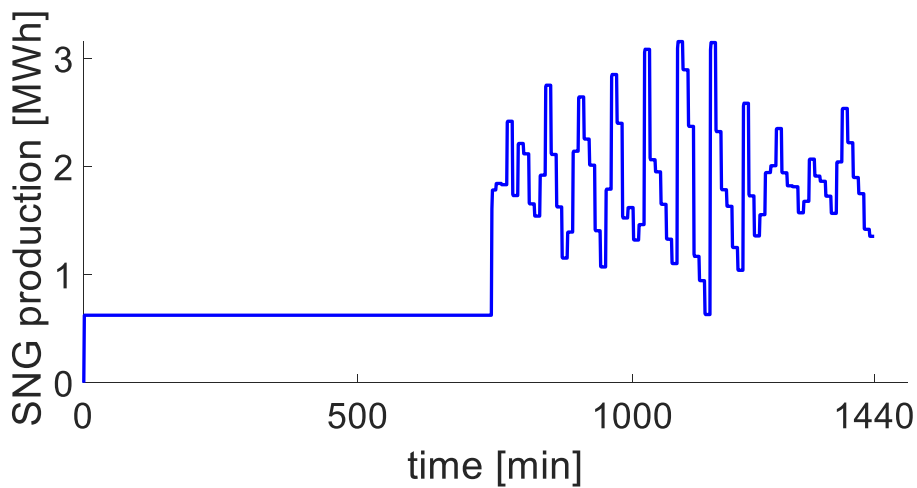


Figure 7-10: Instantaneous SNG production of the 400-MW PtG plant (3<sup>rd</sup> July)

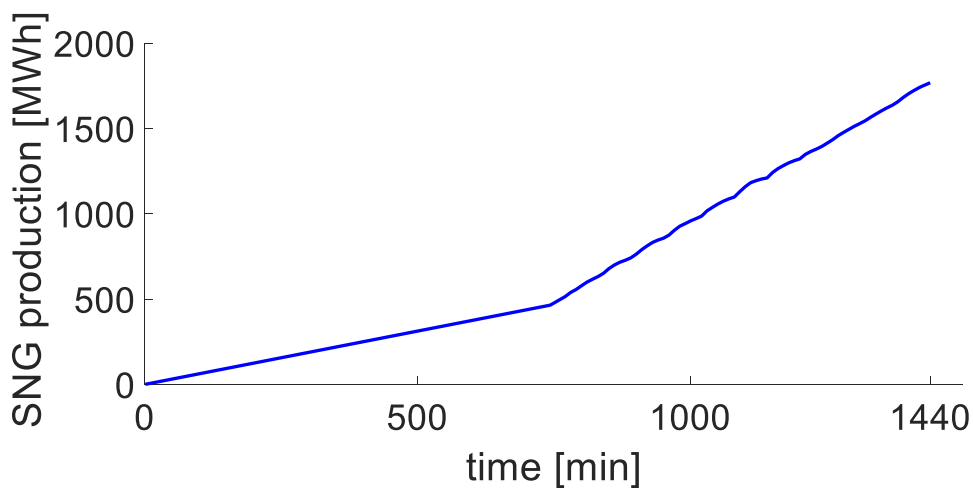


Figure 7-11: Cumulative SNG production of the 400-MW PtG plant (3<sup>rd</sup> July)

For the two days considered, the beneficial effect of the installation of the PtG is shown in Table 7-2: the presence of PtG limits the energy, the duration and the peak of the imbalance, helping the operation of the transmission network. Similarly to the time duration, the reduction of the energy imbalance is almost total, and its peak is reduced significantly by ~40%. The meaning of these results is that the difference between the forecast of the day-ahead market and the actual situation of the intra-day market is almost none. It is possible to observe a correlation between total network imbalance figures and PtG response figures: there is imbalance when PtG units reach their technical upper limit, and therefore the installed capacity of PtG on the network is not enough to fully cover RES imbalances.

Table 7-2: Performance of PtG in the network #T2

Scenario	PtG status	RES imbalance					
		Energy [MWh]	Energy difference [%]	Duration [min]	Duration difference [%]	Peak [MW]	Peak difference [%]
Network #T2 January	Off	1700	-95%	1410	-99%	7910	-36%
	On	89		20		5060	
Network #T2 July	Off	2304	-96%	1410	-95%	6094	-47%
	On	103		70		3244	

## 7.2 Network #T3, present scenario

The results shown for the network #T3 also refer to two days of the year, in January and July, for the same rationale explained at the beginning of this section, and a representation of the load profiles which has been used is shown in Figure 7-12. The capacity of the generators installed used is based on 2013 data (the original ones of the network, shown in Table 7-3) and then updated to 2017 through scenario selection. The loads values are based 2017 data.

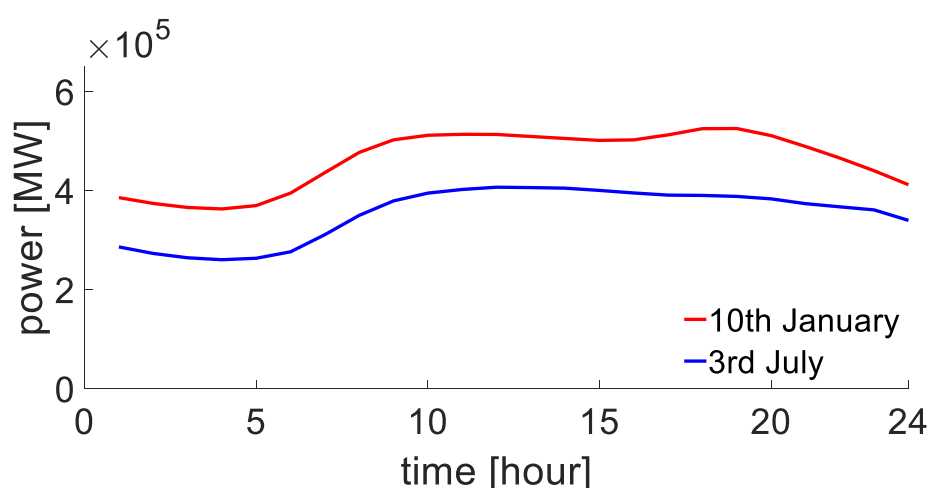


Figure 7-12: Load profiles for 2017 scenario

Figure 7-13 shows the total RES variability from the forecasts of the day-ahead OPF to the actual values in intra-day OPF: this unbalance is representative of the whole network and has to be solved by involving the traditional generators, that should adapt their production for maintaining the system in operation. The same figure shows in dashed blue the effect of 10 GW of PtG, working in different network nodes<sup>6</sup>, on the imbalance of power of the whole network. The redistribution of the power among the different PtG has been based on size criterion. In this particular example, the sizes of the PtG plants has been fixed 1 GW. The model of the PtG plant is the one shown in Section 6.6.

<sup>6</sup> It is worth to note that the siting and sizing of the PtG in the European transmission system, in these case studies, has not been optimized and it will be proper investigate in a future work. In this work, PtG plants has been placed in correspondence of the biggest RES plants.

Table 7-3: Generation capacity in Network #T3, 2013 scenario

Country	Conventional [MW]	Solar [MW]	Wind [MW]	RES penetration <sup>7</sup> [%]
AL	-	-	-	-
AT	19648	1981	404	12.1
BA	-	-	-	-
BE	12690	2172	3068	41.3
BG	5894	701	1041	29.6
CH	22141	60	756	3.7
CZ	7055	277	2067	33.2
DE	100594	43429	38411	81.4
DK	5635	5082	781	104.0
EE	2339	301	6	13.1
ES	58005	23003	6967	51.7
FI	12597	1082	11	8.7
FR	99117	10312	6192	16.7
GB	66505	13563	9000	33.9
GR	10936	1775	2444	38.6
HR	3002	384	44	14.3
HU	5269	328	29	6.8
IE	6132	2400	1	39.2
IT	74374	8750	19100	37.4
LT	1531	290	69	23.4
LU	1644	60	116	10.7
LV	2275	70	2	3.2
ME	-	-	-	-
MK	-	-	-	-
NL	21333	3641	1429	23.8
NO	30470	860	14	2.9
PL	33747	5186	87	15.6
PT	13117	4826	429	40.1
RO	12313	2923	1249	33.9
RS	-	-	-	-
SE	25074	3029	263	13.1
SI	2985	3	532	17.9
SK	6227	3	104	1.7

<sup>7</sup> RES penetration is equal to the total installed capacity of wind and solar generators, divided by the total installed capacity of conventional power plants.

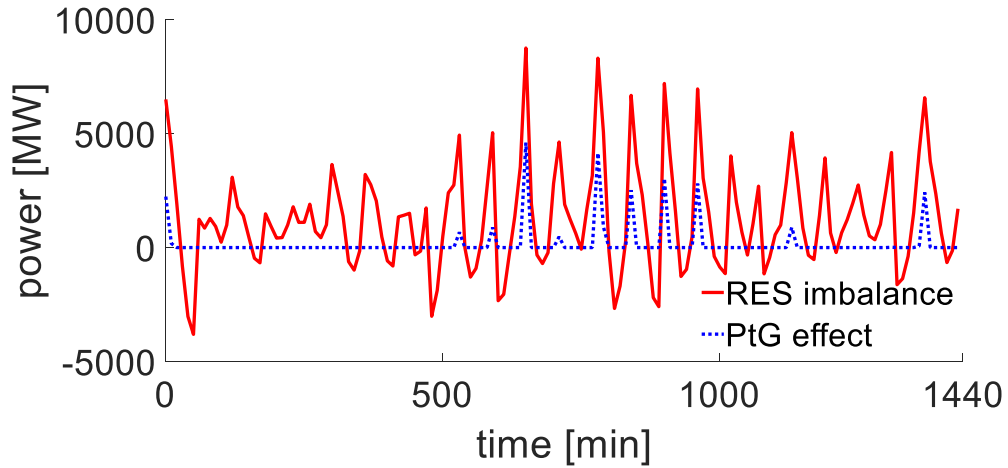


**Figure 7-13: RES imbalance before and after the PtG installation (10<sup>th</sup> January, 2017 scenario), network #T3**

Since PtG plants setpoint is imposed by their size, and their size is the same, the responses of the PtG plants are the same. An example of these responses is shown in Figure 7-14: the model follows in very good way the setpoint imposed. A detail of the response can be seen in Figure 7-15. In particular the delay of the response can be seen. More difficult to observe, but still present, is the exponential part of the response.

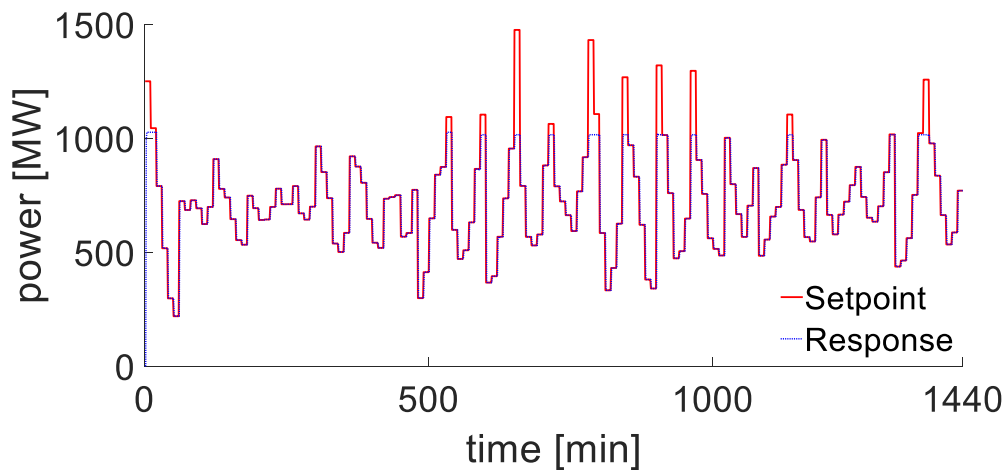


**Figure 7-14: Setpoint and response of 1-GW PtG plant (10<sup>th</sup> January, 2017 scenario), network #T3**

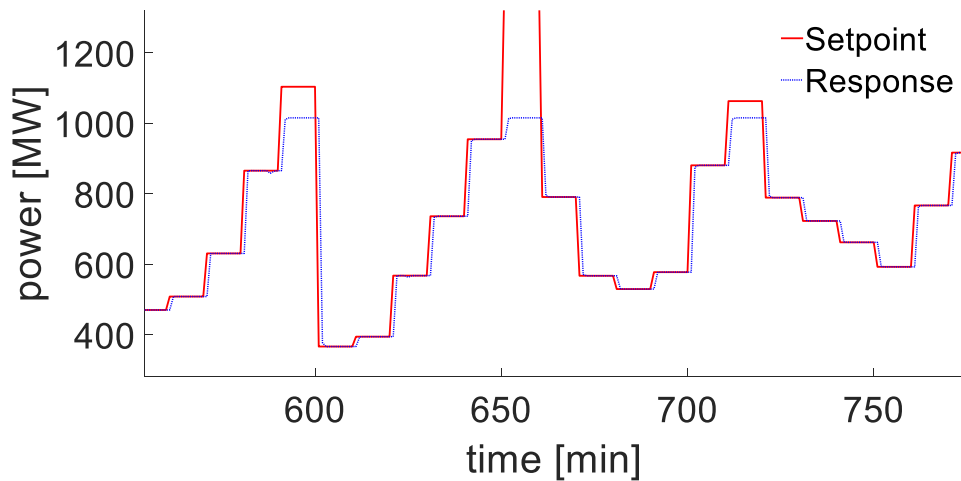


Figure 7-15: Detail of RES imbalance before and after PtG installation (10<sup>th</sup> January, 2017 scenario), network #T3

Finally, the filling of the tank is shown in Figure 7-16: the maximum pressure of the tank is 6 MPa and the time for which the tank guarantees the minim H2 flow at the methanation plant is 24 h. At the initial time step the tank is 50% full. As explained in Section 2.2, filling the hydrogen tank is the priority, reducing the flow rate to the methanation unit until it is full. After this happens, methanation unit gets the priority over hydrogen flow rate, using hydrogen tank as a buffer when necessary.

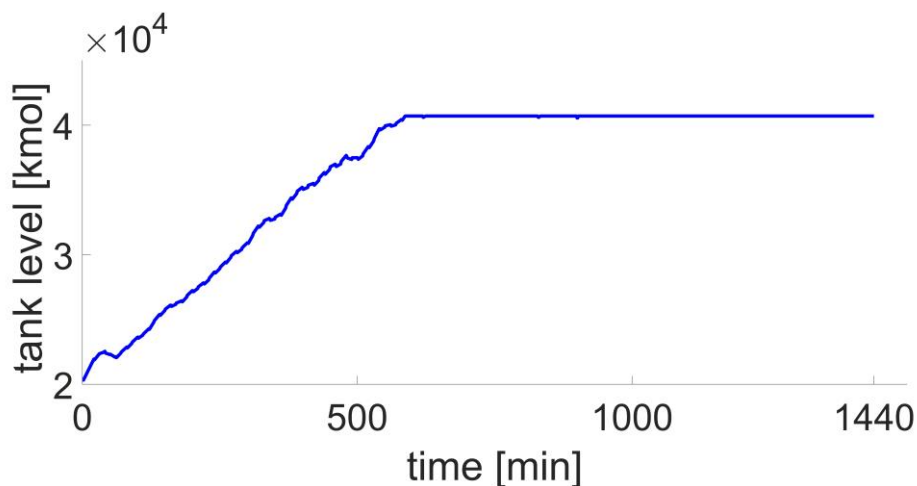


Figure 7-16: Filling of the tank of the 1-GW PtG plant (10<sup>th</sup> January, 2017 scenario)

As explained previously, this can be confirmed by observing Figure 7-18 and Figure 7-17, which represent the SNG output of the methanation unit during the day, both as instantaneous and as a cumulative value.

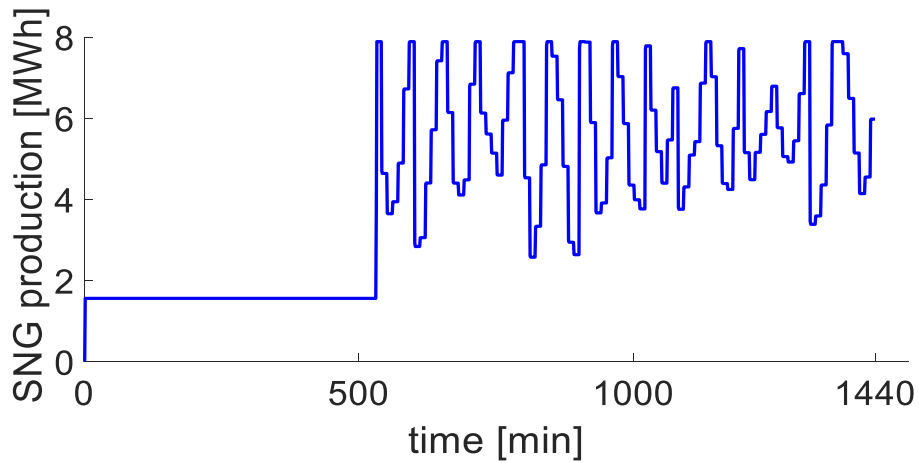


Figure 7-18: Instantaneous SNG production of the 1-GW PtG plant (10<sup>th</sup> January, 2017 scenario)

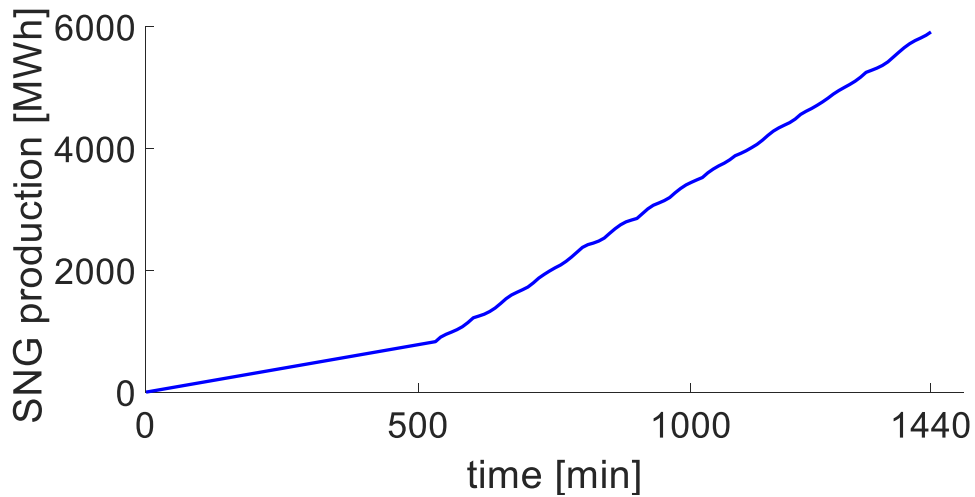


Figure 7-17: Cumulative SNG production of the 1-GW PtG plant (10<sup>th</sup> January, 2017 scenario)

The same results related to July are shown in Figure 7-19, Figure 7-20, Figure 7-21, Figure 7-22 and Figure 7-23: it is clear that there is more variability to be faced in presence of the sunrise and sunset, where the power produced by the sun is increasing/decreasing in monotonic way. PtG unit gets involved more often in those hours, but along the day the SNG production is comparable to the one of the January case.

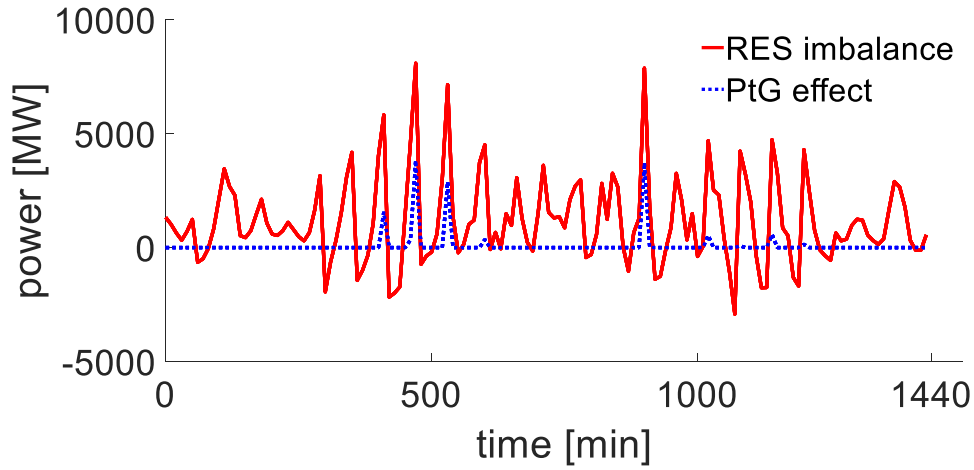


Figure 7-19: RES imbalance before and after the PtG installation (3<sup>rd</sup> July, 2017 scenario), network #T3

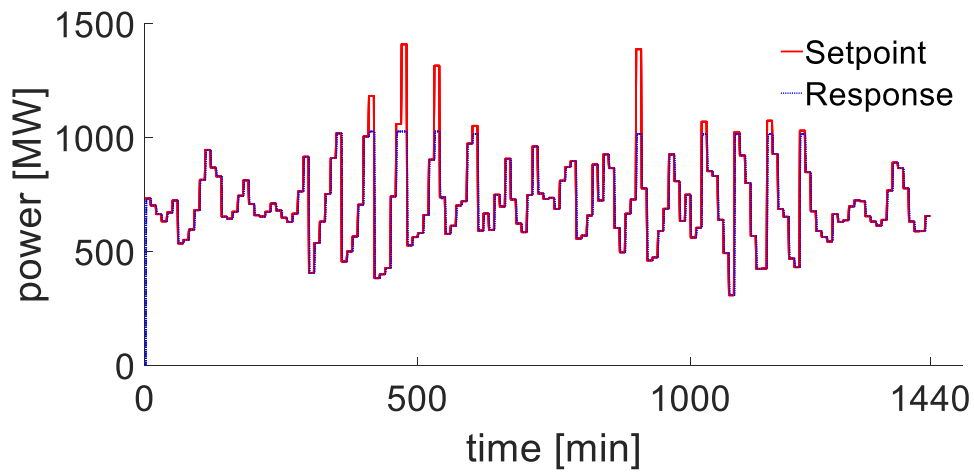


Figure 7-20: Setpoint and response of 1-GW PtG plant (3<sup>rd</sup> July, 2017 scenario), network #T3

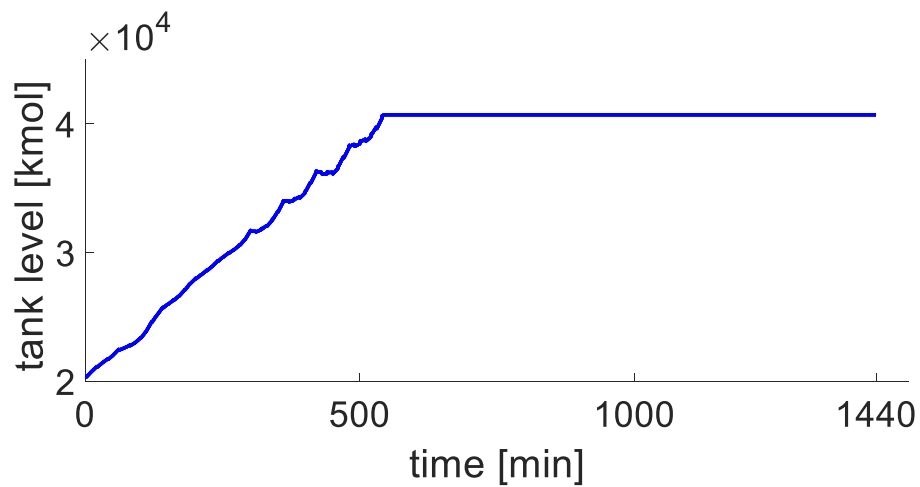


Figure 7-21: Filling of the tank of the 1-GW PtG plant (3<sup>rd</sup> July, 2017 scenario), network #T3

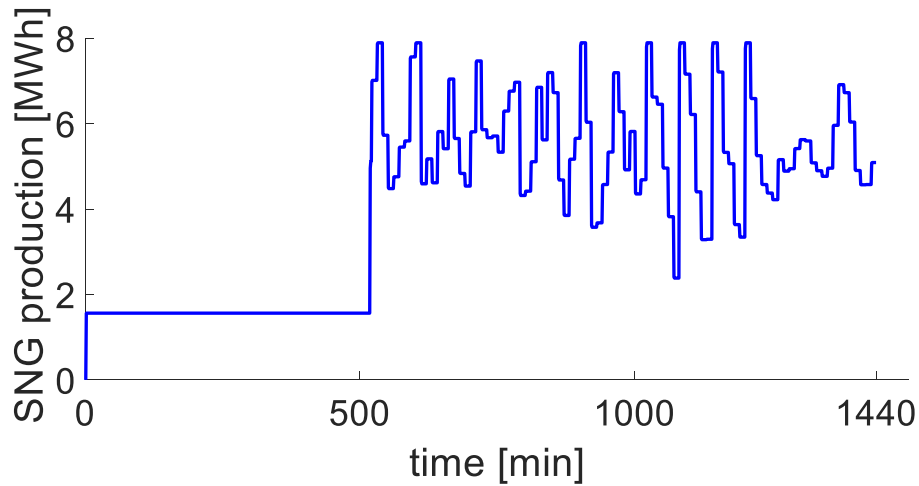


Figure 7-22: Instantaneous SNG production of the 1-GW PtG plant (3<sup>rd</sup> July, 2017 scenario)

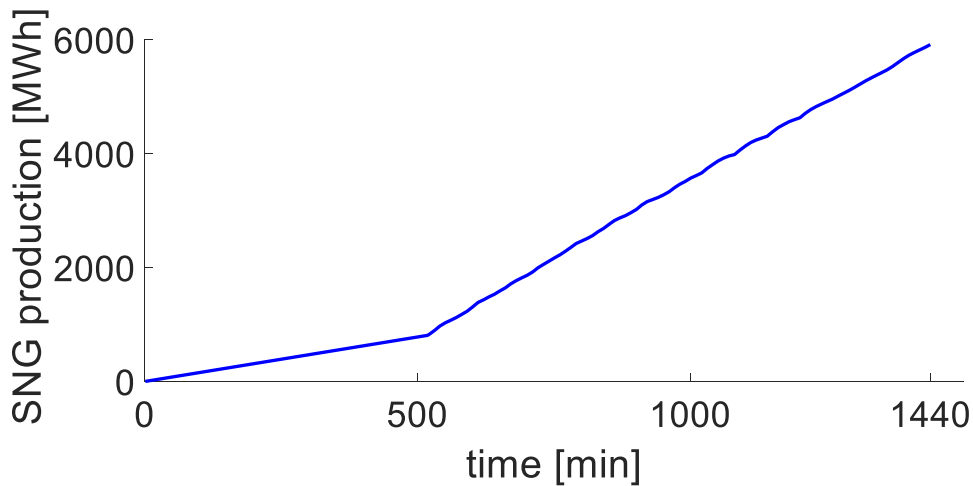


Figure 7-23: Cumulative SNG production of the 1-GW PtG plant (3<sup>rd</sup> July, 2017 scenario)

The PtG effects for the two days of 2017 scenario are shown in Table 7-4: the presence of PtG, also in this case, greatly limits the energy involved by the imbalance and the duration and the peak of the imbalance itself. This reductions help the operation of the transmission network. Despite being a bigger network than #T2, the results are similar, showing the goodness of the approach.

Table 7-4: Performance of PtG in 2017 scenario, network #T3

Scenario	PtG status	RES imbalance					
		Energy [MWh]	Energy difference [%]	Duration [min]	Duration difference [%]	Peak [MW]	Peak difference [%]
Network #T3 January	Off	4581		1440		8758	
	On	431	-91%	150	-90%	4600	-47%
Network #T3 July	Off	3820		1440		8091	
	On	233	-94%	100	-93%	3827	-53%

### **7.3 Network #T3, future scenarios**

Results for 2030 DG and 2040 GCA scenarios are also provided to show scenario selection functionality other than PtG impact. Generation has been scaled for each country and more detailed data is shown in

Table 7-5 and Table 7-6. It is expected RES installed capacity to grow and some types of conventional power plants to be dismissed, and therefore their generation to be scaled down. As explained in Section 5.8, these two scenarios represents an European effort to decarbonisation, as it can be observed in RES penetration compared to 2013 values (visible in Table 7-3). Network's load profiles for these scenarios can be seen in Figure 7-24 and Figure 7-25.

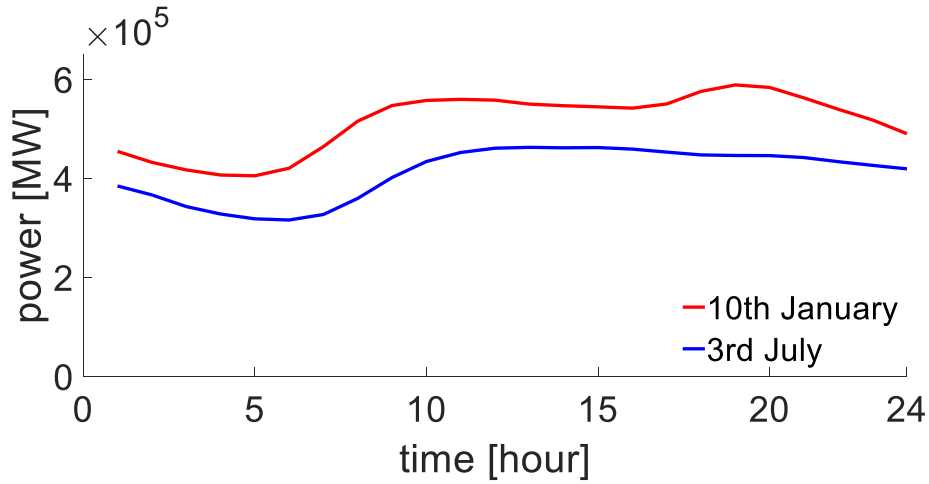


Figure 7-24: Load profiles for 2030DG scenario, 1984 climatic conditions, whole #T3 network

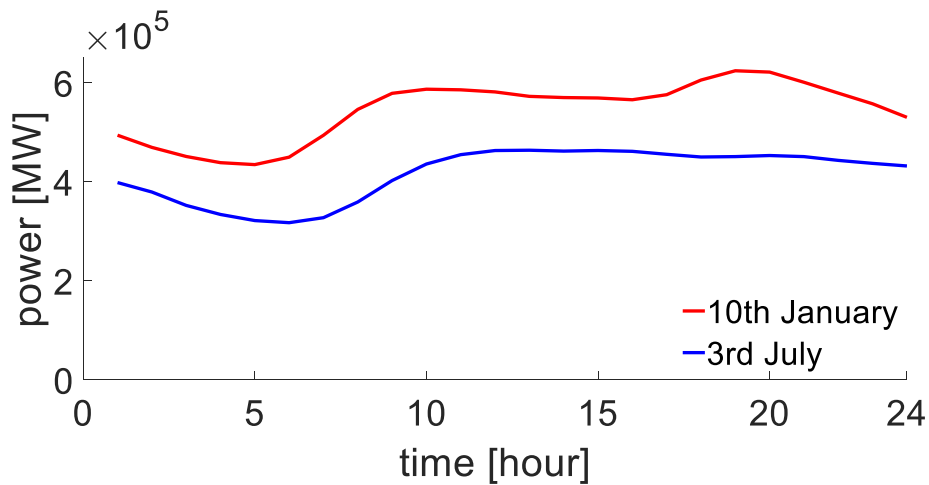


Figure 7-25: Load profiles for 2040GCA scenario, 1984 climatic conditions, whole #T3 network

Table 7-5: Generation capacity in Network #T3, 2030 DG scenario

Country	Conventional [MW]	Solar [MW]	Wind [MW]	RES penetration <sup>8</sup> [%]
AL	3,570	1,974	150	59.5
AT	26,656	8,113	5,310	50.4
BA	4,826	2,396	640	62.9
BE	11,233	7,180	5,937	116.8
BG	12,725	4,386	1,425	45.7
CH	24,487	10,021	1,020	45.1
CZ	13,730	7,577	1,534	66.4
DE	89,218	97,890	76,780	195.8
DK	2,518	5,463	8,851	568.5
EE	816	922	1,563	304.6
ES	72,354	50,732	32,275	114.7
FI	12,383	3,953	4,100	65.0
FR	85,950	43,469	45,155	103.1
GB	44,939	38,734	42,378	180.5
GR	13,762	8,025	6,225	103.5
HR	4,800	2,958	1,700	97.0
HU	6,825	6,405	1,205	111.5
IE	5,721	3,891	6,375	179.4
IT	69,480	49,242	18,856	98.0
LT	3,079	1,875	850	88.5
LU	2,460	381	226	24.6
LV	2,800	1,084	598	60.0
ME	1,721	433	270	40.8
MK	1,833	1,402	113	82.7
NL	16,264	14,338	18,476	201.8
NO	37,367	3,010	3,368	17.1
PL	39,127	25,748	12,328	97.3
PT	18,100	7,003	6,036	72.0
RO	15,038	11,892	4,450	108.7
RS	10,934	5,594	1,127	61.5
SE	23,756	7,486	13,072	86.5
SI	4,539	1,407	114	33.5
SK	9,022	3,831	517	48.2

<sup>8</sup> RES penetration is equal to the total installed capacity of wind and solar generators, divided by the total installed capacity of conventional power plants.

**Table 7-6: Generation capacity in Network #T3, 2040 GCA scenario**

<b>Country</b>	<b>Conventional [MW]</b>	<b>Solar [MW]</b>	<b>Wind [MW]</b>	<b>RES penetration<sup>9</sup> [%]</b>
AL	3,880	4,486	2,970	192.2
AT	25,697	5,910	5,810	45.6
BA	4,062	800	1,200	49.2
BE	11,406	22,329	16,329	338.9
BG	10,173	2,675	1,675	42.8
CH	27,555	13,250	3,240	59.8
CZ	10,210	5,814	1,914	75.7
DE	74,770	144,316	118,666	351.7
DK	1,628	7,803	15,337	1421.7
EE	816	1,063	1,963	370.9
ES	71,230	81,638	52,273	188.0
FI	13,693	7,100	9,400	120.5
FR	80,122	61,796	70,846	165.5
GB	57,652	41,571	50,102	159.0
GR	13,033	17,426	10,725	216.0
HR	6,000	1,046	2,200	54.1
HU	4,353	4,205	2,205	147.3
IE	5,440	2,175	8,875	203.1
IT	72,440	61,234	31,848	128.5
LT	3,079	7,083	1,500	278.7
LU	2,460	1,100	276	55.9
LV	2,800	178	1,448	58.0
ME	1,829	4,856	3,964	482.2
MK	2,313	45	163	9.0
NL	19,528	46,254	31,087	396.1
NO	36,932	3,038	10,474	36.6
PL	37,266	43,385	40,805	225.9
PT	15,705	17,994	13,002	197.4
RO	14,602	6,250	8,250	99.3
RS	8,605	509	1,259	20.5
SE	20,256	8,829	20,848	146.5
SI	5,520	1,011	284	23.4
SK	8,541	1,786	579	27.7

PtG installed capacity and placement have not been altered from 2017 scenario results, in order to show how a solution that worked quite well in 2017 would perform if applied in future scenarios. Results are summarized in Table 7-7 for 2030 DG scenario and in Table 7-8 for 2040 GCA scenario, which shows how a growing RES capacity in the network reduces the effectiveness of the deployment of the same PtG plants set.

<sup>9</sup> RES penetration is equal to the total installed capacity of wind and solar generators, divided by the total installed capacity of conventional power plants.

Table 7-7: Performance of PtG in 2030 DG scenario, network #T3

Scenario	PtG status	RES imbalance					
		Energy [MWh]	Energy difference [%]	Duration [min]	Duration difference [%]	Peak [MW]	Peak difference [%]
Network #T3 January	Off	10329		1440		22186	
	On	3926	-62%	520	-64%	18029	-19%
Network #T3 July	Off	11344		1440		23895	
	On	4882	-57%	580	-60%	19639	-18%

Table 7-8: Performance of PtG in 2040 GCA scenario, network #T3

Scenario	PtG status	RES imbalance					
		Energy [MWh]	Energy difference [%]	Duration [min]	Duration difference [%]	Peak [MW]	Peak difference [%]
Network #T3 January	Off	15815		1440		32534	
	On	8412	-44%	730	-49%	28477	-13%
Network #T3 July	Off	16638		1440		33908	
	On	9380	-47%	770	-47%	29728	-12%

As it can be seen in RES imbalance figures (Figure 7-26, Figure 7-27, Figure 7-28 and Figure 7-29), the effect of PtG units still exists, but it is way less than the one in 2017 scenario. Only the minor imbalances are absorbed, and PtG effects results in a small reduction of the biggest peaks. Referring to the summary tables, the RES imbalance peak grows in future scenarios compared to 2017 one, given the RES installed capacity increase. Therefore, it is necessary to plan PtG sizing and siting in a proper way, referring to future RES penetration.

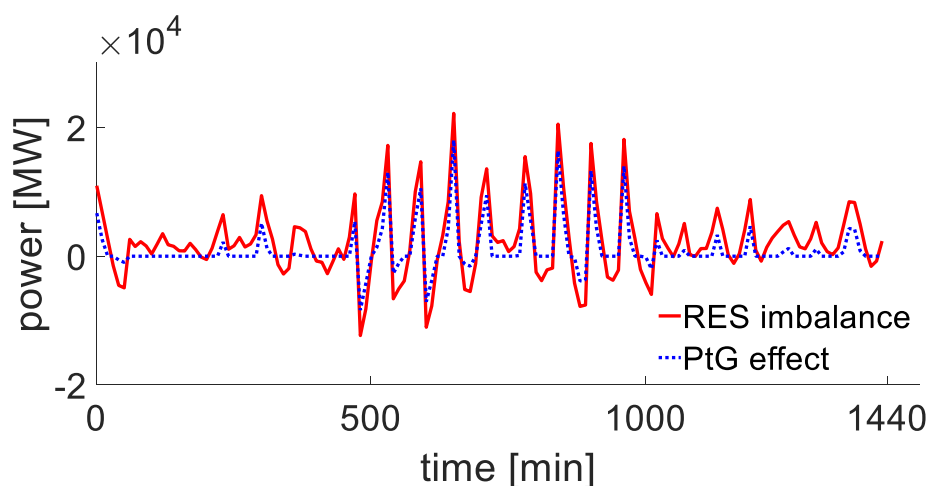


Figure 7-26: RES imbalance before and after the PtG installation (10th January, 2030 DG scenario), network #T3

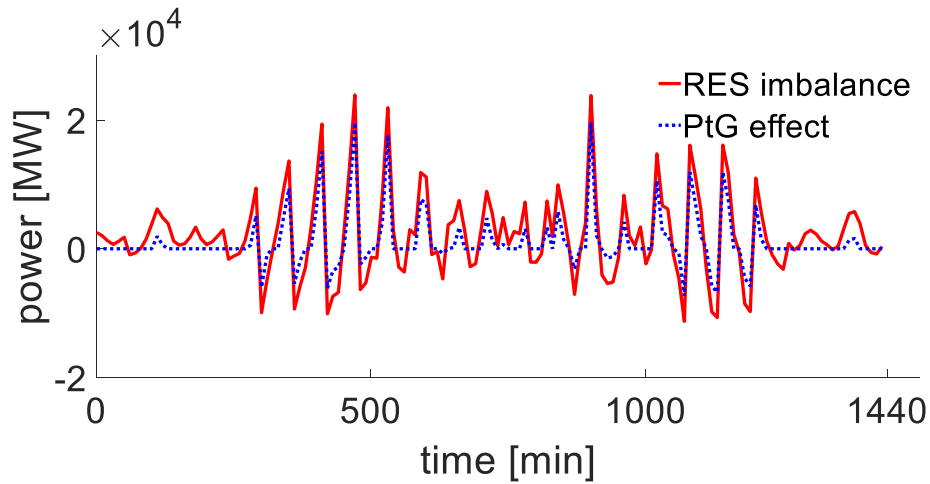


Figure 7-27: RES imbalance before and after the PtG installation (3<sup>rd</sup> July, 2030 DG scenario), network #T3

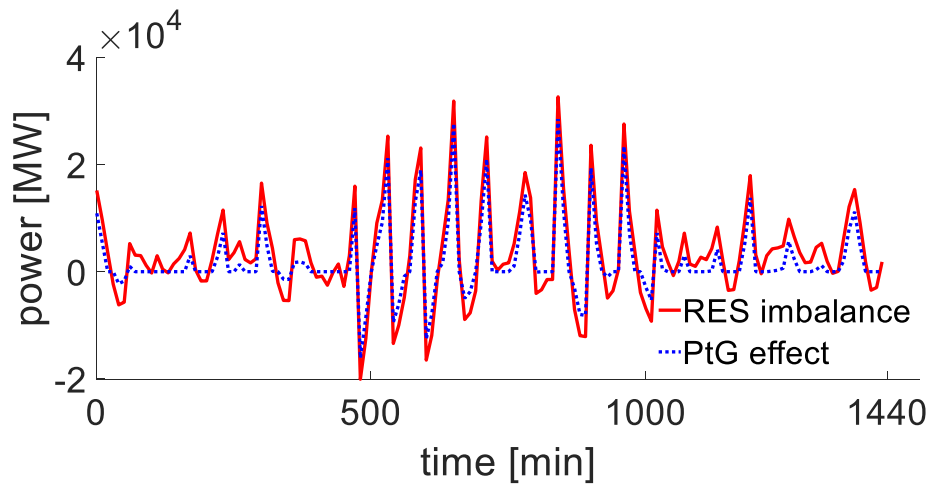


Figure 7-28: RES imbalance before and after the PtG installation (10<sup>th</sup> January, 2040 GCA scenario), network #T3

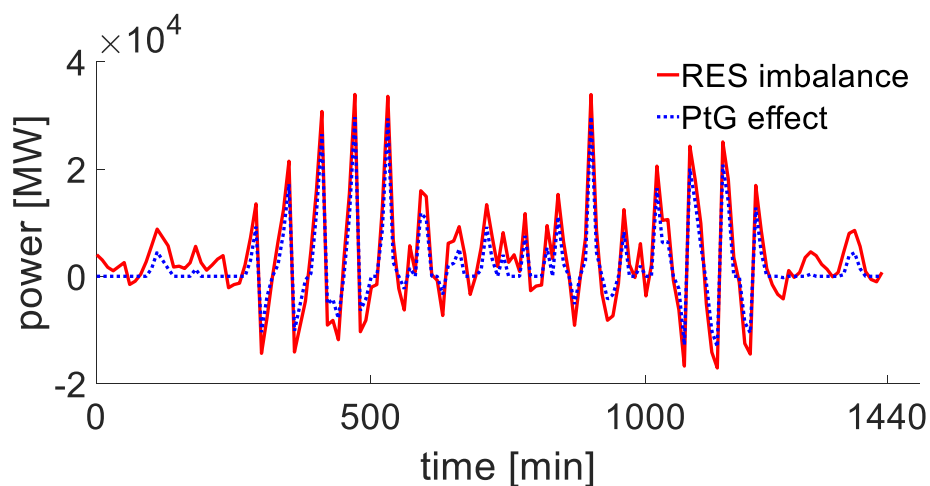


Figure 7-29: RES imbalance before and after the PtG installation (3<sup>rd</sup> July, 2040 GCA scenario), network #T3

PtG unit responses, shown in Figure 7-30, Figure 7-31, Figure 7-32 and Figure 7-33, follow correctly their given setpoints. Compared to 2017 scenario, the maximum setpoint required for each PtG unit doubles for 2030 DG scenario (~1500MW to ~3000MW) and almost triples for 2040 GCA scenario (~1500MW to ~4000MW). This indicates that for properly facing the amount of RES installed,

additional PtG capacity will be necessary. Probably an optimal capacity will be found, since it may be more convenient not to size the installed capacity against the peaks (which are few and do not last long), but to size it over the recovered energy.

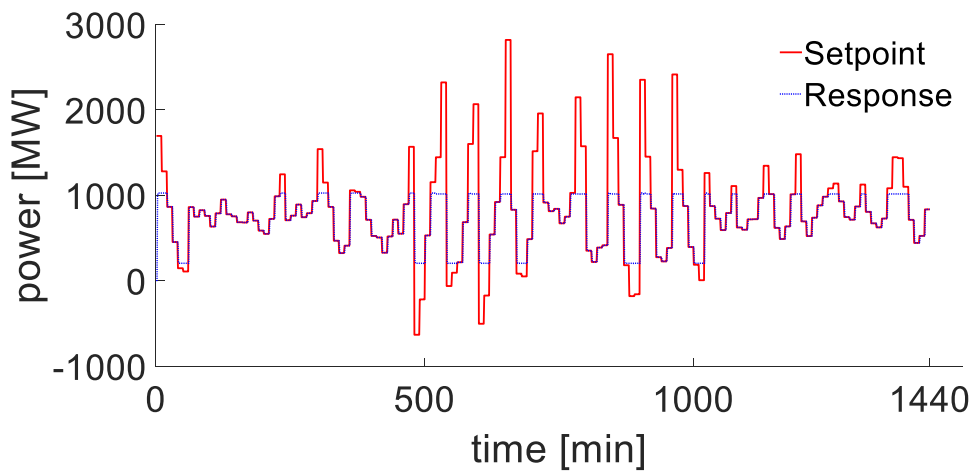


Figure 7-30: Setpoint and response of 1-GW PtG plant (10<sup>th</sup> January, 2030 DG scenario), network #T3

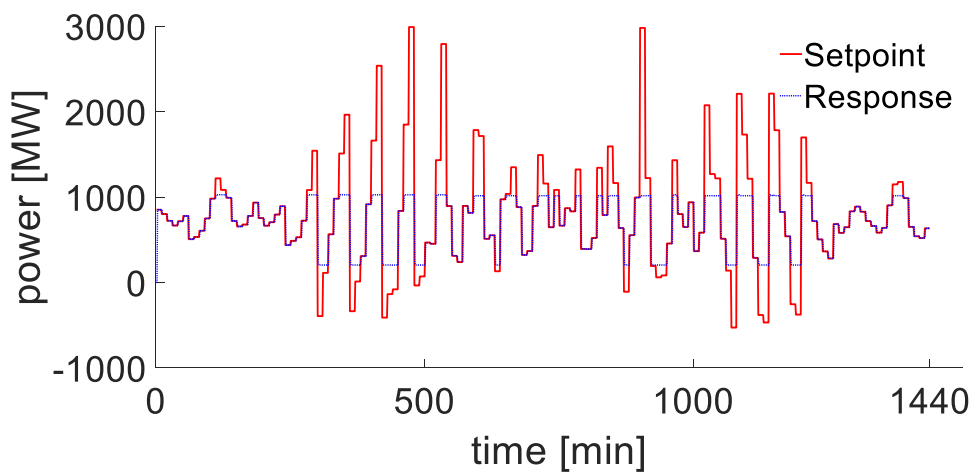


Figure 7-31: Setpoint and response of 1-GW PtG plant (3<sup>rd</sup> July, 2030 DG scenario), network #T3

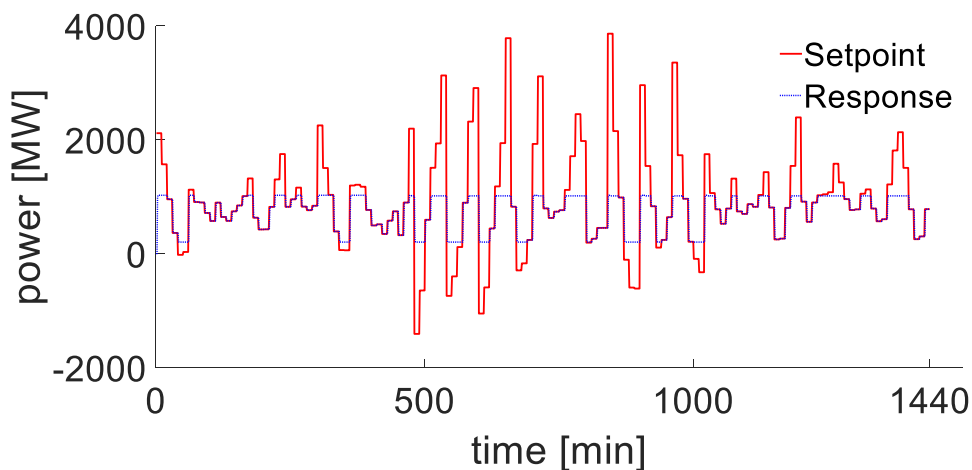


Figure 7-32: Setpoint and response of 1-GW PtG plant (10<sup>th</sup> January, 2040 GCA scenario), network #T3

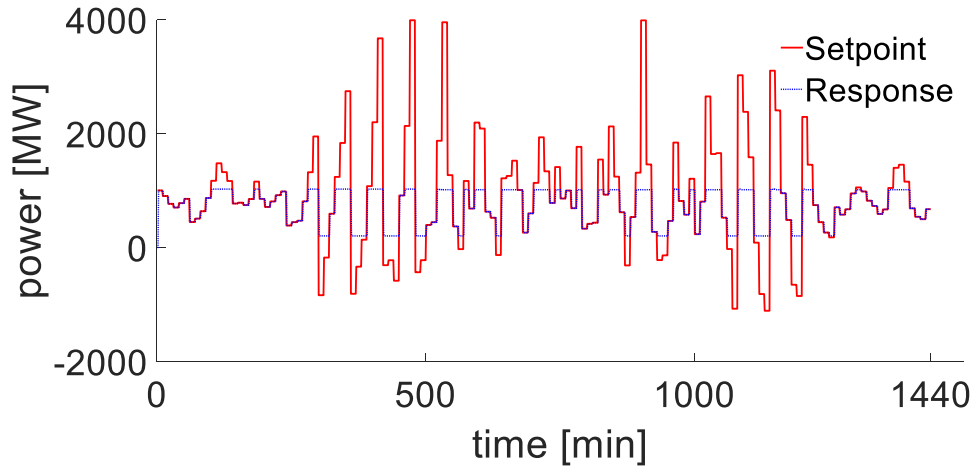


Figure 7-33: Setpoint and response of 1-GW PtG plant (3<sup>rd</sup> July, 2040 GCA scenario), network #T3

Tank levels, presented in Figure 7-34, Figure 7-35, Figure 7-36 and Figure 7-37, rise more quickly compared to 2017 scenario. It is possible to notice that the higher absorptions required for PtG units causes the methanation units to collect more frequently hydrogen not only directly from the electrolyser, but also from the tank, due its slower dynamics compared to the electrolyser.

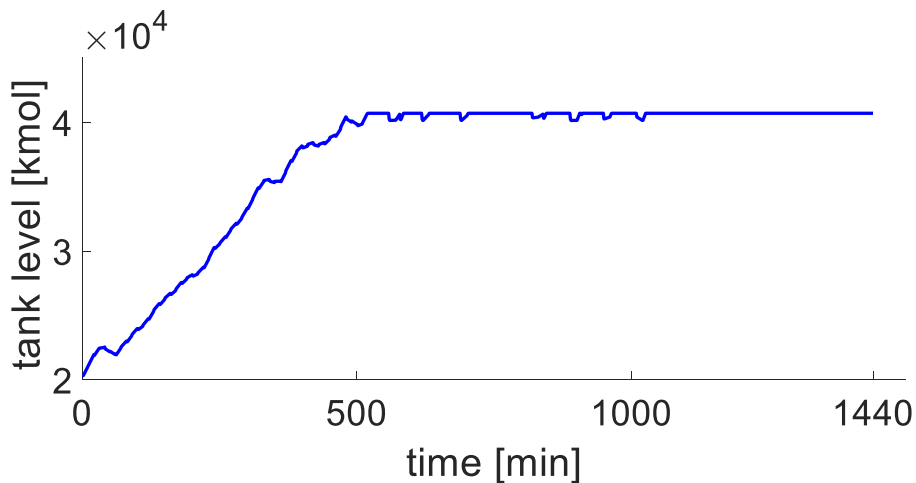


Figure 7-34: Filling of the tank of the 1-GW PtG plant (10<sup>th</sup> January, 2030 DG scenario), network #T3

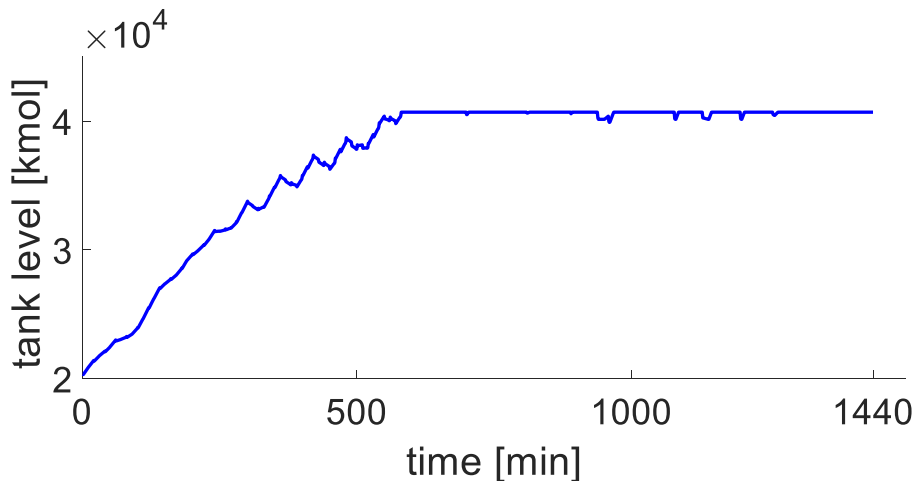


Figure 7-35: Filling of the tank of the 1-GW PtG plant (3<sup>rd</sup> July, 2030 DG scenario), network #T3

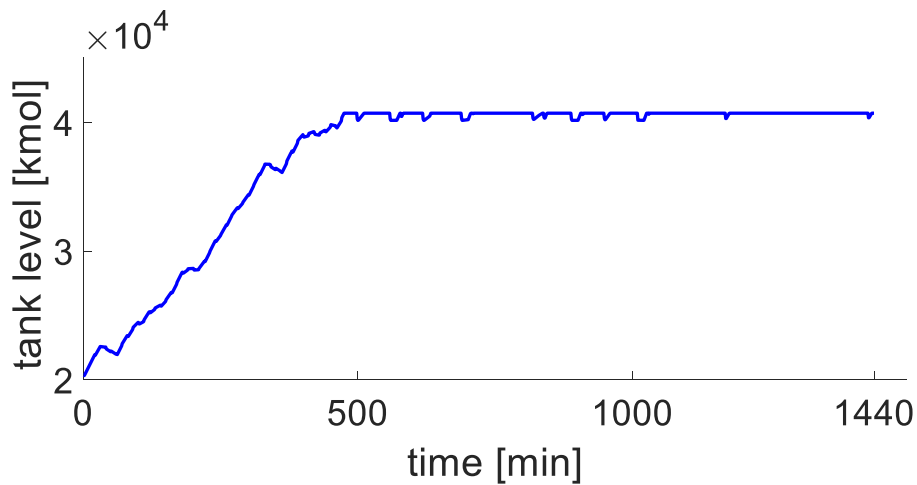


Figure 7-36: Filling of the tank of the 1-GW PtG plant (10th January, 2040 GCA scenario), network #T3

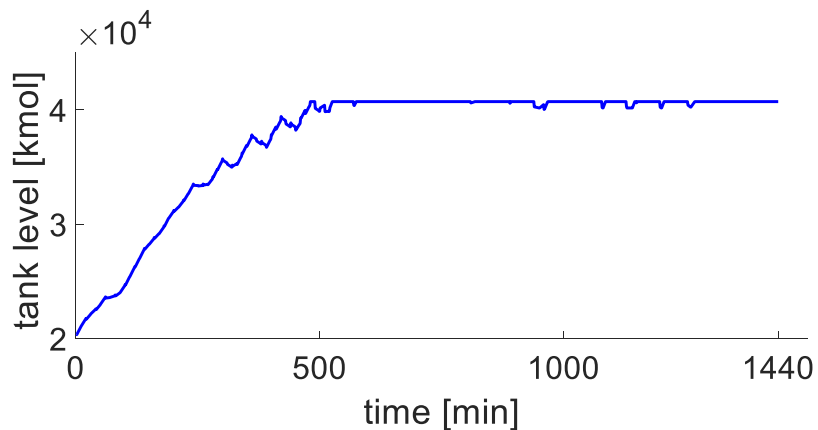


Figure 7-37: Filling of the tank of the 1-GW PtG plant (3<sup>rd</sup> July, 2040 GCA scenario), network #T3

Instantaneous SNG production figures (two example provided, Figure 7-39 and Figure 7-38), if compared to the ones of 2017 scenario (Figure 7-16 and Figure 7-21), show an higher fluctuation of methanation units' working points, compatible with higher RES power variation.

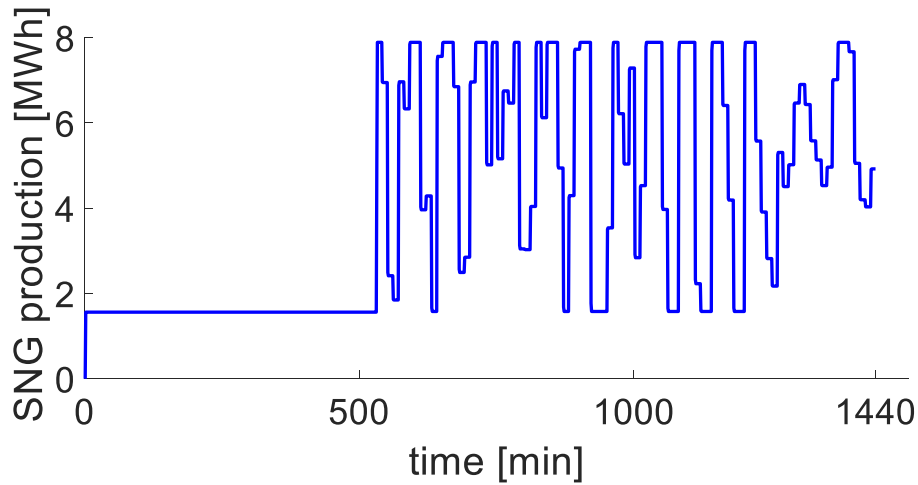


Figure 7-39: Instantaneous SNG production of the 1-GW PtG plant (3<sup>rd</sup> July, 2030 scenario)

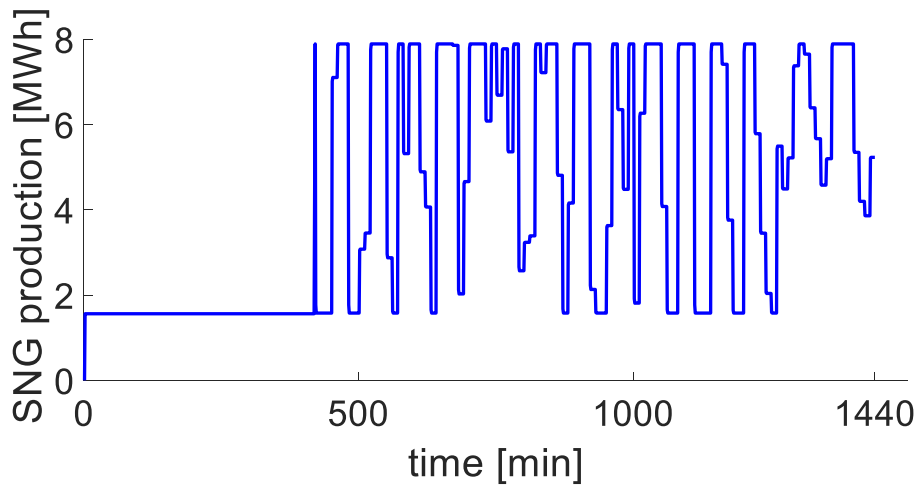


Figure 7-38: Instantaneous SNG production of the 1-GW PtG plant (3<sup>rd</sup> July, 2040 scenario)

It's also important to know that, given the size of the PtG unit and the high variation, the total SNG produced cannot increase much compared to 2017 scenario. The total production cap just above of 6000 MWh as it can be seen in the two examples of cumulative SNG production shown in Figure 7-41 and Figure 7-40.

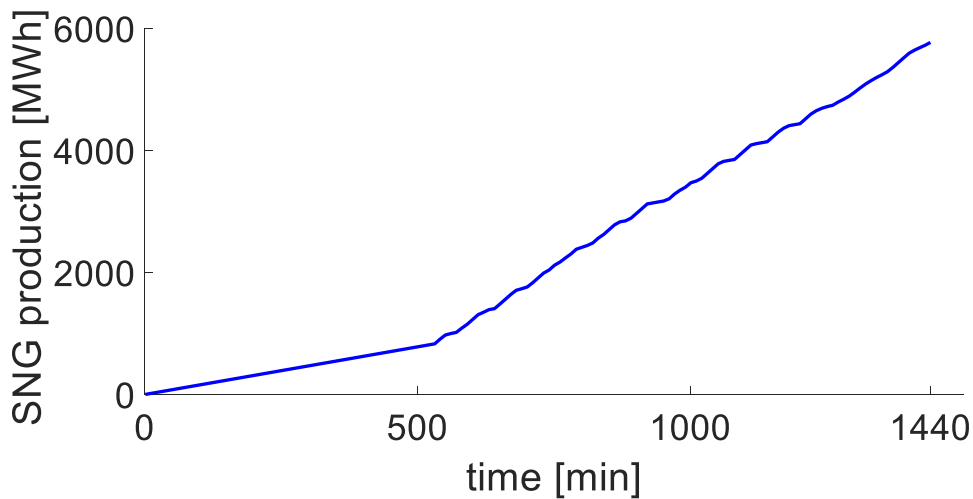


Figure 7-41: Cumulative SNG production of the 1-GW PtG plant (3rd July, 2030 scenario)

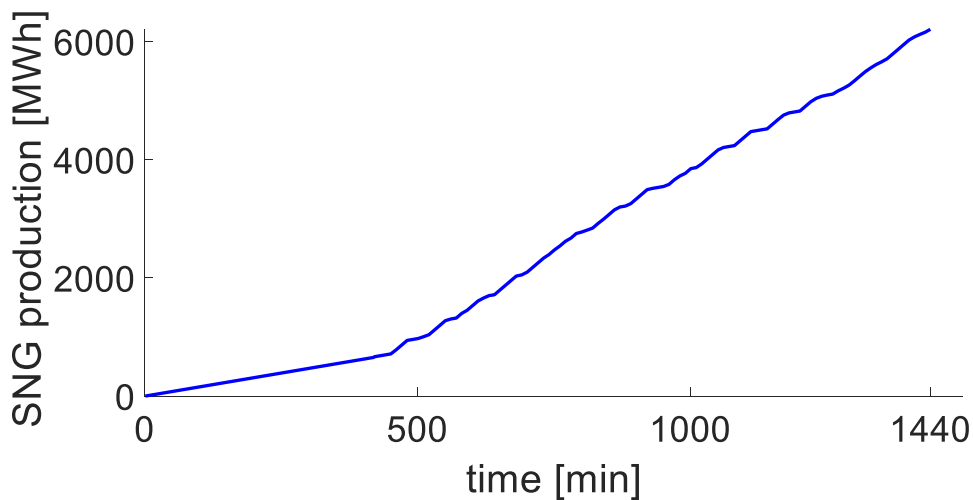


Figure 7-40: Instantaneous SNG production of the 1-GW PtG plant (3<sup>rd</sup> July, 2040 scenario)

As it can be observed in these results, the sizing of PtG plants influences both SNG production and ramping capabilities. Given a certain size, a different RES scenario will not influence much the output of the methanation unit. Future analysis could explore the optimization of the sizing and positioning of PtG based on these two rationales:

- Maximising SNG production for each PtG plant
- Maximising whole PtG system impact on the network

Given the same amount of total PtG installed, the two optimizations could lead to different results since efficiency scales with plant size, and it will be interesting which configuration would be the best for the two cases. In fact, the total capacity of PtG installed is not representative of the effectiveness of the configuration: this capacity can be divided in few big PtG plants or more smaller plants. Besides these considerations, it is clear that PtG configuration has to be designed while looking to future scenarios, else its performance will not be optimal with increased RES capacity

## 8 Conclusions

Three different networks (one test network and two European networks) have been studied: all the cases showed that the introduction of PtG is beneficial for the network operation. The benefits have been calculated in technical terms, seen as the reduction of the variation that the traditional generators have to make on their production for facing the RES variation.

The results obtained from the analysis of all the networks present a common denominator: *PtG helps the transmission networks by absorbing the RES variability*, which cannot be completely foreseen in advance. The magnitude of the RES impact will increase in the next years, as it can be seen comparing 2017 scenario to the 2030 DG and 2040 GCA ones in network #T3, almost up to three times the 2017 level, and transmission networks needs to be ready for the future.

It is possible to understand how important is to proper consider future scenarios, despite their uncertainty: a set of PtG plants that, installed in the conditions corresponding to the 2017 scenario, can reduce RES imbalance energy by ~92%, when applied in 2030 DG and 2040 GCA scenarios sees a reduced effect (from ~92% of RES imbalance energy reduction down to ~60% and ~45%, respectively). The peak power reduction of the RES imbalance on the network follows a similar trend: being directly linked to the total capacity of PtG installed, the peak reduction decreases from ~50% for 2017 scenario down to ~18% and ~12% for the future scenarios.

This has been evaluated by developing a two-level program, where the first part is devoted to simulating an hourly generator dispatching based on the load values and the expected values of the RES, whereas the second part aims to redispatch the traditional generators because of the change of the net load due to the difference between the expected and actual value of RES-based power plants.

All of the previous simulations have been carried out by inserting in the network the “PtG node”, that is the electrical representation of the PtG plant, considering all the production chain (electrolyser, buffer, compressors, methanation step and so on). In this way, the response time of the plant has been properly modelled.

These results make room for further investigations, and the next steps for the continuation of this work will be basically two:

- the impact of optimal PtG placement on network infrastructure
- the complete analysis of the impact on the transmission system operation with long term future scenarios

These two topics are closely connected, because they are both related to the future development of the electricity grids, in terms of future investments already scheduled or under investigation. The PtG technology has been proven to be a solution of the problems introduced by the high penetration of RES, and the computational framework presented in this work represents the instrument needed quantify the economical implication of this solution.

Therefore, “the research must go on”.

## Appendix A PtG plant model

This model has been produced internally at PoliTo in another work but, given its importance in this work, its main features and characteristics are reported in this appendix.

### A.1 AEC electrolyser model

The PtG model used in this work was based on the dynamics (start-ups, shutdowns and partial loads) of a real AEC-based electrolyser. The low temperature-based electrolyser is characterised through to a power-to-hydrogen efficiency (e.g. about 55 %), whereas, the methanation unit is characterized by a certain value of the CO<sub>2</sub> conversion (i.e., about 99 %). In addition, the electrical input to the PtG plant is comparable with the load of the electrolyser, thus all the auxiliary consumptions were considered.

The dynamic AEC-electrolyser response was obtained from the data of a test carried out at the project demonstration site in Falkenhagen on a 2 MW AEC-electrolyser, which was constituted of 6 AEC modules (330 kW each one). The test had a duration of about 11 hours, and the set point of the electrolyser was changed following a profile created to explore a large number of operating conditions, as shown in Figure A-1. These tests showed a fast response in relation to conventional generators. Therefore, its response could be modelled for the purpose of forecasting the behaviour of the AEC-based electrolyser when it is coupled with an intermittent RES-based electric profile.

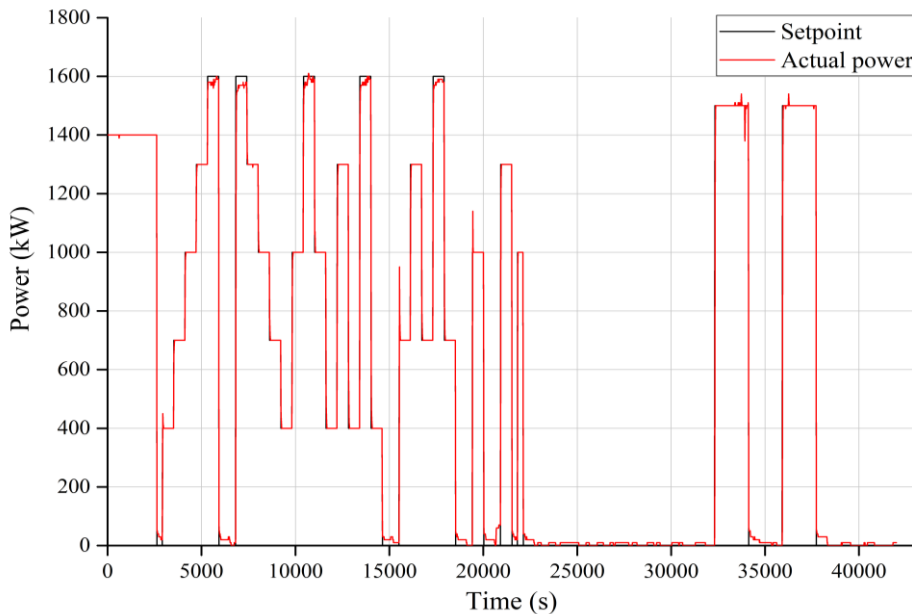


Figure A-1: Falkenhagen test on an AEC-based electrolyser

Analysing Falkenhagen test data, the AEC-based electrolyser behaviour could be modelled as a first order system with delay, which is characterized by 3 parameters; the mathematical model of its response to a step is described by means of equation (8) [29][30].

$$\begin{cases} y(t) = 0 & \text{If } t < \alpha \\ y(t) = A \cdot K \cdot \left[ 1 - \exp\left(-\frac{t - \alpha}{\tau}\right) \right] & \text{If } t \geq \alpha \end{cases} \quad (8)$$

In this equation,  $y$  is the actual power of the AEC-based electrolyser (MW),  $A$  is the step amplitude of the set point (MW),  $K$  is the gain of the system,  $\alpha$  is the time delay of the response (s),  $\tau$  is the

time constant of the system (s) and  $t$  represents the time (s). The gain could be evaluated by means of equation (9), where  $y(\infty)$  is the actual power of the electrolyser after a large period of time (stationary condition).

$$K = \frac{y(\infty)}{A} \quad (9)$$

Whereas, the two time parameters ( $\alpha$  and  $\tau$ ) were estimated by means of the Sundaresan and Krishnaswamy's method [31], according to equations (10) and (11), respectively. The two parameters were calculated using two characteristic points of the response curve:  $t_1$  represents the time in which the response reaches the 35.3% of the stationary value  $y(\infty)$ ; while,  $t_2$  is estimated as the time in which the response reaches the 85.3% of the final value  $y(\infty)$ .

$$\alpha = 1.3 \cdot t_1 - 0.29 \cdot t_2 \quad (10)$$

$$\tau = 0.67 \cdot (t_2 - t_1) \quad (11)$$

For the purpose of evaluating the three parameters ( $K$ ,  $\tau$  and  $\alpha$ ), four steps with the same amplitude were considered. More in detail, the four steps were obtained between 3450 s and 5400 s (see Figure A-1), where the step amplitude ( $A$ , MW) was 0.3 MW. Therefore, the first order system with delay model interpolates carefully the actual power data, as illustrated in Figure A-2. The estimated parameters ( $K = 1$ ;  $\tau = 11.73$  s;  $\alpha = 14.62$  s) allow the actual power of the AEC-based electrolyser to be calculated by means of the model of its dynamic response. The response is exponential, thus, the stationary condition could be reached after about 60 s (the difference between the set point and the actual power is lower than 2 %), as it can be shown in the example response in Figure A-2.

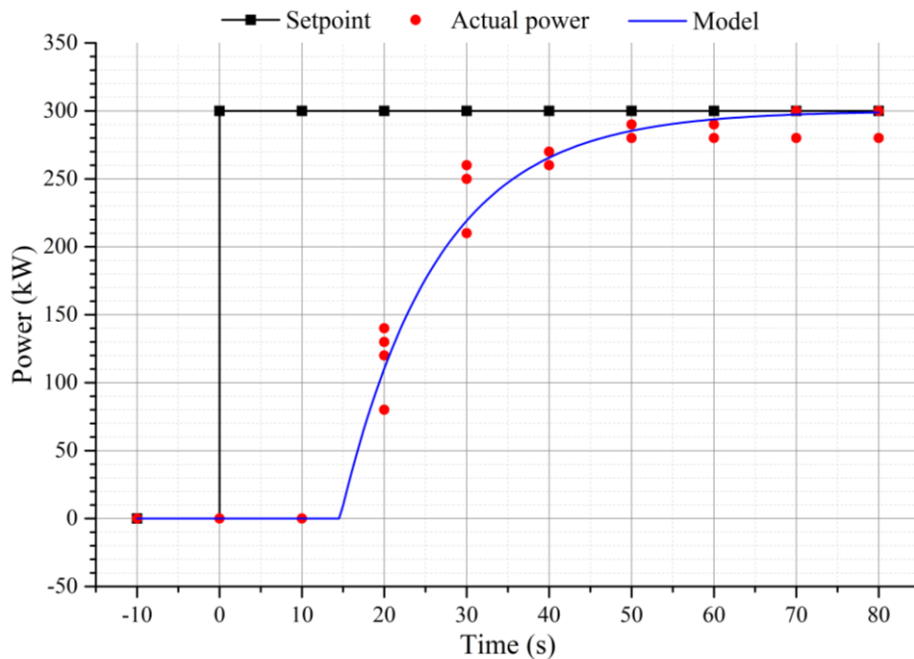


Figure A-2: AEC-based electrolyser response model estimated using Falkenhagen test data (first order system with delay:  $K = 1$ ;  $\tau = 11.73$  s;  $\alpha = 14.62$  s).

It is worth to note that, in general, these parameters depend on the characteristics of the single electrolyser, but they do not depend on the step amplitude of the setpoint variation, which is applied to that electrolyser. They could change, if the stack size varies; but in our case, 330 kW AEC stacks are considered. Thus, this size could be considered as an average size between 300 kW and 2-3 MW electrolysers due to the modularity of the technology.

## A.2 AEC electrolyser efficiency

After modelling the electrical response of the electrolyser it's important to analyse the efficiency curve, which relates the absorbed electric power with the hydrogen chemical power. The power-to-H<sub>2</sub> efficiency ( $\eta_{el\_H_2}$ , lower heating value (LHV) based) was estimated by means of Falkenhagen test data (see Figure A-1).

As it can be seen in Figure A-3, the interpolation between the actual electric power ( $P_{AEC}$ , MW) and the actual hydrogen power ( $P_{H_2}$ , MW) produced by the electrolyser, is a line, therefore the efficiency was evaluated as the slope of the line, and therefore it can be considered constant at various electric power levels, as shown in equation (12). The neglected experimental data correspond to values of power-to-hydrogen efficiency greater than 75 % or lower than 45 % (LHV basis), which are considered as reference efficiencies of low temperature-based electrolysers [32][33].

The resulting average value of power-to-H<sub>2</sub> efficiency is about 57.6%. In addition, the hydrogen power was calculated using the volumetric hydrogen flow ( $\dot{V}_{H_2}$ , m<sup>3</sup>/h) measured during the test, according to equation (13). In this equation,  $p$  is the normal pressure (10<sup>5</sup> Pa),  $T$  the normal temperature (273.15 K),  $R$  is the ideal gas constant (8314 J·kmol<sup>-1</sup>·K<sup>-1</sup>),  $MW_{H_2}$  represents the molar weight of the hydrogen (2.016 kg/kmol) and  $LHV_{H_2}$  is the lower heating value of the hydrogen (120 MJ/kg).

$$P_{H_2} = \eta_{el\_H_2} \cdot P_{AEC} \quad (12)$$

$$P_{H_2} = \frac{p \cdot \dot{V}_{H_2}}{R \cdot T} \cdot \frac{MW_{H_2} \cdot LHV_{H_2}}{3600} \quad (13)$$

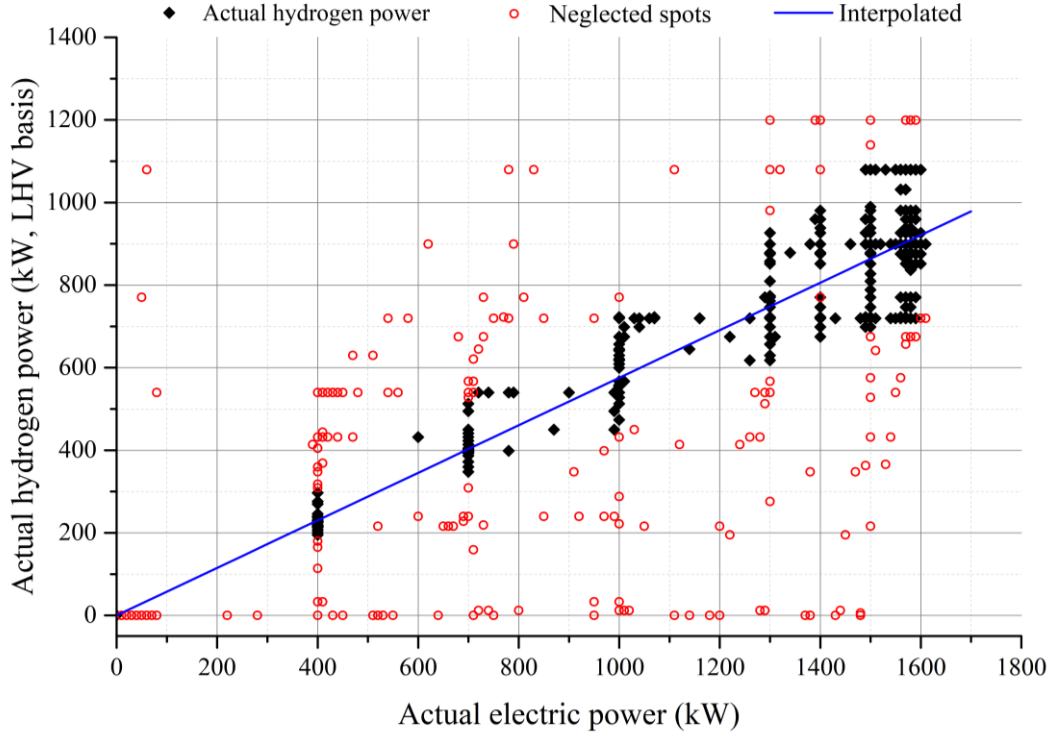


Figure A-3: AEC-based electrolyser power-to-H<sub>2</sub> efficiency (LHV based) obtained using Falkenhagen test data.

### A.3 Methanation unit

The overall CO<sub>2</sub> conversion within the methanation unit was assumed about 99 % [14] to ensure the synthetic natural gas (SNG) quality. Hence, the thermodynamic hydrogen-to-methane efficiency corresponds to 83 % on LHV basis (it is defined as the ratio between the chemical energy of the produced methane and the chemical energy of the hydrogen which is fed to the methanation unit). However, the methanation reaction is strongly exothermic, thus, 17 % of the hydrogen chemical energy (LHV basis) is released as heat of reaction (-164 kJ/mol) [33]. Moreover, all high-temperature items of equipment were thermally insulated to minimize heat losses and dissipations. Heat losses ( $Q$ , MW) were estimated according to equation (14), in which  $k$  represents the thermal conductivity ( $W \cdot m^{-1} \cdot K^{-1}$ ) of a microporous insulation material [34],  $S$  is the surface heat exchange area ( $m^2$ ),  $x$  is the insulation panel thickness (m),  $T_1$  and  $T_2$  are the temperatures (K) of the internal and external surface area, respectively.

$$Q = \frac{k \cdot 10^{-6}}{x} \cdot S \cdot (T_2 - T_1) \quad (14)$$

### A.4 Compression and pumping power consumptions

The hydrogen produced within the AEC-based electrolyser could be compressed in a storage tank or it could be mixed with carbon dioxide in stoichiometric ratio equal to 4. In addition, the carbon dioxide may be compressed up to the methanation unit pressure. Finally, the water has to be pumped in the electrolyser. For all these processes electricity is needed, thus the power of the compressors ( $P_{c,j}$ , MW) and the power of the pump ( $P_{p,H_2O}$ , MW) must be estimated according to equations (15)

and (16), respectively. In these correlations,  $Z$  is the compressibility factor,  $R$  is the molar ideal gas constant,  $\gamma$  is the heat capacity ratio and  $\eta_c$  is the compression efficiency, which was set at 85% [35].  $T_{1,j}$  (K) and  $p_{1,j}$  (bar) are the temperature and the pressure at the inlet of the  $j$ -th compressor; and lastly,  $p_{2,j}$  (bar) is the pressure at the outlet of the equipment. Moreover,  $\dot{n}_{in,j}$  is the molar flow (kmol/s) of the gas mixture at the inlet of the  $j$ -th compressor. In addition,  $p_M$  and  $p_{ATM}$  are the methanation unit pressure (MPa) and the atmospheric pressure (0.101325 MPa), respectively;  $MW_{H_2O}$  is the water molar weight (18.016 kg/kmol),  $\eta_p$  is the efficiency of the pump which was assumed equal to 85 %,  $\rho_{H_2O}$  the water density (about 1000 kg/m<sup>3</sup>),  $\dot{n}_{H_2}$  is the hydrogen molar flow (kmol/s) produced by the electrolyser and  $WC$  is the water conversion of the AEC-based electrolyser which was set equal to 75%.

$$P_{c,j} = Z_j \cdot \frac{R}{10^6} \cdot T_{1,j} \cdot \frac{\gamma_j \cdot \eta_{c,j}}{\gamma_j - 1} \cdot \left[ \left( \frac{p_{2,j}}{p_{1,j}} \right)^{\frac{\gamma_j - 1}{\gamma_j \cdot \eta_{c,j}}} - 1 \right] \cdot \dot{n}_{in,j} \quad (15)$$

$$P_{p,H_2O} = \frac{(p_M - p_{ATM}) \cdot MW_{H_2O}}{\eta_p \cdot WC \cdot \rho_{H_2O}} \cdot \dot{n}_{H_2} \quad (16)$$

For instance, the specific energy consumption for CO<sub>2</sub> compression is 83.4 kJ/kg, while the specific energy consumption for H<sub>2</sub> compression is about 3300 kJ/kg, which correspond to 3.8 % of the produced SNG energy. In addition, the water flow has to be heated up to the electrolyser temperature, hence the molar enthalpy variation of the water flow is about 3770 kJ/kmol (1.9 % of the produced SNG energy).

## Appendix B Calculation of the AC power for PV fields

The irradiance can be converted in power through the model shown in this appendix. In particular, the model allows to pass from the irradiance (expressed in  $W/m^2$ ) to an adimensional value representing the ratio between the power produced by the PV plant at AC side ( $P_{AC}$ , expressed in [W]) and the nominal power of the plant ( $P_{nom}$ , expressed in [Wp]), i.e.,  $\frac{P_{AC}}{P_{nom}}$ . Eventually, this ratio represents the production profile, i.e., the power produced by the plant expressed in per unit (pu).

This step is made by calculating the temperature of the PV panel  $T_c$  by starting from the temperature of the air, as shown in (17), and then using it to calculate the *thermal efficiency*  $\eta_{th}$  which is used for calculating the pu PV production (formulas (18) and (19)) [25]:

$$T_c = T_a + \frac{NOCT-20}{800} \cdot G \quad (17)$$

$$\eta_{th} = 1 - \alpha_{th} \cdot (T_c - 25) \quad (18)$$

$$\frac{P_{AC}}{P_{nom}} = \eta_{DC-AC} \cdot \frac{G}{1000} \cdot \eta_{th} \quad (19)$$

Where  $T_c$  is the estimated temperature of the PV panel (expressed in  $^{\circ}C$ ),  $T_a$  is the air temperature,  $NOCT$  is nominal operating cell temperature (imposed equal to  $45^{\circ}C$ ),  $\eta_{th}$  is the reduction of production due to the temperature of the PV panel,  $G$  [ $W/m^2$ ] is the radiation,  $\alpha_{th} = 0.45\%$  is the loss coefficient due to the temperature, and  $\eta_{DC-AC} = 0.828$  represent the efficiency due to cables, connections, inverter and so on.

## Appendix C Wind Profile Elaboration

Accurate and reliable wind data has been hard to gather. Wind's bond with the height, terrain conformation, geographical location brings the need of punctual data from the actual wind farms in order to reach an absolute accuracy. Therefore, an approach similar to the one used in Appendix B for solar generation is not applicable. The only accurate wind power time series found were using one-hour time steps, too long for our purposes, since one-hour averages do not reflect wind variability. Ideally our aim was to reach 1-minute time step for wind profiles, but for the European networks it has been decided to use 10-minutes time steps since there is a market at that interval of time.

Many iterations of elaboration have been needed in order to obtain reliable and accurate wind profiles, and the history of the main passages is presented here.

### C.1 Network #T1

In the test network only one wind generator without any geographical information is present, and, since the network is not representative of any real network, the power output has been chosen equal to the power output of a real wind farm, which data was available to us. The data was from a wind farm composed by five turbines of 2.5MW nominal power each, and it was gathered with a sample rate of 32 Hertz. Almost one-year worth of data was accessible. By summing the power output and dividing for the number of active turbines, a per unit profile was created, ready to be applied to the desired installed capacity. An example of per unit profiles is presented in Figure C-1.

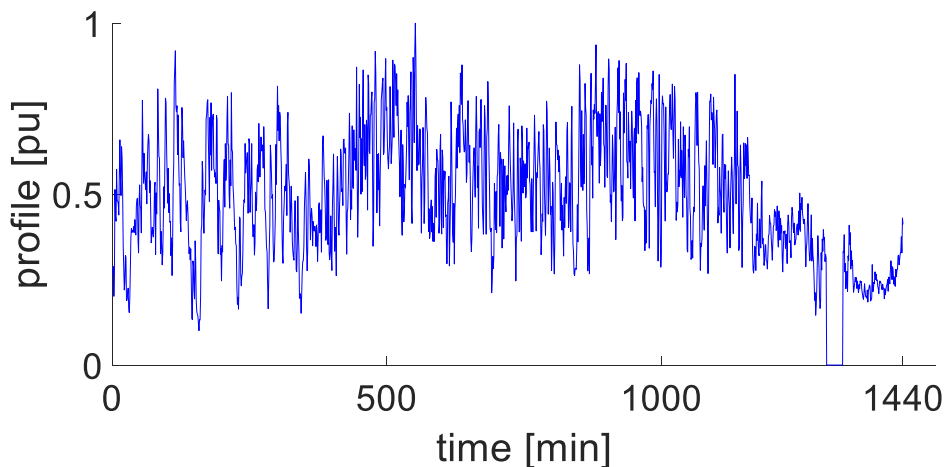


Figure C-1: Example of Per-Unit profiles

### C.2 First approach for Europeans networks

The first idea in order to have reliable wind power variability for each node was to replicate some profiles similar to the real ones. A transition probability matrix approach was used, followed by a discrete Markov chain process.

In order to create a transition probability matrix, it was necessary to discretize the real data into discrete states. By assigning each point of the real data to its state, a sequence of states represents the real data. A transition probability matrix is a square matrix with rows as input state, and columns as output state. It's created row by row, by considering a state, and analysing which states follows the input state in the time series. Therefore, a value in the matrix equals to the probability for that row# state to transition to the column# state. It follows that a property of the transition probability matrixes is that the sum of the values of each row equals to one.

After creating the transition probability matrix, it can be used to transition to a state to another, using an extraction, through the execution of a discrete Markov chain process. Multiple Markov chain processes has been used, one for each bus, in order to have a unique, yet accurate, wind power profile for each bus.

By using a month worth of data for the creation of the transition probability matrix, by replicating the approach to each month twelve profiles have been made for each bus, granting seasonality differences to our study. An example of 10-states profile simulated through the use of the example transition probability matrix in Table C-1 is shown in Figure C-2. Figure C-3 show a 50-states profile simulated starting from the same real data.

**Table C-1: Example of a 10-states probability transition matrix**

		Output state									Sum
Input state	0.97	0	0	0.03	0	0	0	0	0	0	1
	0	0.55	0.37	0.08	0	0	0	0	0	0	1
	0	0.09	0.60	0.23	0.06	0.01	0.01	0	0	0	1
	0.00	0.01	0.13	0.44	0.27	0.10	0.04	0.00	0	0	1
	0	0	0.03	0.30	0.34	0.16	0.11	0.04	0.01	0	1
	0	0	0.00	0.09	0.28	0.30	0.22	0.09	0.02	0	1
	0	0	0	0.02	0.11	0.34	0.29	0.18	0.05	0.00	1
	0	0	0	0	0.03	0.16	0.31	0.38	0.11	0.01	1
	0	0	0	0	0.02	0.12	0.25	0.31	0.27	0.04	1
	0	0	0	0	0	0	0	0.40	0.40	0.20	1

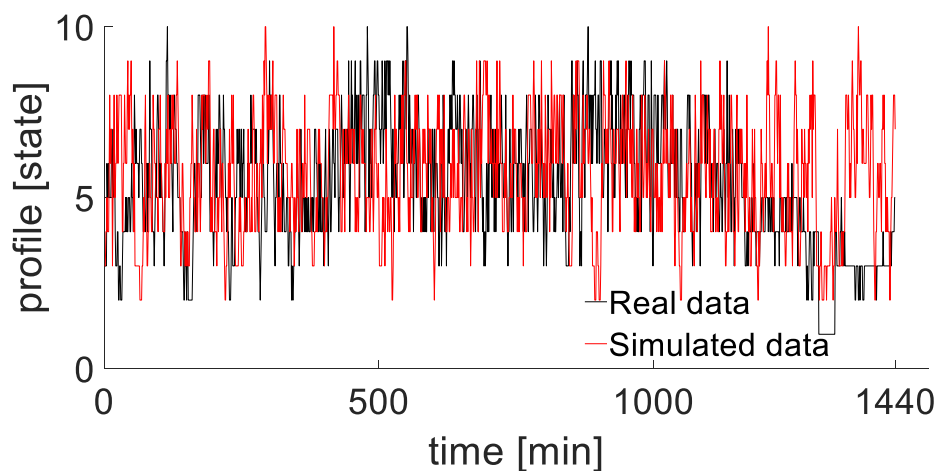


**Figure C-2: Example of discrete profiles – 10 states**

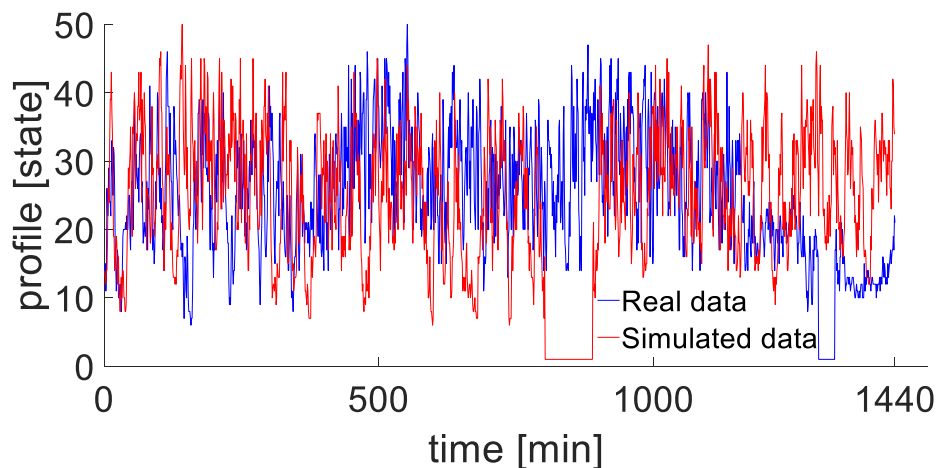


Figure C-3: Example of discrete profiles - 50 states

### C.3 Second approach for Europeans networks

When executing network #T2 simulations the problem with the first approach was clear: by applying a wind profile derived from a relatively small wind farm to a bus which its installed wind power plants capacity represents an aggregate of wind farms, the wind power output variance is overestimated, therefore not representative of the real variation. The network could not follow wind variation, causing non-convergence of the power flow, until it has been decided to apply the variation to only 50% of the installed capacity, unveiling that the problem was the unrealistic power variation.

In fact, it is plausible that few turbines could go from full power to almost zero in a matter of minutes, but it is far less probable to happen to all the turbines of a region, or a country. Moreover, there was not only no correlation between with the historical one-hour average data, but also with the yearly energy produced by wind power plants. This required to analyse the situation in a deep manner.

Then a different approach has been tested: gathering 1-hour power time series from [22], and then extracting the variance from real data. Real data this time was taken from another wind farm, composed by 69 turbines of 2.6MW nominal power each.

The average value was assigned to each node based on the installed capacity. At first the variance has been correlated with the per unit average value of production, with the installed capacity, and then both. But what at first glance seemed a good solution for the variance, revealed to be inconsistent when the installed wind capacity was scaled, since the variance would scale differently than predicted. In fact, aggregating wind power plants resembles aggregating domestic loads. Domestic loads are unpredictable when considered singularly but become predictable when they are aggregated. The same thing happens to wind farms; therefore, it is expected to have less variance for an increase in capacity and vice versa. By using these methods, the variance would scale the opposite way.

It's important to highlight the importance of correlating the variance with the per unit average value. When assigning an average value, and trying to overlap a variance to it, the correlation between a value of variance and when it happened gets lost. A single transition probability matrix for the variance is not applicable.

This can be understood easily with an example: consider an hourly average value of 0.1 pu of the installed capacity. Time step is ten minutes; therefore, the hourly average value is calculated from six measurements. Variance around that value could be for example five times -0.1 pu and 0.5 pu once. This kind of variance can happen only when the average value is low enough, else in other situations, for example for an average value of 0.8, the singular power production can go over the installed capacity, for example  $0.8 \text{ pu} + 0.5 \text{ pu} = 1.3 \text{ pu}$ .

#### **C.4 Final approach for Europeans networks**

Between these two problems, the latter was the most important. As shown in the example, a variance profile calculated from a given average pu value could be applied to a different average pu value. This generates inaccurate variance (bigger for example) at a certain installed capacity, and this variance would be even increased if the installed capacity is scaled up. It has been chosen to address the latter problem and leave room for improvements and additional studies for the future.

Analysing variance succession from a time step to another through transition probability matrixes was not an option anymore after introducing hourly average values from sources external to the wind farm data. Therefore, a clustering method has been chosen:

- Hourly average profiles calculated from [22] have been converted to ten states, representing each one an interval of per unit values, for example state one represents 0:0.1 pu, state two 0.1:0.2 pu, and so on.
- Each month of wind farm data has been analysed, characterizing hourly average values as states in the same manner as [22] data. Variance profiles within each hour has been assigned to the corresponding hourly average state. The result is a population of variance profiles for each month and for each hourly average state.
- A clustering of these populations of variance is applied, in our case ten clusters for each population, using a k-mean algorithm. The result is for each population ten typical variance profiles, and their probabilities.
- For each bus and for each hourly average value an extraction from the relative state's variance clusters is performed, assigning a variance cluster.

The logical assumptions seemed acceptable, but validation for this method was needed, and it has been performed by analysing the autocorrelation figures of:

- the real data
- the real data's averages with the variance calculated via the described method overlapped
- the real data's averages with the variance values (not entire profiles) extracted randomly from the populations.

An example of the resulting profiles is presented in Figure C-4, and shows the genuineness of the approach. The autocorrelation of this method is clearly closer to the one of the real data than the random approach. This can be observed in Figure C-5 at low lag values, and at the value of the negative peak.

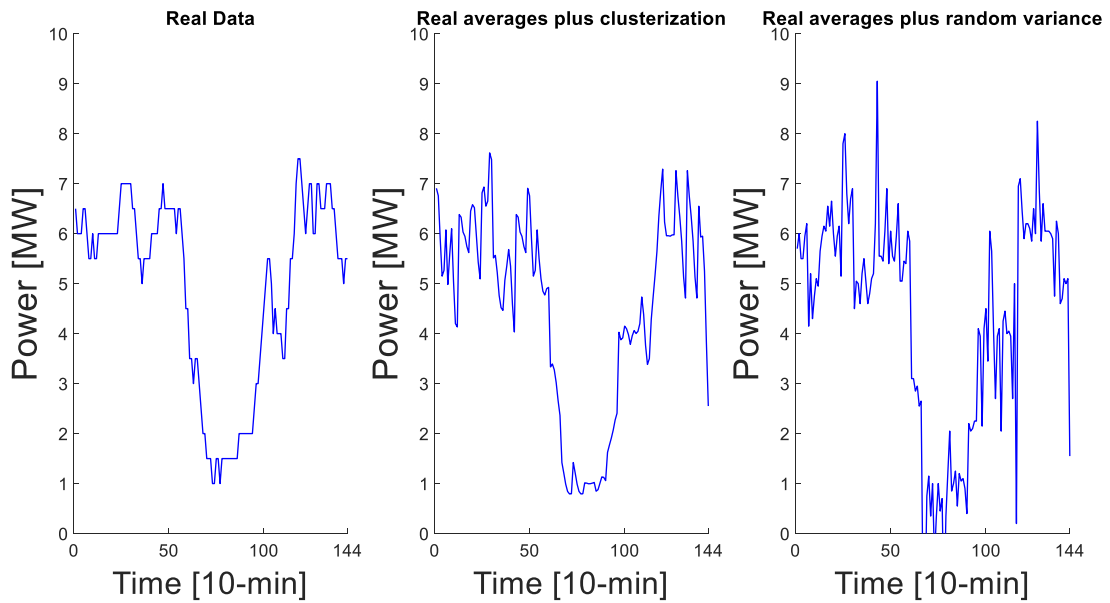


Figure C-4: Profiles used for autocorrelation test

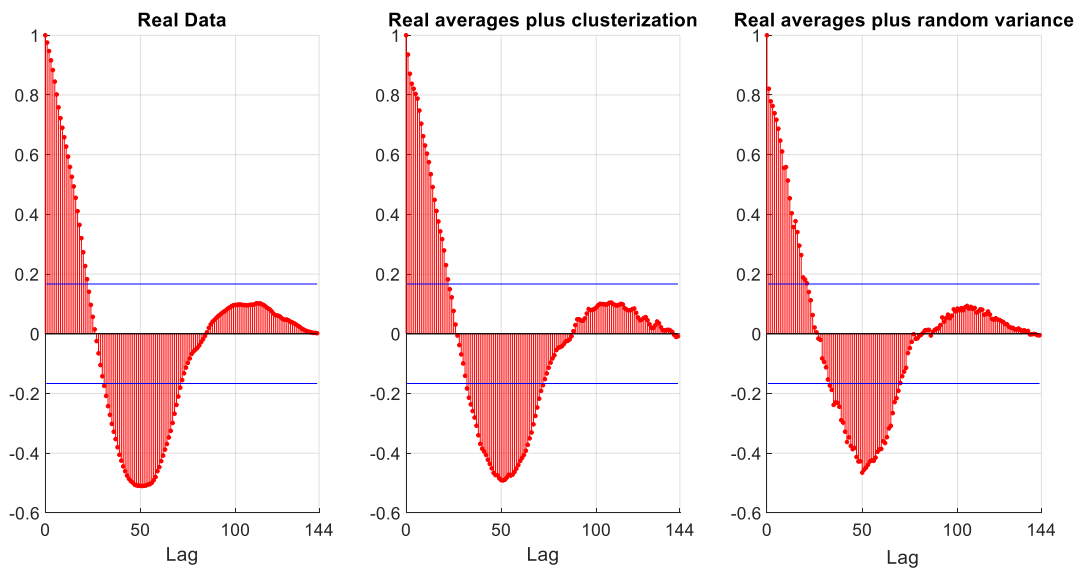


Figure C-5: Autocorrelation

The limitations of these model are clear, the data is from a single location only, and a single wind farm, and the scaling of the installed capacity is not fully correct, but the scarcity of available data, both as spatial and temporal resolution, gives merit to the choices taken. It's important to keep in mind that the aim of this work was the study of the network, and not the study and the creation of accurate high-resolution wind profiles. But in the light of these findings, and in the spirit of the research, additional studies will be conducted in the future about this matter, seen the lack of information in the literature.

A first evolution of the method could consist in studying more wind farms, characterized by different sizes, and assigning to the installed capacity for each bus the clusters of variance calculated from a real wind farm with the most similar size. A second step could be the characterization of wind farms with different sizes and from different locations.

## Appendix D NUTS 2 and Regions association

NUTS stands as French acronym of “Nomenclature des Unités Territoriales Statistiques” is the standard repartition of the territory created by Eurostat in 1988. It is divided in four levels, 0 to 3, from the less to the bigger level of detail.

- NUTS 0 represents the 28 European countries
- NUTS 1 represents areas with a maximum population of 7 million people and a minimum of 3 million. For the small countries it corresponds to the NUTS 0 level, and for the bigger ones it represents an over-regional subdivision
- NUTS 2 reassumes the territorial division in “regions” used by the administration of each country
- NUTS 3 the same as NUTS 2, but a district level

More detailed information is reported in Table D-1, and a graphical representation of NUTS 1 and 2 is shown in Figure D-1.

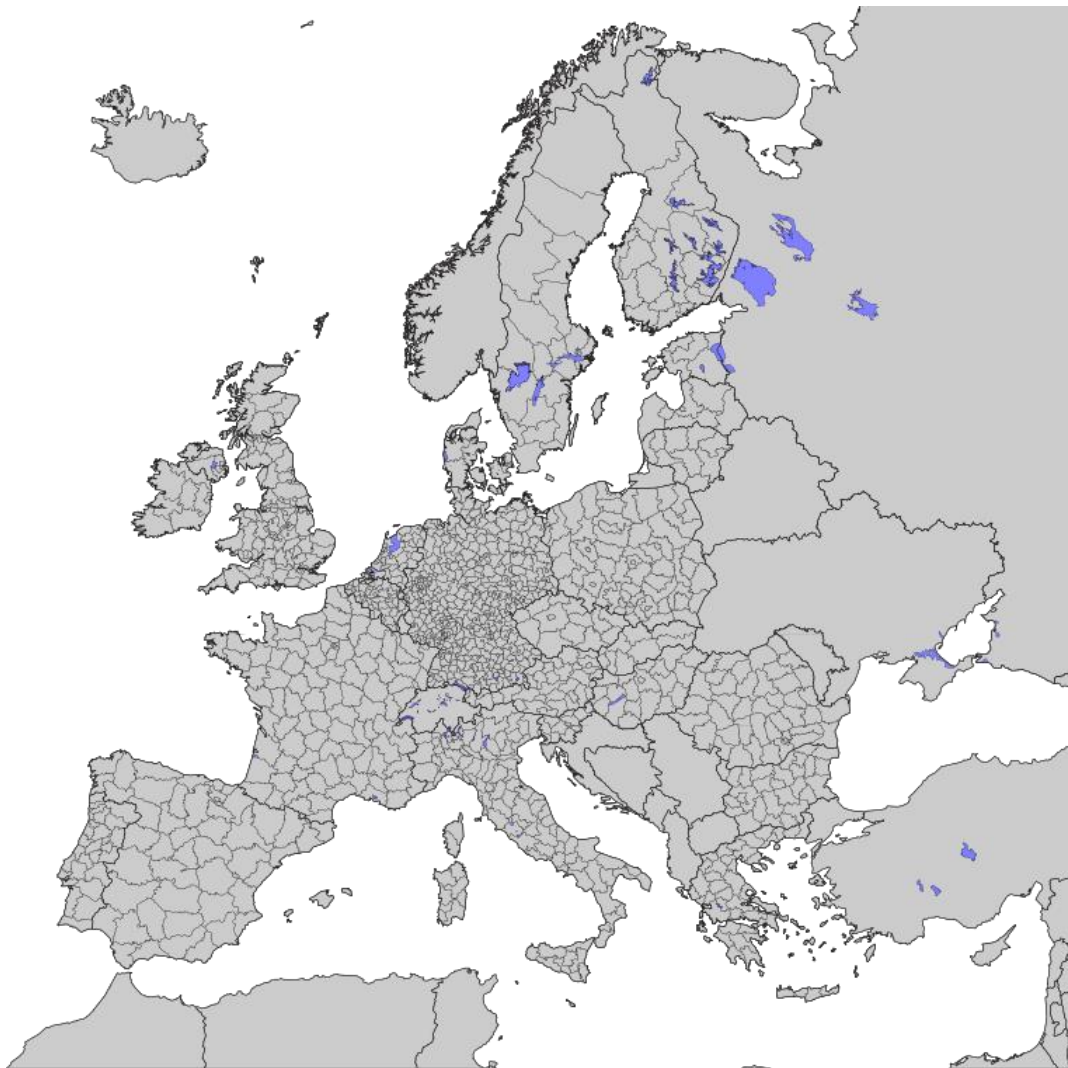


Figure D-1: Representation of European NUTS 1 and NUTS 2 borders

**Table D-1: European NUTS classification**

<b>Class</b>	<b>Maximum population</b>	<b>Minimum Population</b>	<b>Number of regions</b>
NUTS 0	-	-	28
NUTS 1	7000000	3000000	97
NUTS 2	3000000	800000	270
NUTS 3	800000	150000	1318

An interesting problem has been to correlate a coordinate to the belonging NUTS 2 region. Despite there could be other ways using GIS programs, the method used involved the use of the program R. The script downloads a vectorial map of the NUTS 2 regions straight from the European Commission website, places the desired coordinates on the map, and by edge checking assigns each coordinate to the relative country and NUTS 2 region. Both a graphical and table output are created, as it can be seen in Figure D-2 and Figure D-3

```

R Console
-----
  NUTS_ID STAT_LEVL SHAPE_Leng SHAPE_Area
1      ES11         2    9.563231  3.25958242
2      PT11         2    7.485377  2.28624994
3      PT11         2    7.485377  2.28624994
4      PT11         2    7.485377  2.28624994
5      PT11         2    7.485377  2.28624994
6      PT11         2    7.485377  2.28624994
7      PT11         2    7.485377  2.28624994
8      PT11         2    7.485377  2.28624994
9      PT16         2    9.126782  2.99222053
10     PT16         2    9.126782  2.99222053
11     PT16         2    9.126782  2.99222053
12     PT16         2    9.126782  2.99222053
13     PT16         2    9.126782  2.99222053
14     PT16         2    9.126782  2.99222053
15     PT16         2    9.126782  2.99222053
16     PT16         2    9.126782  2.99222053
17     PT16         2    9.126782  2.99222053
18     PT16         2    9.126782  2.99222053
19     PT16         2    9.126782  2.99222053
20     PT18         2    8.985369  3.27592726
21     PT17         2    3.455519  0.26474301
22     <NA>        NA         NA         NA
23     PT17         2    3.455519  0.26474301
24     PT18         2    8.985369  3.27592726
  
```

**Figure D-2: Example of script's output**



**Figure D-3: Geographical representation of network #T2 buses**

## Appendix E OPF convergence problems and their possible solutions

During of debugging of the code and of networks' implementation in Matpower many problems about PF and OPF convergence have been solved. In order to understand the reason behind non-convergence, a little collection of easy checks have been created. This can be helpful also for people new to Matpower, and maybe to whom will continue this work.

First troubleshooting step would be to check the total network load and total network generation capacity online. Obviously, if the former is bigger than the latter, the situation is infeasible. In order to check this eventuality:

```
sum(mpc.bus(:,PD))>sum(mpc.gen((mpc.gen(:,GEN_STATUS)==1),PMAX)
```

If 1, this is the case.

If this is not the case, it could be that total minimum power generation online is bigger than the total load, leading to another infeasibility. In order to check if this is the case:

```
sum(mpc.bus(:,PD))<sum(mpc.gen((mpc.gen(:,GEN_STATUS)==1),PMIN)
```

If 1, this is the case.

If neither of these situations apply, then it could be a problem caused by some crucial line which is overloaded, creating imbalances between regions. Keep in mind that is highly probable that the problematic line is one connecting two different countries. The mpc can be modified to increase branch limits, and another power flow can be executed. If it converges, that is the problem.

```
mpc.branch(:,RATE_A)=2*mpc.branch(:,RATE_A)
```

Another way to relax branch limits is to enable soft limits. It is possible only for DC OPF since it enables lines overloads at the cost of a price penalty, so an branch overload would be the least possible, since it causes additional costs to the system, and OPF tries to minimize the system costs. Soft limits can be enabled via this command:

```
mpc = toggle_softlims(mpc, 'on')
```

A subtle situation could be when a region is connected to the rest of the network via DC lines. MATPOWER implements DC lines internally as generators, and previous method for increase lines rates works only for AC lines. In order to increase DC lines limits it is necessary to:

```
mpc.dcline(:,10:11)=2*mpc.dcline(:,10:11)
```

And then try another power flow.

About DC lines: differently from AC lines, it is not enough to add them into mpc in the dedicated dcline field. They need to be specifically enabled through this command:

```
mpc = toggle_dcline(mpc, 'on')
```

it is important to note that when DC lines are not enabled, and islands are created, MATPOWER fails to inform the user that the network is actually two separated networks. This could be due to DCOPF, since slack is not required, being zero the network losses.

If non-convergence happens on real time script, reasons could be different. Maximum and minimum power outputs of the generators change along each hour in the script. Therefore, if there is an incongruence of total minimum power/maximum power and load, the cause is a total network ramp rate lower not high enough to cover RES variability. The solution is to run the second part of day ahead script, add more generators online other than the one decided by DUOPF, and try again the real time market. The problem could be the monotone behaviour of PV variability during sunrise and sunset, which stresses a lot the ramp rate requirement, so additional generators could be added only at certain hours.

## References

- [1] A. Mazza, E. Bompard, and G. Chicco, Applications of power to gas technologies in emerging electrical systems, *Renewable and Sustainable Energy Reviews*, vol.92, pp. 794-806, 2018
- [2] E. Giglio, F.A. Deorsola, M. Gruber, S. R. Harth, E. A. Morosanu, D. Trimis, S. Bensaid, and R. Pirone, Power-to-Gas through High Temperature Electrolysis and Carbon Dioxide Methanation: Reactor Design and Process Modelling, *Ind. Eng. Chem. Res.*, vol. 57, pp. 4007–4018, 2018.
- [3] J.J. Grainger, and W.D. Stevenson, *Power System Analysis*, McGraw-Hull Series in Electrical and Computer Engineering, 1994.
- [4] K. Mayer, S. Truck, Electricity markets around the world, *Journal of Commodity Markets*, Volume 9, March 2018, pages: 77-100
- [5] EPRI, Wholesale electricity market design initiatives in the United States: Survey and research needs, Electric Power Research Institute, 2016 Technical Update
- [6] R. D. Zimmerman, C. E. Murillo-Sanchez, and R. J. Thomas, Matpower: Steady-State Operations, Planning and Analysis Tools for Power Systems Research and Education, *IEEE Transactions on Power Systems*, vol. 26, pp. 12-19, Feb. 2011 <http://dx.doi.org/10.1109/TPWRS.2010.2051168>
- [7] Task Force C6.04 “Benchmark Systems for Network Integration of Renewable and Distributed Energy Resources”, CIGRE, April 2014
- [8] ENTSO-E, Ten Years Network Development Plan 2016: Grid data, <https://docstore.entsoe.eu/stum/>, (on line 18<sup>th</sup> July 2018)
- [9] DIW Berlin, ELMOD: The original Version of Europe, [https://www.diw.de/de/diw\\_01.c.528493.de/forschung\\_beratung/nachhaltigkeit/umwelt/verkehr/energie/modelle/elmod.html#ELMOD](https://www.diw.de/de/diw_01.c.528493.de/forschung_beratung/nachhaltigkeit/umwelt/verkehr/energie/modelle/elmod.html#ELMOD), (on line 18<sup>th</sup> July 2018)
- [10] F.U. Leuthold, H. Weigt, and C. von Hirschhausen, A Large-Scale Spatial Optimization Model of the European Electricity Market, *Network and Spatial Economics*, vol.12, pp. 75-107, 2012
- [11] Power World, Updated and Validated Power Flow Model of the Main Continental European Transmission Network, <https://www.powerworld.com/knowledge-base/updated-and-validated-power-flow-model-of-the-main-continental-european-transmission-network> (on line 8<sup>th</sup> March 2018)
- [12] B. Wiegman, Unofficial ENTSO-E dataset processed by GridKit, <https://zenodo.org/record/55853#.WpA8cjtG2Co> (on line 18<sup>th</sup> July 2018)
- [13] T. Jensen, H. de Sevin, M. Greiner, P. Pinson, The RE-Europe data set, <https://zenodo.org/record/999150#.W303ry1aagQ>
- [14] J. Hörsch, and Tom Brown, The role of spatial scale in joint optimisations of generation and transmission for European highly renewable scenarios, 14<sup>th</sup> Int. Conference of the European Energy Market, Dresden, Germany, 2017
- [15] J. Hörsch, F. Neumann and T. Brown, Python for Power System Analysis (PyPSA), Model of the European Energy System, <https://github.com/PyPSA/pypsa-eur>

- [16] J. Hörsch, F. Hofmann, D. Schlachtberger, and T. Brown, Supplementary Data: Code, Input Data and Model data: PyPSA-Eur: An Open Optimisation Model of the European Transmission System, [https://zenodo.org/record/1246852#.W307ay1aY\\_V](https://zenodo.org/record/1246852#.W307ay1aY_V) (on line 19<sup>th</sup> July 2018)
- [17] J. Hörsch, F. Hofmann, D. Schlachtberger, and T. Brown, PyPSA-Eur: An Open Optimisation Model of the European Transmission System, Preprint submitted to International Journal of Energy Strategy Reviews, June 2018, <https://arxiv.org/pdf/1806.01613.pdf>
- [18] ENTSO-E, Union for the Coordination of the Transmission of Electricity (UCTE), <https://www.entsoe.eu/news-events/former-associations/ucte/Pages/default.aspx> (on line on 8<sup>th</sup> March 2018)
- [19] ENTSO-E, Home page, <https://www.entsoe.eu/Pages/default.aspx> (on line on 8<sup>th</sup> March 2018)
- [20] ENTSO-E, European Grid Map, <https://www.entsoe.eu/data/map/> (on line on 17<sup>th</sup> July 2018)
- [21] D. Oeding, B. Oswald, Elektrische Kraftwerke und Netze, 7th Edition, Springer, 2011 (in German)
- [22] European Commission, European Meteorological derived high resolution renewable energy source generation time series, <https://ec.europa.eu/jrc/en/scientific-tool/emhires> (on line 18<sup>th</sup> July 2018)
- [23] Bright Solar Resource Model, <http://jamiembright.github.io/BrightSolarModel/>, (online 18<sup>th</sup> July 2018)
- [24] J.M. Bright, C.J. Smith, P.G. Taylor, and R. Crook, "Stochastic generation of synthetic minutely irradiance time series derived from mean hourly weather observation data", Solar Energy, vol. 115, pp. 229-242, 2015, DOI: <http://dx.doi.org/10.1016/j.solener.2015.02.032>
- [25] F. Spertino, F. Corona and P. Di Leo, "Limits of Advisability for Master–Slave Configuration of DC–AC Converters in Photovoltaic Systems," in IEEE Journal of Photovoltaics, vol. 2, no. 4, pp. 547-554, Oct. 2012. doi: 10.1109/JPHOTOV.2012.2203793
- [26] ENTSO-E, Power Statistics, [https://www.entsoe.eu/data/power-stats/hourly\\_load/](https://www.entsoe.eu/data/power-stats/hourly_load/) (on line on 17<sup>th</sup> July 2018)
- [27] ENTSO-E, TYNDP, <http://tyndp.entsoe.eu/maps-data/> (on line on 17<sup>th</sup> July 2018)
- [28] ENTSO-E, TYNDP 2018 Scenario Report, <https://tyndp.entsoe.eu/tyndp2018/scenario-report/> (on line on 26<sup>th</sup> July 2018)
- [29] B. A. Ogunnaike, W. H. Ray, Process Dynamics, Modeling, and Control, Oxford University Press, 1994.
- [30] D. E. Seborg, T. F. Edgar, D. A. Mellichamp, Process Dynamics and Control, 2<sup>nd</sup> ed., John Wiley & Sons, 2004
- [31] K. R. Sundaresan and P. R. Krishnaswamy, "Estimation of Time Delay Time Constant Parameters in Time, Frequency, and Laplace Domains", The Canadian Journal of Chemical Engineering, 56(2), 1978, pp. 257–262, <http://dx.doi.org/10.1002/cjce.5450560215>.
- [32] O. Schmidt, A. Gambhir, I. Staffell, A. Hawkes, J. Nelson, S. Few, "Future cost and performance of water electrolysis: An expert elicitation study, International Journal of Hydrogen Energy, Volume 42, Issue 52, 2017, pp. 30470-30492, DOI: <https://doi.org/10.1016/j.ijhydene.2017.10.045>.
- [33] S. McDonagh, R. O'Shea, D. M. Wall, J.P. Deane, J. D. Murphy, "Modelling of a power-to-gas system to predict the levelised cost of energy of an advanced renewable gaseous transport fuel", Applied Energy, Volume 215, 2018, pp. 444-456, <https://doi.org/10.1016/j.apenergy.2018.02.019>.

- [34] F. Petipas, A. Brisse, and C. Bouallou, Model-based behaviour of a high temperature electrolyser system operated at various loads, *J. Power Sources*, vol. 239, pp. 584–595, 2013.
- [35] R. K. Sinnott, *Coulson & Richardson's Chemical Engineering Design*, 4th ed., vol. 6. Oxford, 2005.

## Ringraziamenti

Un lungo percorso della mia vita è giunto al termine, ed è difficile da realizzare. Non solo il percorso universitario, ma una parte della mia vita ed esistenza che è stata dedicata completamente allo studio. Un lungo ed estenuante percorso fatto da interrogazioni, esami, lezioni, notti insonni e imprecazioni varie, ma anche di entusiasmo, curiosità e di amicizia. Di affetti e di dolori, di interessi e noia, di persone che sono arrivate e sono rimaste altre che magari se ne sono andate. Voglio prendermi poche righe per poter ringraziare tutte le persone che sono state importanti per me e che mi hanno aiutato a crescere e arrivare fino a questo traguardo, e che spero mi continueranno a sostenere nelle nuove sfide che si prospettano davanti a me.

Voglio prima di tutto ringraziare chi mi ha aiutato e supportato nello sviluppo e nella stesura di questa tesi. Il Dr. Andrea Mazza per la sua professionalità e attenzione ai dettagli, per le ore passate al telefono per far convergere le reti e per avermi mostrato che anche l'università può avere un lato umano. Il Prof. Francesco Ettore Bompard, per il suo contributo nella mia formazione come Professore e per l'interesse che ha manifestato in questa mia tesi. Il Dr. Abouzar Estebarsari per avermi aiutato ad approcciare questo problema e avermi spinto a formalizzarne una soluzione completa. Shaghayegh Zalzar che, pur non essendo direttamente coinvolta in questa tesi, ha dedicato il suo tempo e le sue capacità per aiutarmi a risolvere svariati problemi riscontrati.

Voglio ringraziare la mia famiglia, che mi ha supportato (sopportato) costantemente in tutti questi anni di studio e per i sacrifici fatti per non farmi mai pesare nulla e potermi dare la possibilità di studiare al meglio possibile (a parte quando ci sono tonnellate di legna per il camino da sistemare). Grazie a mamma per non aver ancora compreso bene il funzionamento del sistema universitario, ma comunque per tifare sempre per me. Grazie a mio padre per spronarmi sempre (anche a calci in culo se necessario) e avermi spinto ad iniziare questa carriera. Grazie alla nonna, che finalmente potrà vedermi finire gli studi. Grazie a mio fratello... ah no niente. Scherzo, grazie per garantirmi sempre un po' di svago e stacco tra una sessione di studio e l'altra.

Voglio ringraziare il mio amore Irene, per tutti questi anni passati tra libri, quaderni e compiti a casa, ma sempre insieme. Per volermi così come sono, interessato alla tecnologia, all'informatica e alla scienza e a tutte queste cose che grazie agli inglesi posso riassumere con cose "nerd". Per avermi supportato (sopportato) fin dal liceo (\*colpo di tosse\* avanguardie \*colpo di tosse\*) e per procurarmi sempre cose buone per soddisfare la mia fame nervosa prima di un esame. Oppure per festeggiare dopo un esame. Oppure per consolarmi dopo un esame. Per i pomeriggi rilassanti passati a studiare uno accanto all'altra, e quelli un po' più disperati in cui davo la priorità allo studio e non a te. E soprattutto grazie per avermi sempre aspettato dopo quei pomeriggi disperati.

Voglio ringraziare gli amici di sempre, Angelo, Luca, Stefano e Fabio, per esserci sempre stati. Ormai non sappiamo bene come sia iniziato il tutto, ma l'importante è che continui. Grazie per tutti i "giretti per Sanbe" che mi hanno sempre permesso di svagarmi e pensare ad altro dopo lunghe giornate passate sui libri, e di sfogarmi quando necessario (un esempio a caso, quando questa tesi infinita si incagliava. Posso dirlo no? Tanto il Dr. Andrea Mazza non legge fino a questo punto... Vero?). E grazie a Grazia e Silvia per trattarmi bene Angelo e Stefano.

Voglio ringraziare gli amici che per una circostanza o per l'altra si sono aggiunti in momenti diversi della mia vita. Grazie a Luca e Daniele (brah) per avermi spinto ad esplorare diversi hobby nei più disparati campi, dal tiro con l'arco alle saldature elettroniche, dall'enduro con le moto al rafting giù per la Dora e l'Orco, dall'informatica alla forgiatura. Grazie a Mara, Walter, Chiara, Sara, Arianna, Francesco, Giulia e Luca, per avermi accolto sì al tempo in qualità di "ragazzo di Ire", ma per poi non avermi mai fatto sentire fuori luogo, e anzi per aver vissuto bei viaggi ed esperienze e risate

insieme (spero che tutto questo non sia solo per ottenere consulenze tecnico-informatiche, vi tengo d'occhio).

Voglio ringraziare i compagni di università, Luca, Matteo, Simone, Giorgio, Erik e Beppe, per aver condiviso sventure e gioie di questo percorso masochista che è l'ingegneria elettrica (la prossima volta gestionale vero? Che pagano di più per saper fare non si sa bene cosa), perché un percorso così non sarebbe stato sopportabile da una persona sola (e grazie a Beppe per gli appunti, sono dei capolavori e dovrebbero farla affrescare a te la Cappella Sistina). Anzi a Luca no, che mi ha portato ad accettare questa tesi (tanto il Dr. Andrea Mazza continua a non leggere). Ovviamente scherzo, grazie perché questa tesi "in parallelo" mi ha aiutato molto nello svilupparla e nel viverla, e le mille mila ore di vocali e gli ormai gigabytes di foto che ci siamo scambiati penso che siano una prova del sentimento reciproco.

Grazie a tutti, anche a chi non ho nominato, e a chi non c'è più, perché se sono qui e sono diventato ciò che sono è grazie a voi.

Grazie a tutti.